PAUL SCHERRER INSTITUT

Aeroradiometric Measurements in the Framework of the Swiss Exercise ARM21

Gernot Butterweck, Benno Bucher, David Breitenmoser, Ladislaus Rybach,
Cristina Poretti, Stéphane Maillard, Adrian Hess , Malgorzata Kasprzak,
Gerald Scharding, Sabine Mayer

PSI Bericht Nr. 22-02
March 2022
ISSN 1019-0643

PAUL SCHERRER INSTITUT

Aeroradiometric Measurements in the Framework of the Swiss Exercise ARM21

Gernot Butterweck[1], Benno Bucher[2], David Breitenmoser[1], Ladislaus Rybach[3], Cristina Poretti[4], Stéphane Maillard[5], Adrian Hess[4] Malgorzata Kasprzak[1], Gerald Scharding[4], Sabine Mayer[1]

1 Department of Radiation Safety and Security, Logistics Division, Paul Scherrer Institute (PSI), Forschungsstrasse 111, 5232 Villigen PSI, Switzerland
2 Swiss Federal Nuclear Safety Inspectorate (ENSI), Industriestrasse 19, 5201 Brugg, Switzerland
3 Institute of Geophysics, Swiss Federal Institute of Technology Zürich (ETHZ), 8092 Zürich, Switzerland
4 Swiss National Emergency Operations Center (NEOC), 3003 Bern, Switzerland
5 NBC-EOD Centre of Competence (Nuclear Biological Chemical Defense and Explosive Ordnance Disposal), 3700 Spiez, Switzerland

Paul Scherrer Institut (PSI)
5232 Villigen PSI, Switzerland
Tel. +41 56 310 21 11
Fax +41 56 310 21 99
www.psi.ch

PSI Bericht Nr. 22-02
March 2022
ISSN 1019-0643

Abstract

The flights of the civil part (ARM21c) of the exercise were performed between June 28th and July 2nd and the flights of the military part (ARM21m) were performed between August 30th and September 2nd, 2021.

Both parts of the exercise included the measurement of an altitude profile over Lake Neuchâtel with sufficient altitude range to determine the slope of the altitude dependent cosmic correction.

According to the alternating schedule of the annual ARM exercises, the environs of the nuclear power plants Gösgen (KKG) and Mühleberg (KKM) were surveyed, the former extended with an area to the south-east of the power plant. The measurements showed no artificial radionuclides outside of the plant premises.

The series of background measurements over Swiss cities was continued with flights over Frauenfeld, Lugano, Nyon and Wil.

As a follow-up of the Caesium deposition in the wake of the Chernobyl accident, measurements were performed over areas in western and southern Switzerland. Residual ^{137}Cs activity can still be detected in the vicinity of Lugano and several other sites tested during ARM21 as a follow-up of the Chernobyl deposition. Comparison to results of ground measurements, maps published in the scientific literature and previous airborne measurements yielded reasonable agreement to the measurement results.

Detector RLL001 used in ARM21c continues to operate as specified. Problems with one NaI(Tl) crystal of detector RLL004 used during ARM21m indicates that not all of the crystals with poor quality have been identified in previous exercises.

Contents

List of Figures

List of Tables

1 Introduction

Swiss airborne gamma spectrometry measurements started in 1986. Methodology and software for calibration, data acquisition and mapping were developed at the Institute of Geophysics of the Swiss Federal Institute of Technology Zurich (ETHZ). Between 1989 and 1993 the environs of Swiss nuclear installations were measured annually on behalf of the Swiss Federal Nuclear Safety Inspectorate (ENSI) during exercises performed as system check and drill for the operators. This schedule was changed to biannual inspections in 1994, together with an organizational inclusion of the airborne gamma-spectrometric system (ARM) into the Emergency Organization Radioactivity (EOR) of the Federal Office for Civil Protection (FOCP). The deployment of the airborne gamma-spectrometric system is organized by the National Emergency Operations Centre (NEOC). NEOC is also responsible for the recruitment and instruction of the measurement team and the operational readiness of the system. Aerial operations are coordinated and performed by the Swiss Air Force with Super Puma helicopters. The gamma-spectrometric equipment is stationed at the military airfields of Dübendorf and Payerne. The gamma-spectrometry system can be airborne within four hours. Responsibility for scientific support, development and maintenance of the aeroradiometric measurement equipment passed from ETHZ to the Radiation Metrology Section of the Paul Scherrer Institute (PSI) in 2003 in cooperation with ENSI. General scientific coordination and planning of the annual measuring flights is provided by the Expert Group for Aeroradiometrics (FAR). FAR was a working group of the Swiss Federal Commission for NBC protection (ComNBC) and consists of experts from all Swiss institutions concerned with aeroradiometry. FAR was re-organized as an expert group of NEOC in 2008. Additional information can be found at `https://far.ensi.ch/`.
In 2018 the ARM measuring system used by NEOC in past exercises was replaced with the RLL (Radiometrie Land-Luft) system owned by the Swiss armed forces. The maintenance of the RLL systems is performed by the manufacturer according to a service agreement with Swiss armed forces. Of the four systems available, under normal circumstances two systems are operated by staff of the NBC-EOD Centre of Competence (NBC-EOD) for measurement tasks with military character and two systems are assigned to NEOC for the deployment in case of civil emergencies with a radiological component. Since 2018 the scientific report includes as before measuring flights of NEOC (ARM21c) together with measuring flights performed by NBC-EOD (ARM21m).
This report focuses on methodological aspects and thus complements the respective short reports available at `https://www.naz.ch` (ARM21c) and `https://www.vtg.admin.ch/de/organisation/kdo-ausb/lvb-g-rttg-abc/komp-zen-abc-kamir.html` (ARM21m).

1.1 Measuring system RLL

The measuring system RLL (Radiometrie Land-Luft) used both for civil and military measurements consists of a radiation detector with four NaI(Tl) scintillation crystals with a total volume of 16.8 litres, associated photo-multipliers and multichannel analysers (MCA) for low level measurements and one Geiger-Müller tube and associated electronics for high-level dose rate measurements. The spectroscopic measuring chain provides a linear energy calibration of the MCA up to 3 MeV divided into 1024 channels. Detectors, Geiger-Müller tube and associated electronics are installed in an aluminium case with thermal insulation foam. The detection container is mounted in the cargo bay below the centre of the helicopter. The RLL system uses position, air pressure, air temperature and radar altitude data provided by the helicopter via the internal ARINC bus. Figure 1 shows the complete system packaged for storage. The equipment control, data acquisition and storage are performed with a rugged computer working as a data server. Two further rugged redundant client computers are used as operator interface for real-time evaluation, data mapping and communication. All computers are installed in an equipment rack including a battery backed-up power supply. Both operators can operate the system with their associated client computer, display, keyboard and trackball. The additional third central display of the operator's console is mirrored on a screen in the cockpit located between both pilots and is used for information exchange with the pilots and general radiological situation awareness (Figure 2). The measuring system RLL is mounted in an Aerospatiale AS 332 Super Puma helicopter (TH 06) of the Swiss Air Forces (Figure 3). This helicopter has excellent navigation properties and allows emergency operation during bad weather conditions and night time.

Figure 1: Components of the RLL system. 1. Lifting platform for the installation of the detection container. 2. Floor plates and accessories case. 3. Monitors and operator console. 4. Detection container. 5. Operator seats and equipment rack.

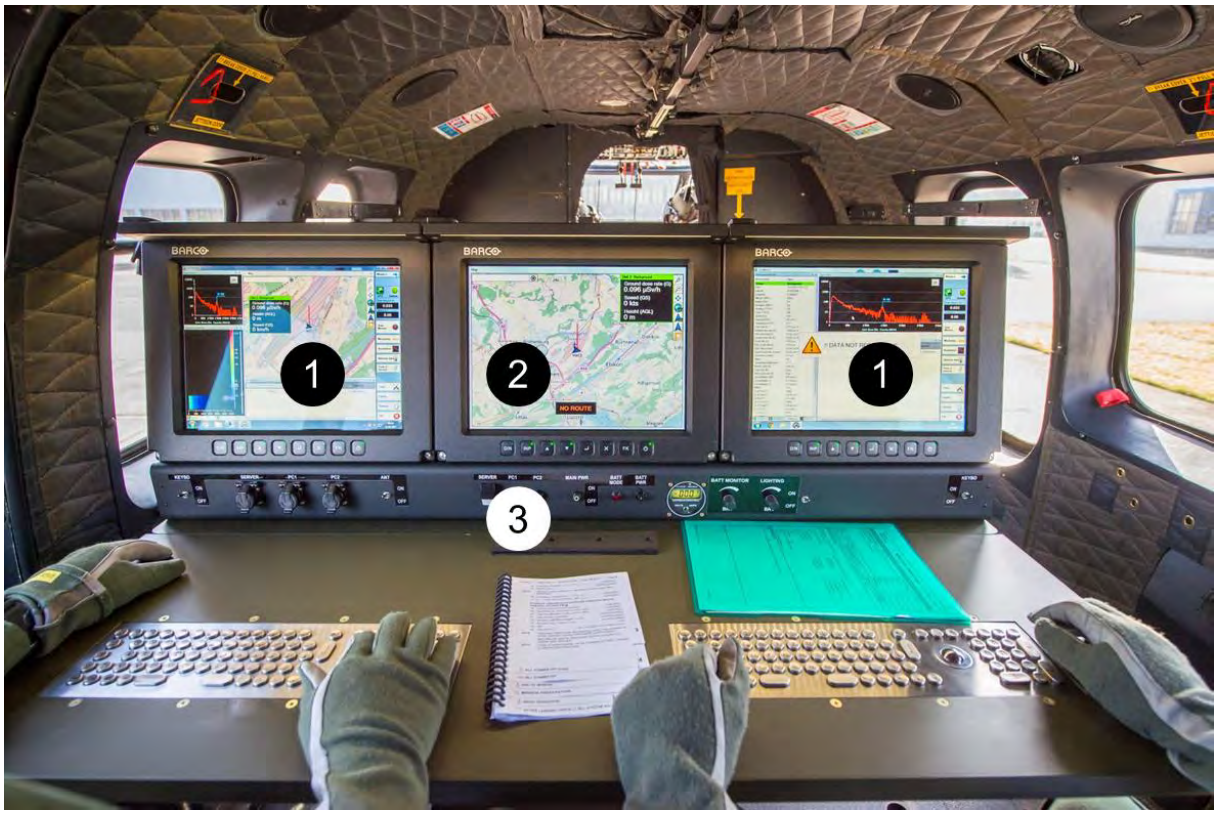

Figure 2: Operator console of the RLL system. 1. Displays of the client computers. 2. Common display (mirrored in the cockpit). 3. Control panel with switches for power, lighting and communication and USB ports for file exchange.

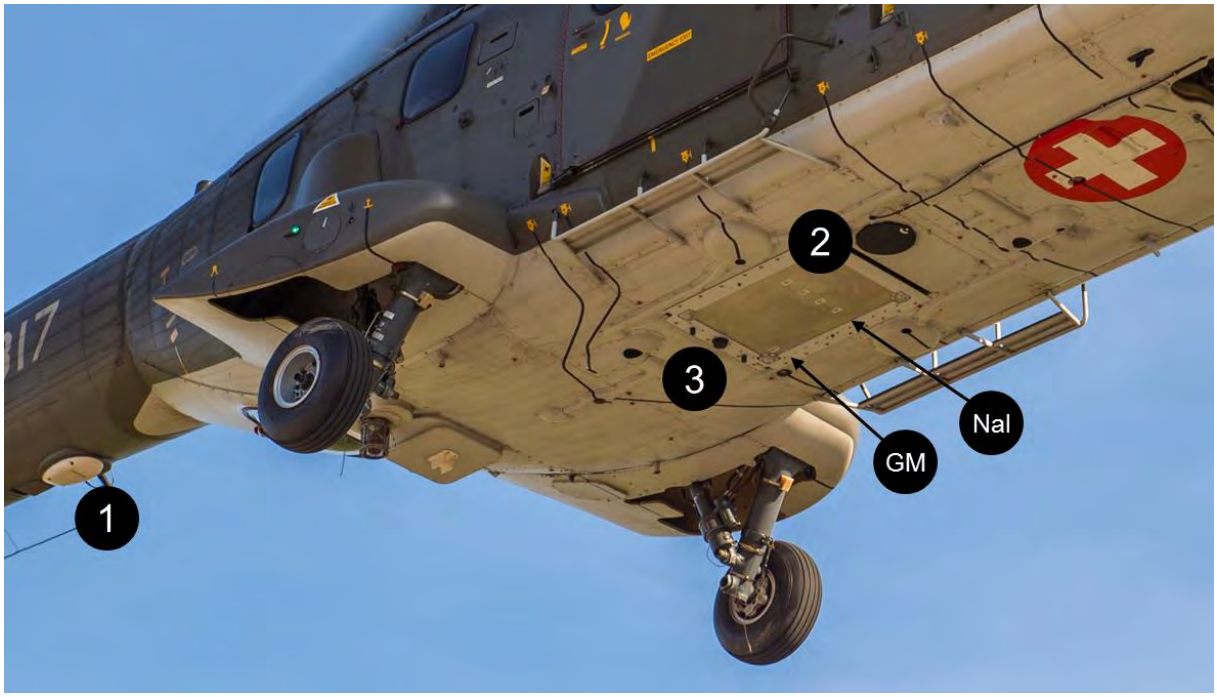

Figure 3: RLL detector mounted in the cargo bay of a Super Puma helicopter. 1. Radar altimeter. 2. Detection container marked with detector reference points. 3. UMTS antenna for data upload.

1.1.1 Quality issues

A quality check of positioning and spectral performance was performed during the exercise according to the procedure described in PSI report 21-01. The flights of exercise part ARM21c were performed with detector RLL001 already used throughout exercise ARM20. The spectral resolution was checked daily and showed good values during the exercise. Exercise part ARM21m was performed with detector RLL004 to test the detector performance during flights. Whereas the spectral resolution of all four crystals at the photon peak at 662 keV of ^{137}Cs was tested sufficient, problems with the automatic energy calibration adjustment of crystal 2 were observed. Figure 4 shows average spectra of three flights measured over the vicinity of Nyon. Whereas the energy calibration of crystals 1, 3 and 4 was adjusted sufficiently to the target value of 3 keV per channel, the automatic adjustment of the energy calibration of crystal 2 was inadequate, best visible for the 2615 keV photon peak of ^{208}Tl. Laboratory measurements with radionuclide sources for the determination of stripping factors performed after ARM21m confirmed this observation. The spectra of crystal 2 of detector RLL004 measured during ARM21m were replaced for the further data evaluation with spectra of crystal 3 according to the procedure described by Butterweck et al. (2018) and the stripping factors were determined accordingly.

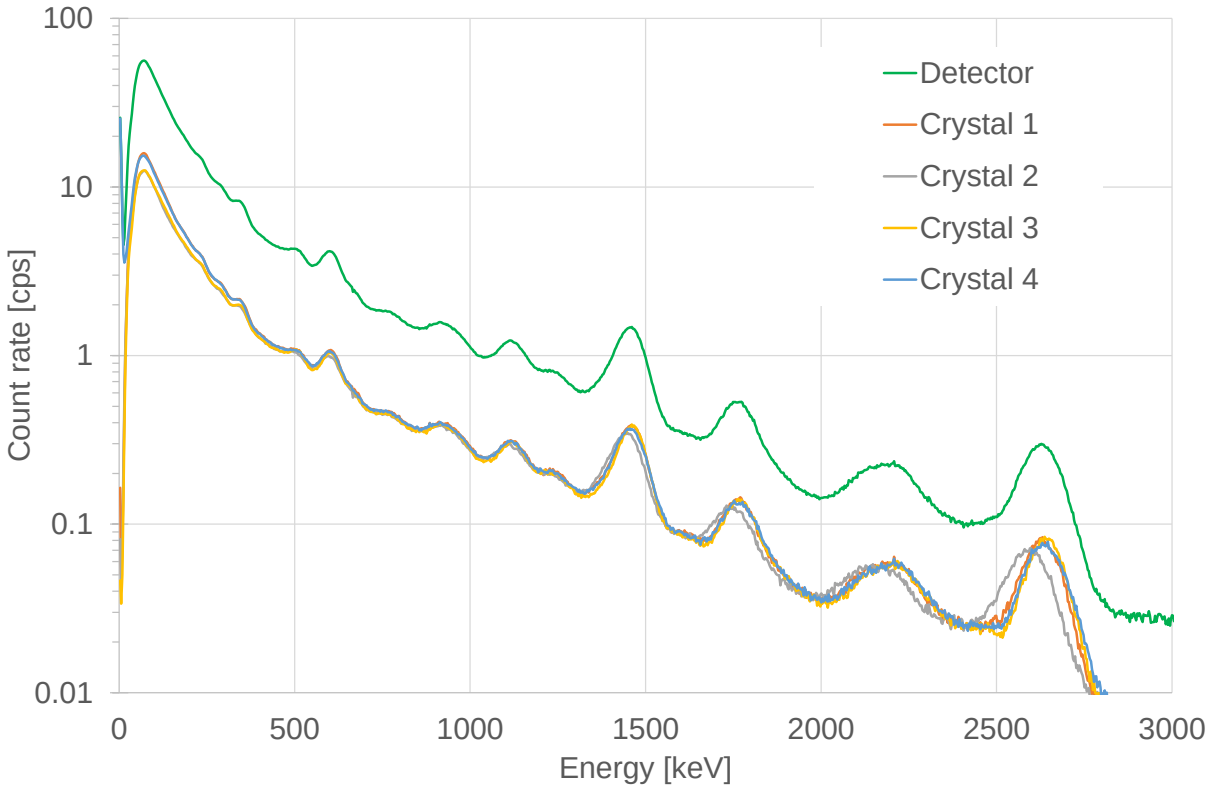

Figure 4: Average spectra of three flights measured over the vicinity of Nyon.

1.2 Measuring flights

The advantage of aeroradiometric measurements lies in the high velocity of measurements in a large area, even over rough terrain. Uniform radiological information of an area is obtained from a regular grid of measuring points. This grid is composed from parallel flight lines which are 100 m to 1000 m apart, depending on the scope of the measurement. The flight altitude above ground is aspired to be constant during the measuring flight. Typical values lie between 50 m and 150 m above ground. The spectra are recorded in regular time intervals of typical one second, yielding integration over 28 m of the flight line at a velocity of 100 km/h.

1.3 Data evaluation

The proprietary software for data acquisition and evaluation provided by the manufacturer of the RLL system was tested sufficient for supplying data to support decisions in radiological emergencies. An outline of the algorithms used can be found in Butterweck et al. (2018). An additional off-line data evaluation software (named AGS_CH) following the methodology developed at ETHZ described in Schwarz (1991) and Bucher (2001) is used to produce the results presented throughout the PSI reports since 2020.

1.3.1 Background and cosmic correction

Both civil and military parts of exercise ARM21 included an altitude profile over Lake Neuchâtel. Figure 5 shows the altitude above sea level along the flight paths. Both altitude profiles had more than 2000 m between lowest and highest altitude and were used together with three already existing altitude profiles to determine the slope of the cosmic correction using Deming regression with δ limited to values above 1 (Table 1) as described in Butterweck et al. (2021). The determination of the uncertainty of the slope derived with Deming regression is not trivial. As the five selected altitude profiles can be assumed to have unknown systematic differences additional to the stochastic variations, the sample standard deviation over the slopes of the five altitude profiles is given in Table 1 as an estimate of uncertainty. The slope averaged over the five available altitude profiles with sufficient altitude range is used in a second step to calculate the background count rates listed in Table 2 for each energy window. The use of unified slopes for all altitude profiles reduces the variation of background count rates. The background count rates are determined annually from flights over extended water bodies near the main measuring areas for the individual detector-helicopter combination. The background and slope for the current exercise are stored under identifiers ISWB_winname and ISWC_winname in the header section of all ERS 2.0 files (Section 6) generated for ARM21 data.

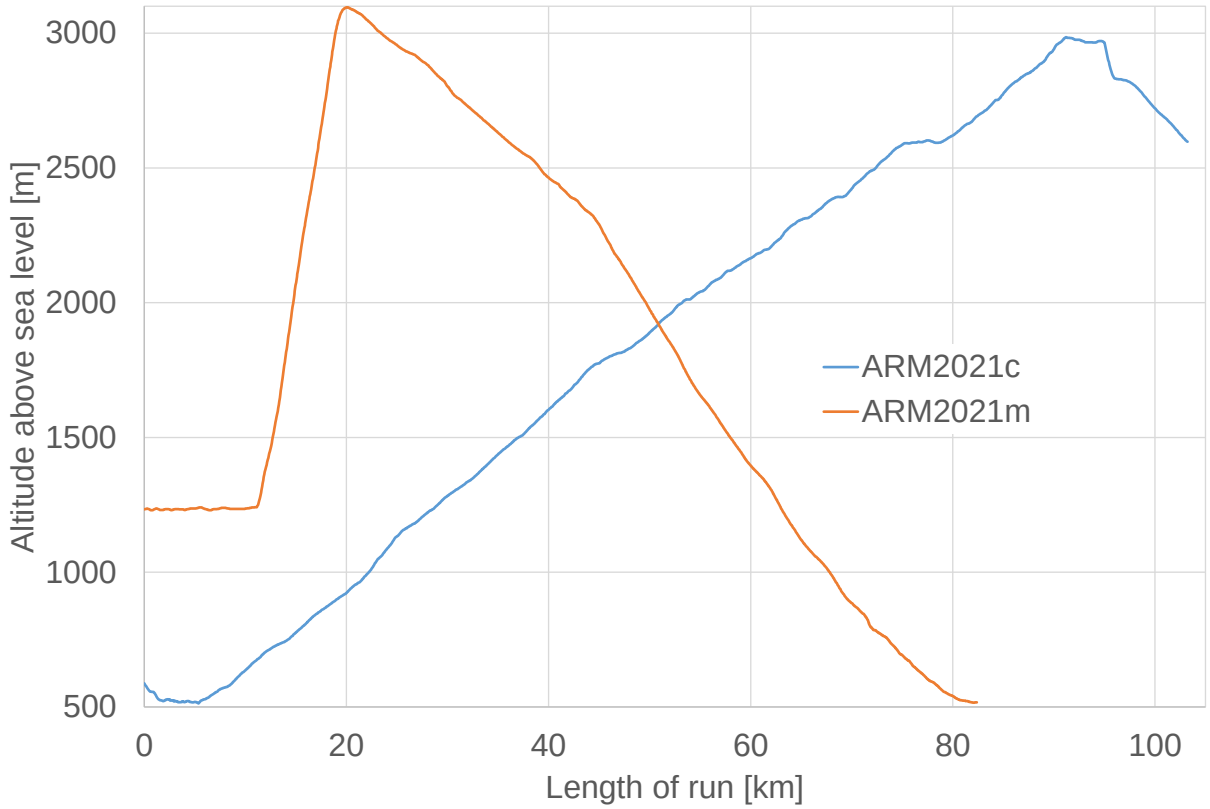

Figure 5: Altitude profiles over Lake Neuchâtel measured during both parts of the exercise. Length of run is the length of the flight path projected to the lake surface including turns.

	Slope of cosmic correction [ ]						
Energy Window	Total	Potassium	Uranium	Thorium	Caesium	Cobalt	SDI
Lake Geneva 2018	5.20	0.28	0.21	0.29	0.45	0.60	3.96
Lake Neuchâtel 2019	5.48	0.31	0.23	0.26	0.60	0.66	4.09
Lake Neuchâtel 2021c	5.68	0.33	0.23	0.29	0.57	0.72	4.28
Lake Neuchâtel 2021m	5.92	0.30	0.24	0.27	0.59	0.60	4.43
Lake Zug 2017	5.96	0.31	0.25	0.29	0.61	0.69	4.31
Average	5.65	0.30	0.23	0.28	0.58	0.65	4.26
Standard deviation	0.32	0.02	0.02	0.02	0.08	0.06	0.23

Table 1: Determination of the average slope for cosmic correction from five altitude profiles.

	Background count rate [cps]						
Energy Window	Total	Potassium	Uranium	Thorium	Caesium	Cobalt	SDI
Lake Geneva 2018	150	11	7	0.7	24	17	103
Lake Neuchâtel 2016	133	8	6	1.6	22	12	90
Lake Neuchâtel 2019	108	9	5	-0.6	18	12	72
Lake Neuchâtel 2021c	125	9	6	0.5	20	12	86
Lake Neuchâtel 2021m	150	10	8	0.9	25	16	101
North Sea 2018	36	5	1	0.1	6	2	23
Lake Thun 2020A	76	6	4	0.0	12	7	50
Lake Thun 2020B	76	6	3	0.0	13	7	50
Lake Zug 2017	60	6	2	0.2	10	5	40

Table 2: Determination of the background count rate using the average slope of cosmic stripping of Table 1

.

1.3.2 Characterisation of spectral cross-talk

Several factors can lead to registering a photon emitted by a radionuclide on or in the ground in an energy window associated with a different radionuclide:

- Photons emitted from the soil are scattered due to the Compton effect in the soil, in buildings, in vegetation, in the air between surface and helicopter and in the detector. The associated energy loss may lead to a registration of the photon in a lower photon energy window.
- The poor energy resolution of a NaI(Tl)-detector compared to modern solid-state detectors can cause photons with energies near the energy limits of a photon energy window to be registered in the adjacent energy window.
- ^{238}U and ^{232}Th are parent radionuclides of complex decay series emitting photons throughout the complete energy spectrum registered by the detector.

The stripping factors between energy windows are determined in the laboratory with point sources in about 1 m distance to the detector. For the natural radionuclides ^{40}K, ^{238}U and ^{232}Th, these values are adjusted for infinite sources measured with 100 m ground clearance according to Schwarz (1991).
The stripping factors for detector RLL001 determined in 2020 were also used for the data evaluation of the ARM21c exercise part. The stripping factors of detector RLL004 were determined with laboratory measurements after the ARM21m exercise part for the configuration with replacement of crystal 2 spectra with crystal 3 spectra (Section 1.1.1). Table 3 shows the resulting stripping factors, which are stored in the header of the respective ERS 2.0 files under identifier ISWS_winname1_winname2 (Section 6).

"'from"'-window	"'to"'-window	Stripping factor	
		RLL001	RLL004
Uranium	Potassium	0.93	0.92
Thorium	Potassium	0.48	0.47
Cobalt	Potassium	0.07	0.04
Thorium	Uranium	0.36	0.34
Uranium	Thorium	0.05	0.05
Potassium	Caesium	0.45	0.37
Uranium	Caesium	3.16	2.78
Thorium	Caesium	1.65	1.44
Cobalt	Caesium	0.15	0.12
Potassium	Cobalt	0.76	0.66
Uranium	Cobalt	2.37	2.26
Thorium	Cobalt	0.68	0.65

Table 3: Stripping factors for relevant energy windows of detectors RLL001 and RLL004.

1.3.3 Calibration

The calibration factors from stripped count rate to activity concentration or dose rate were adjusted lastly in 2020 using a comparison of detector RLL001 with in-situ gamma-spectrometric ground measurements at Thun military training ground Butterweck et al. (2021). During the evaluation of ARM21 data, the relation between the calibration factors for activity per volume and activity per area was revised for the radioisotope ^{137}Cs. The latter quantity is rarely used for routine evaluation of Swiss exercises. After the first determination in 2003, the area calibration factor in Becquerel per square meter was adjusted proportional to applied adjustments of the volume calibration factor in Becquerel per kilogram with a proportionality factor of 17.5 kilogram per square meter. Setting up a relation between activity per volume and activity per area is valid for natural radionuclides, for which assuming a vertically homogeneous distribution in soil and rock is considered appropriate. For the man-made radionuclide ^{137}Cs, mainly deposited in Europe in the wake of the Chernobyl accident, this assumption does not represent the real vertical distribution at all. The vertical distribution of ^{137}Cs was found to follow an exponential decrease with depth (see ICRU Report 53, 1994), according to

$$A_m(\zeta) = A_{m,0}\, e^{-\zeta/\beta} \tag{1.3.1}$$

with:

ζ: Mass per unit area [g/cm²]
$A_{m,0}$: Activity per unit mass at the surface of the soil [Bq/g]
$A_m(\zeta)$: Activity distribution with depth [Bq/g]
β: Relaxation mass per unit area [g/cm²]

The mass per unit area is the integral over the soil density depth profile

$$\zeta = \int_0^z \rho(z')\, dz' \tag{1.3.2}$$

with:

z: Soil depth [cm]
$\rho(z')$: Soil density in depth z' [g/cm³]

Assuming a constant soil density ρ for all relevant soil depths, the mass per unit area for a depth z can be calculated as

$$\zeta(z) = \int_0^z \rho dz' = \rho z \tag{1.3.3}$$

allowing to calculate the contribution of a soil layer A_{S12} between depths z_1 and z_2 to the activity per surface area:

$$A_{S12} = \rho \int_{z_1}^{z_2} A_{m,0} e^{-\rho z'/\beta} dz' = A_{m,0}\beta(e^{-\rho z_1/\beta} - e^{-\rho z_2/\beta}) \tag{1.3.4}$$

The total activity per area A_S integrated over the complete depth profile ($z_1 = 0, z_2 \to \infty$) is

$$A_S = A_{m,0}\beta \tag{1.3.5}$$

and the fraction of activity per area of a soil layer A_{S12} between depths z_1 and z_2 to the total activity per area A_S is calculated to

$$\frac{A_{S12}}{A_S} = e^{-\rho z_1/\beta} - e^{-\rho z_2/\beta} \tag{1.3.6}$$

A analogous calculation to determine A_S for a vertically homogeneous distribution of radionuclides in a slab with infinite depth will yield an infinite activity per area. Thus, an additional step has to be introduced to estimate a relation between activity per soil mass and activity per area. Due to the attenuation of the 662 keV photons emitted by ^{137}Cs in soil, the dose rate in 1 m above ground is limited even for a homogeneous vertical activity concentration. Using the dose rate conversion coefficients published by LeMercier et al. in 2007 and targeting identical dose rate for both exponential and homogeneous vertical activity concentrations, a relation between both models of vertical activity concentration can be established.

$$DR_e = F_e(\beta)A_S = F_h A_M = DR_h \tag{1.3.7}$$

with:

DR_e: Dose rate in 1 m above ground generated by an exponential ^{137}Cs concentration profile [nSv/h]
A_S: Activity per area of an exponential ^{137}Cs concentration profile [Bq/m²]
$F_e(\beta)$: Conversion coefficient between dose rate and activity per area of an exponential ^{137}Cs concentration profile with relaxation mass β [nSv/h per Bq/m²]
A_M: Constant activity per soil mass of a homogeneous ^{137}Cs concentration profile [Bq/kg]
F_h: Conversion coefficient between dose rate and activity per soil mass of a homogeneous ^{137}Cs concentration profile [nSv/h per Bq/kg]
DR_h: Dose rate in 1 m above ground generated by a homogeneous ^{137}Cs concentration [nSv/h]

The stripped counts in the Caesium energy window can be calibrated both to activity per unit mass and activity per area.

$$A_M = CF_M\, CR \tag{1.3.8}$$

with:

A_M: Constant activity per soil mass of a homogeneous ^{137}Cs concentration profile [Bq/kg]
CF_M: Calibration factor of the measured count rate in the Caesium energy window to the activity per soil mass of a homogeneous ^{137}Cs concentration profile [Bq/kg per cps]
CR: Count rate in the Caesium energy window [cps]

$$A_S = CF_S(\beta)\, CR \tag{1.3.9}$$

with:

A_S: Activity per area of an exponential ^{137}Cs concentration profile [Bq/m²]
$CF_S(\beta)$: Calibration factor of the measured count rate in the Caesium energy window to the activity per area of an exponential ^{137}Cs concentration profile with relaxation mass β [Bq/m² per cps]
CR: Count rate in the Caesium energy window [cps]

Assuming further that the photon flux 1 m above ground is proportional to the photon flux at the measuring altitude of airborne gamma spectrometry, a relation between the calibration factors of measured count rate in the Caesium energy window to activity per area of an exponential activity distribution and to activity per soil mass for a homogeneous activity concentration can be generated.
Combining equations 1.3.7, 1.3.8 and 1.3.9 renders the proportionality between both calibration factors

$$\frac{CF_S(\beta)}{CF_M} = \frac{F_h}{F_e(\beta)} \tag{1.3.10}$$

The procedure to determine both calibration factors is summarised in the following list:

1. Determine CF_M with in-situ gamma-spectrometric ground measurements calibrated for homogeneous activity distribution
2. Determine β from activity profile measurements in soil samples using equation 1.3.6
3. Interpolate according dose rate conversion coefficient from table in LeMercier et al., 2007
4. Calculate $CF_S(\beta)$ using equation 1.3.10

Step 1 of the procedure was already performed during ARM20 resulting in $CF_M = 1.02$ Bq/kg per cps. For step 2, the average activity concentrations of soil samples in Canton Ticino published by Togni, et al. in 2016 were used. Table 4 shows the average activity concentrations of soil layers with 5 cm thickness measured in Canton Ticino. The relative contributions of the soil layers were compared to the relative activity concentrations according to equation 1.3.6 for different values of β normalised to 100% in the upper 25 cm of soil. A value of

β = 9.5 g/cm² rendered the smallest squared deviation between measured and calculated values. This values agrees with values published for aged caesium depositions (Table 3.5, ICRU, 1994). A linear interpolation of the values published by LeMercier et al., 2007 yields F_h = 0.221 nSv/h per Bq/kg for the homogeneous ^{137}Cs activity concentration and $F_e(9.5)$ = 0.00112 nSv/h per Bq/m². Using equation 1.3.10, the ratio of calibration factors can be calculated to 197 kg/m², resulting in a calibration factor of 201 Bq/m² per cps. These values differ massively from the values used in the past (17.5 kg/m² and 17.8 Bq/m² per cps for a surface contamination (β = 0)). Some of the differences can be attributed to different assumptions used in the procedure outlined above. Nevertheless, the effect of different assumptions does not support the magnitude of difference observed, making a scale error in past estimations of the calibration factor for activity per area most likely. The revised calibration factor for activity per area was implemented into the calibration section of the ERS files for all RLL detectors (Table 5).

Layer	^{137}Cs activity	Relative contribution	
	concentration [Bq/kg]	Measured	Exponential ($\beta = 9.5$ [g/cm²])
0 - 5 cm	289	56.9%	57.8%
5 - 10 cm	137	27.0%	24.9%
10 - 15 cm	54	10.6%	10.7%
15 - 20 cm	20	3.9%	4.6%
20 - 25 cm	8	1.6%	2.0%

Table 4: Average ^{137}Cs activity concentrations in soil samples of Canton Ticino.

Quantity	Nuclide	ERS2.0 Identifier	Value	Unit
Activity per wet weight	^{40}K	ISWA_AW_K-40	5.58	Bq/kg per cps
Activity per wet weight	^{238}U	ISWA_AW_U-238	3.57	Bq/kg per cps
Activity per wet weight	^{232}Th	ISWA_AW_Th-232	1.22	Bq/kg per cps
Activity per wet weight	^{137}Cs	ISWA_AW_Cs-137	1.02	Bq/kg per cps
Activity per area	^{137}Cs	ISWA_AA_Cs-137	201	Bq/m^2 per cps
Source activity	^{137}Cs	ISWA_AP_Cs-137	2511000	Bq per cps
Source activity	^{60}Co	ISWA_AP_Co-60	1505000	Bq per cps
Dose rate dH*(10)/dt	Total (SDI)	ISD_SDI	5.65E-08	µSv/h per cps keV
Dose rate dH*(10)/dt	^{40}K	ISWD_K-40	0.000289	µSv/h per cps
Dose rate dH*(10)/dt	^{238}U	ISWD_U-238	0.00197	µSv/h per cps
Dose rate dH*(10)/dt	^{232}Th	ISWD_Th-232	0.000917	µSv/h per cps
Dose rate dH*(10)/dt	^{137}Cs	ISWD_Cs-137	0.000191	µSv/h per cps

Table 5: Conversion factors used in the data evaluation.

As the model of a vertical homogeneous ^{137}Cs activity distribution is unrealistic, correction factors for the comparison with samples of different soil layers were estimated based on an exponential distribution with β = 9.5 g/cm² = 95 kg/m². Using the ratio of calibration factors of 197 kg/m² derived above, the activity per unit area A_S can be associated with A_M using

equation 1.3.5. Inserting equation 1.3.5 into equation 1.3.4 and dividing by the layer mass per unit area $\rho(z_2 - z_1)$ calculates the average activity per unit mass of the soil layer A_{M12}:

$$A_{M12} = \frac{A_{S12}}{\rho(z_2 - z_1)} = \frac{A_S(e^{-\rho z_1/\beta} - e^{-\rho z_2/\beta})}{\rho(z_2 - z_1)} = \frac{197 A_M(e^{-\rho z_1/\beta} - e^{-\rho z_2/\beta})}{\rho(z_2 - z_1)} = F_{he} A_M \tag{1.3.11}$$

with:

A_{M12}: Average activity per soil mass of a soil layer [Bq/kg]
F_{he}: Correction factor from vertically homogeneous activity concentration to the average activity concentration in a soil layer of an exponential profile [ ]

Table 6 repeats the average activity concentrations measured in soil layers of Canton Ticino of Table 4 together with correction factors F_{he}, based on the assumption of a constant soil density of 1.6 g/cm³. The activities per unit mass A_M of a vertically homogeneous activity profile were calculated by dividing the measured activity concentrations by the correction factor, rendering roughly constant estimates of the activity per unit mass of a homogeneous activity profile with an average of 197 Bq/kg.

Layer	^{137}Cs activity concentration [Bq/kg]	F_{he} [ ]	A_M [Bq/kg])
0 - 5 cm	289	1.402	206
5 - 10 cm	137	0.604	227
10 - 15 cm	54	0.260	208
15 - 20 cm	20	0.112	178
20 - 25 cm	8	0.048	166

Table 6: Factor to transfer ^{137}Cs activity concentrations between soil samples and a vertically homogeneous activity distribution.

1.4 Data presentation

Brief reports of the measurement results are compiled by the respective measurement teams and published immediately after the end of the exercise on the homepage of NEOC and the homepage of NBC-EOD Centre of Competence. These reports are archived at `https://far.ensi.ch`.
A combined detailed analysis of both parts of the exercise is published in the form of a PSI-report within the responsibility of the FAR. These reports are also archived at `https://far.ensi.ch`.
For all measuring areas, a map of the total dose rate (measuring quantity dH*(10)/dt extrapolated to 1 m above ground) and the flight lines is presented together with a map of the Man-Made-Gross-Count (MMGC) ratio. A map of the ^{232}Th activity concentration (measuring quantity activity per wet mass) yields quality information as it can be expected that this quantity is constant over time. As an additional quality measure, an appendix with the basic parameters of the data evaluation is added to simplify a re-evaluation of the data in the future. If the MMGC-ratio indicates elevated values, maps of individual radionuclides are added based on the average photon spectrum over the affected area. In the case of large changes of topography in the measured area, a map of the terrestrial dose rate consisting of the total dose rate reduced by the altitude dependent cosmic component is included. In the case of measuring flights with the main purpose of mapping natural radionuclide concentrations, a supplementary map of the ^{40}K activity concentration (measuring quantity activity per wet mass) may also be presented.
A discrete colour scale was defined by the Swiss Expert Group for Aeroradiometrics (FAR) in 2019. The colours and their representation as red, green and blue (RGB) values are listed in Table 7 together with the represented ranges of measured values. The unit of dose rates used in previous reports, $[$nSv/h$]$, was changed with the new representation to $[\mu$Sv/h$]$, the unit used to store dose rate values in the ERS 2.0 format (Butterweck et al. (2018)).
An additional colour scale for maps of the activity per area measured in kilo-Becquerel per square meter was added in this report. For better comparability with maps of the activity per unit mass measured in Bq/kg, a conversion factor from activity per volume to activity per area of 0.2 kBq/m² per Bq/kg was assumed based on an exponential decrease of ^{137}Cs with soil depth and a relaxation mass β = 9.5 g/cm² (Section 1.3.3).

Colour	Red	Green	Blue	Dose rate [μSv/h]	MMGC-ratio [ ]	Activity per mass [Bq/kg] ^{40}K	Activity per mass [Bq/kg] ^{238}U, ^{232}Th, ^{137}Cs	Activity per area [kBq/m^2] ^{137}Cs (β=9.5 g/cm^2)
	153	0	153	> 10	> 100	> 10000	> 5000	> 1000
	204	0	102	5 - 10	50 - 100	5000 - 10000	1000 - 5000	200 - 1000
	204	0	0	2 - 5	15 - 50	2000 - 5000	500 - 1000	100 - 200
	255	0	0	0.5 - 2	9 - 15	1500 - 2000	250 - 500	50 - 100
	255	176	51	0.3 - 0.5	8 - 9	1000 - 1500	200 - 250	40 - 50
	255	235	51	0.2 - 0.3	7 - 8	800 - 1000	150 - 200	30 - 40
	230	255	128	0.15 - 0.2	unused	600 - 800	100 - 150	20 - 30
	173	255	153	0.1 - 0.15	unused	400 - 600	75 - 100	15 - 20
	073	255	106	0.08 - 0.1	6 - 7	200 - 400	50 - 75	10 - 15
	102	255	255	0.06 - 0.08	5 - 6	100 - 200	25 - 50	5 - 10
	77	148	255	0.04 - 0.06	unused	50 - 100	12.5 - 25	2.5 - 5
	51	102	179	< 0.04	< 5	< 50	< 12.5	< 2.5

Table 7: Quantification of the colour scale.

2 Results of the exercise ARM21

The flights of the civil part ARM21c of the exercise were performed between June 28th and July 2nd and the flights of the military part ARM21m were performed between August 30th and September 2nd, 2021. Both parts of the exercise included the measurement of an altitude profile over Lake Neuchâtel with sufficient altitude range to determine the slope of the altitude dependent cosmic correction (Section 1.3.1).
According to the alternating schedule of the annual ARM exercises, the environs of the nuclear power plants Gösgen (KKG) and Mühleberg (KKM), the latter under ongoing decommissioning, were surveyed in ARM21c.
Background measurements over Swiss towns were continued with measurements over Frauenfeld, Lugano, Nyon and Wil.
Several regions in southern and western Switzerland with reported ^{137}Cs deposition in the wake of the Chernobyl accident in 1986 were measured to determine the residue of the deposited activity.
Two transverses were measured over central Switzerland to expand airborne gamma-spectrometry coverage of Switzerland.
Flight velocity of the Super Puma helicopters of the Swiss Air Force was around 30 m/s with a target ground clearance of 90 m for all measuring flights. The counting interval of the spectra was one second.
Personnel of the military units Stab BR NAZ and ABC Abwehr Einsatzkompanie performed the measurements supported by experts from ENSI, PSI, ETHZ, NBC-EOD Centre of Competence and NEOC.
Flight parameters of the measuring flights are listed in Table 8 and an overview of the according flight lines is shown in Figure 6.

Location	Flight number	Measuring time [s]	Length of run [km]	Area [km^2]
		ARM21c		
Lake Neuchâtel	Heli 1_20210628 1341	1826	82	-
KKM	Heli 1_20210628 0931	8124	411	98
KKG	Heli 1_20210629 0836	6393	287	67
Extended area KKG	Heli 1_20210629 1036 Heli 1_20210701 1347	10648	540	477
Frauenfeld	Heli 1_20210701	1573	62	15
Lugano	Heli 1_20210630 0942 Heli 1_20210630 1112	5573	226	50
Wil	Heli 1_20210701	2066	77	18
Balerna	Heli 1_20210630 0935	524	17	3
Demanio	Heli 1_20210630 1343	440	15	3
Lodrino	Heli 1_20210630 1408	369	11	2
Monti di Paudo	Heli 1_20210630 1357	306	7	1
Ronchini	Heli 1_20210630 1330	402	13	1
Stabio	Heli 1_20210630 0924	456	14	2
Transverses	Heli 1_20210702 0910	8514	371	-
		ARM21m		
Lake Neuchâtel	Heli 4_20210902 1110	2064	103	-
Nyon	Heli 4_20210902 1350 Heli 4_20210903 0850 Heli 4_20210903 1345	22451	1022	239
Joux	Heli 4_20210830 0910 Heli 4_20210830 1350 Heli 4_20210901 1350 Heli 4_20210902 0840	35258	1694	414

Table 8: Flight data of ARM21.

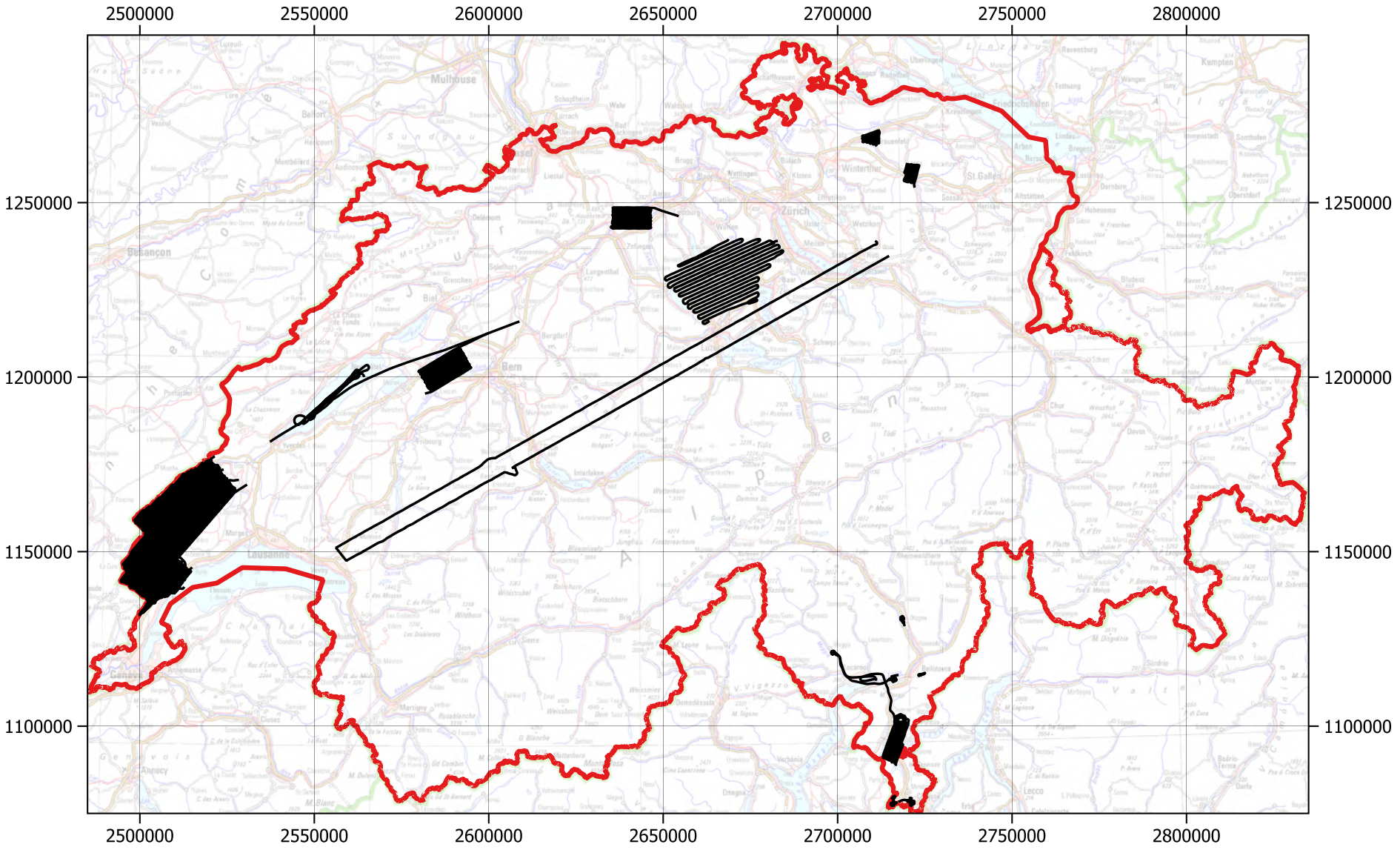

Figure 6: Overview of the measurement areas of ARM21. Geodaten©swisstopo.

2.1 Nuclear power plant Mühleberg (KKM)

The nuclear power plant Mühleberg (KKM), under decommissioning since 2019, was inspected during ARM21c following a bi-annual schedule introduced in 1994. The map of dose rate dH*(10)/dt one meter above ground (Figure 7) shows elevated values over the plant premises. The map of the MMGC-Ratio indicates man-made radionuclides as source of the elevated dose rate (Figure 8). The spectrum over the region with elevated dose rate and MMGC-ratio in comparison to a background spectrum outside of the plant premises clearly identifies the radionuclide ^{60}Co (Figure 9). During decommissioning, activated components are disassembled, removed from the well shielded reactor building and processed on the plant site. Due to the reduced shielding, the photon emissions of these components can be detected from above. No elevated readings outside of the plant premises were noticed. The map of the naturally occurring radionuclide ^{232}Th (Figure 10) used as an additional quality indicator displays the spatial distribution of the radionuclide and the absorbing effect of water layers on terrestrial photon emissions.

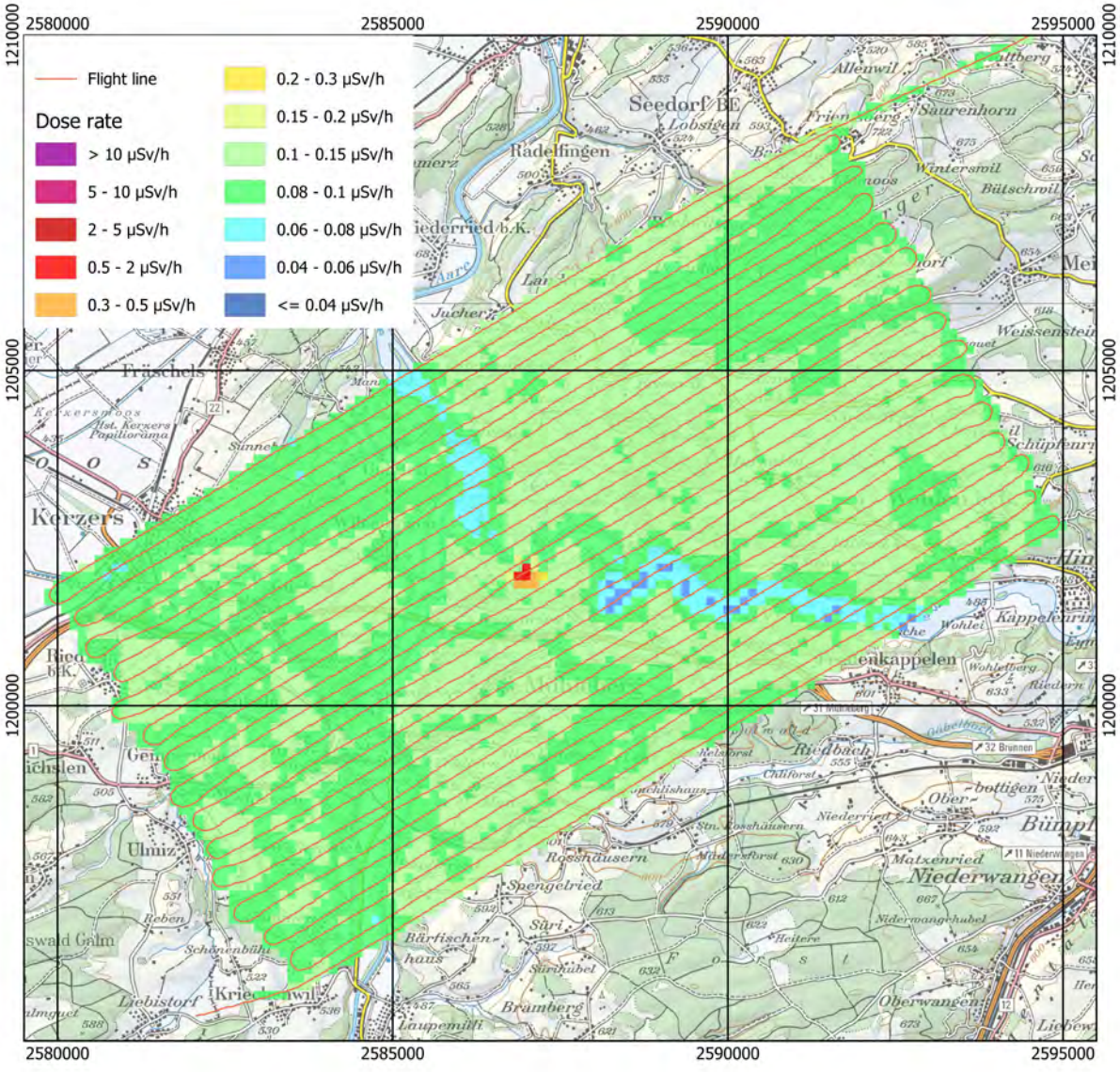

Figure 7: Dose rate over the environs of nuclear power plant Mühleberg (KKM). Geodaten©swisstopo.

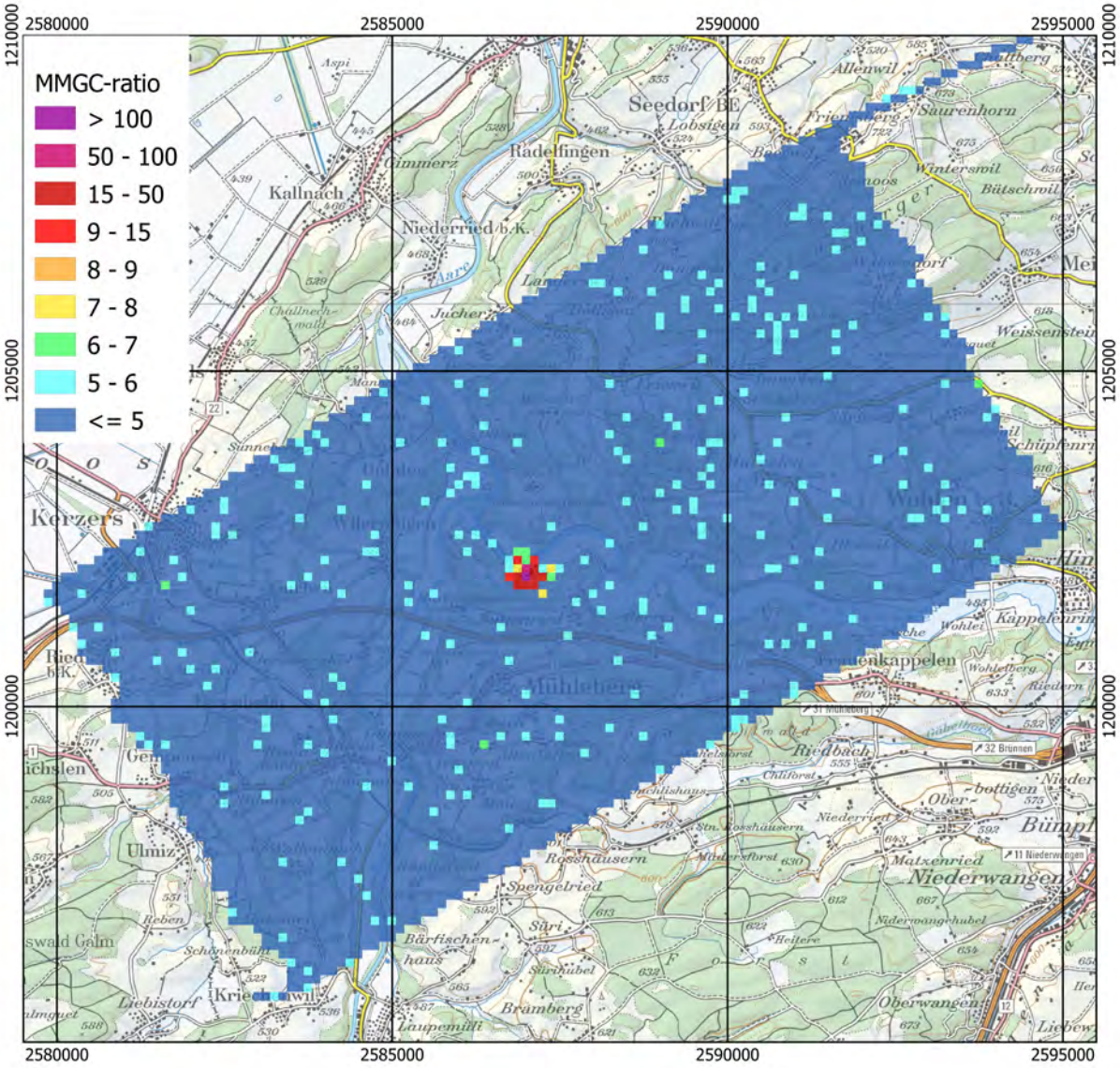

Figure 8: Man-made gross count (MMGC) ratio over the environs of nuclear power plant Mühleberg (KKM). Geodaten©swisstopo.

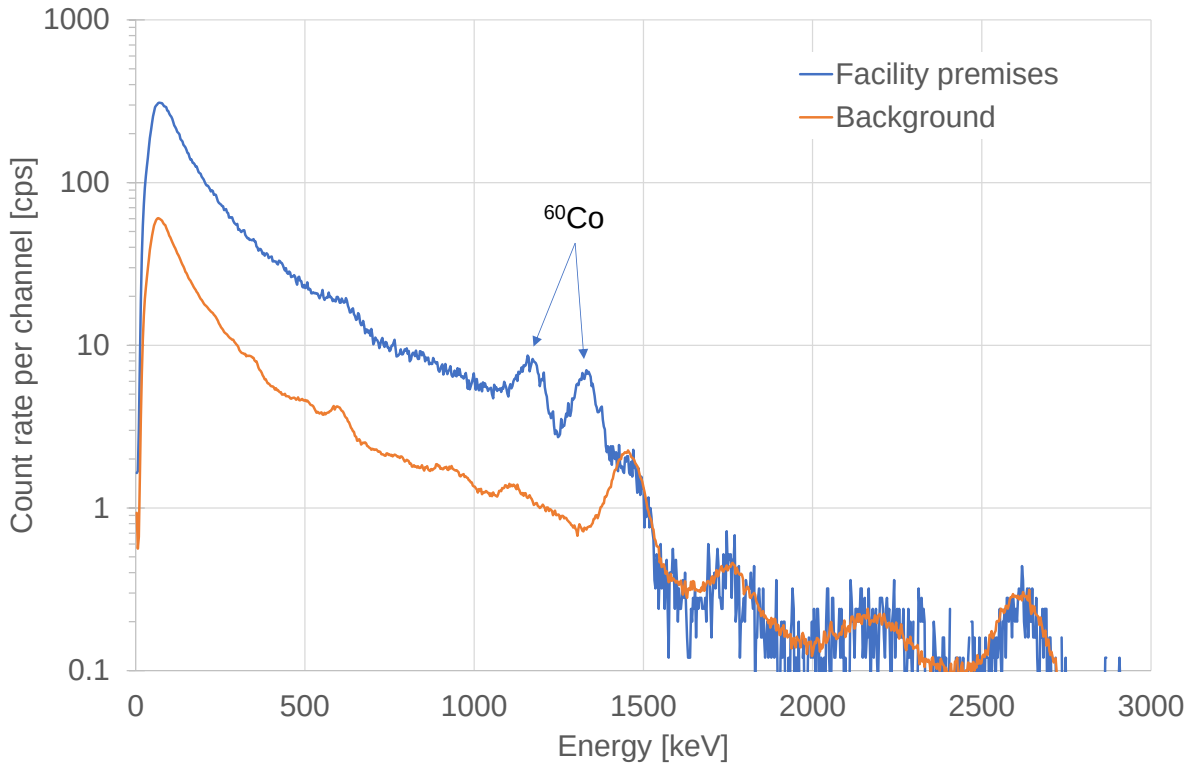

Figure 9: Photon spectrum over nuclear power plant Mühleberg (KKM) in comparison to the background outside of the plant premises.

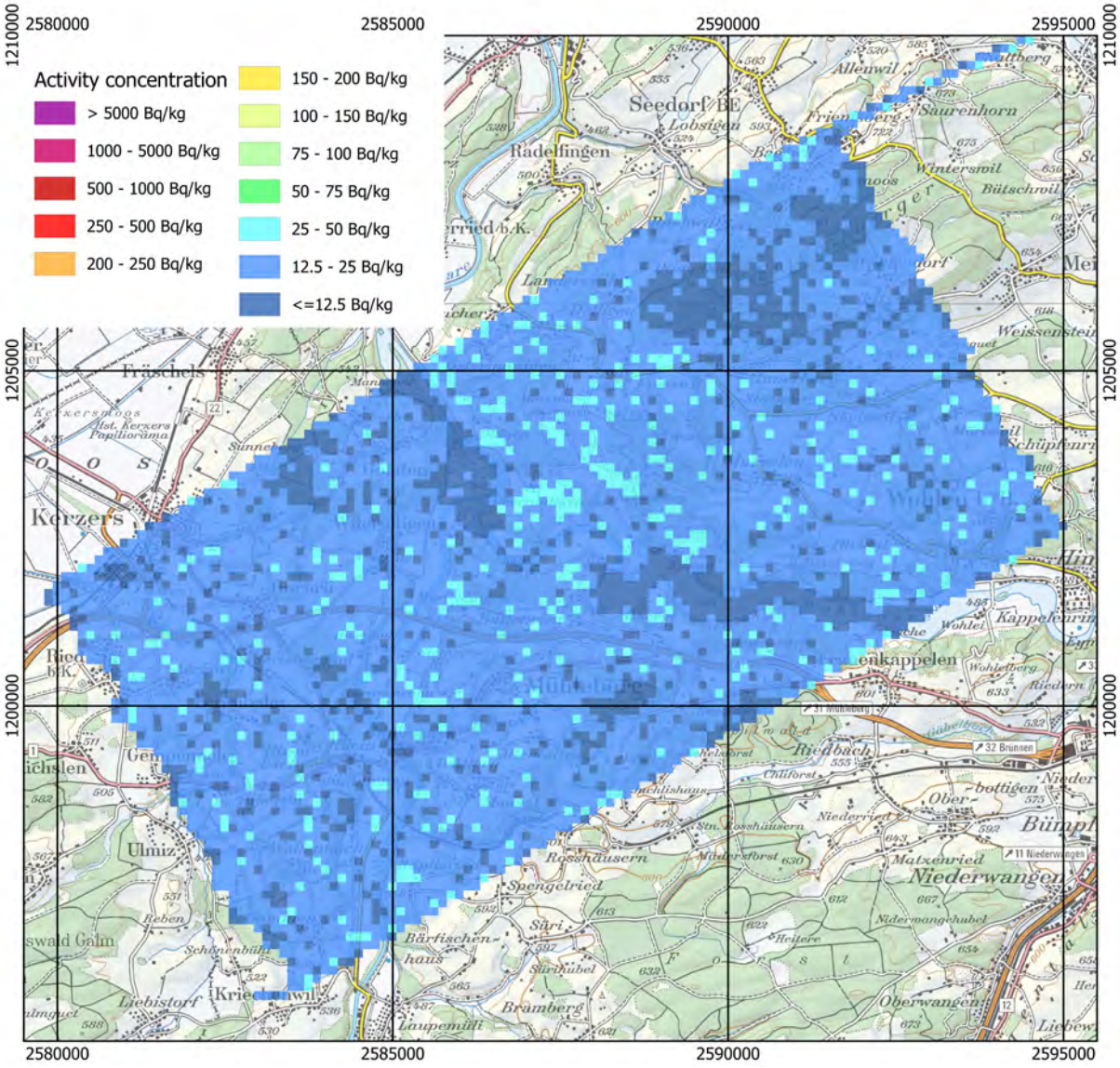

Figure 10: ^{232}Th activity concentration measured over the vicinity of nuclear power plant Mühleberg (KKM). Geodaten©swisstopo.

2.2 Nuclear power plant Gösgen (KKG)

Following the biannual measurement schedule of the Swiss nuclear installations, the vicinity of the nuclear power plant Gösgen (KKG) was inspected during ARM21c. At the pressurised water reactor of KKG, activated water is confined to the well shielded reactor building, rendering the power plant unobtrusive in maps of dose rate (Figure 11) and MMGC-ratio (Figure 12). The map of the naturally occurring radionuclide ^{232}Th activity concentration (Figure 13) used as an additional quality indicator displays the spatial distribution of the radionuclide and the absorbing effect of water layers on terrestrial photon emissions.
The long term goal to map an extended area up to 50 km around KKG was advanced with a sector to the south-east of KKG. The maps of dose rate (Figure 14) and ^{232}Th activity concentration (Figure 15) show typical values for northern Switzerland. The map of MMGC-ratio (Figure 16) yields no indication for the presence of man-made radionuclides in the area measured.

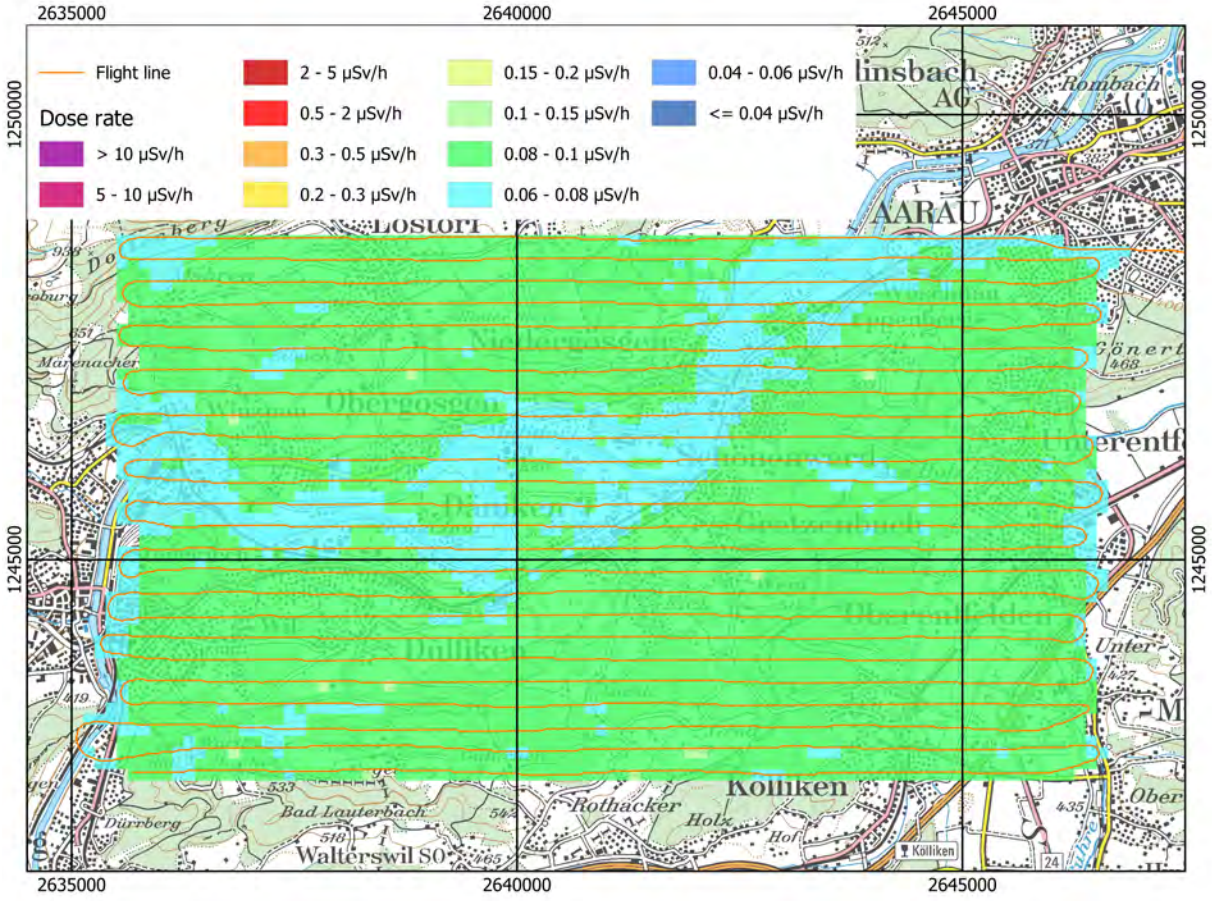

Figure 11: Dose rate over the environs of nuclear power plant Gösgen (KKG). Geodaten©swisstopo.

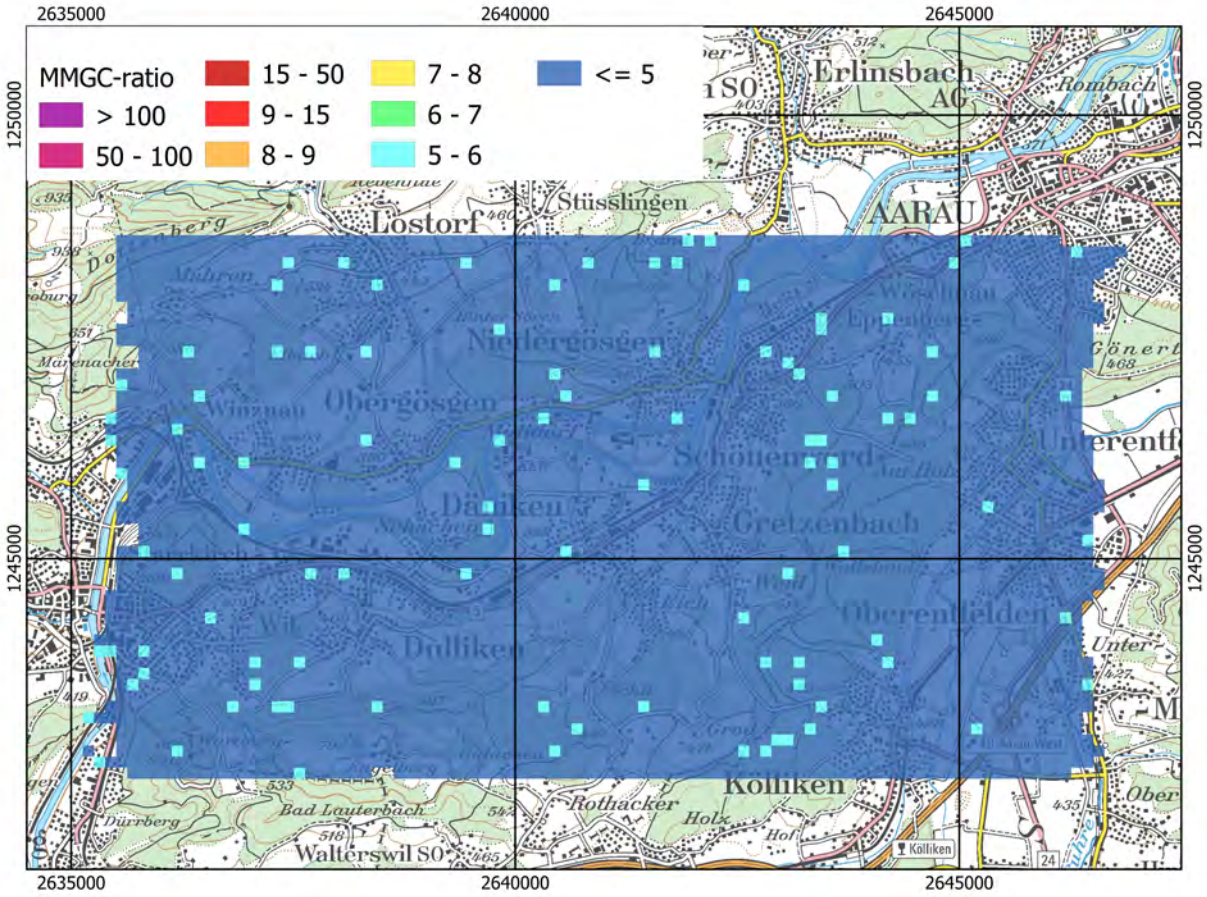

Figure 12: Man-made gross count (MMGC) ratio over the environs of nuclear power plant Gösgen (KKG). Geodaten©swisstopo.

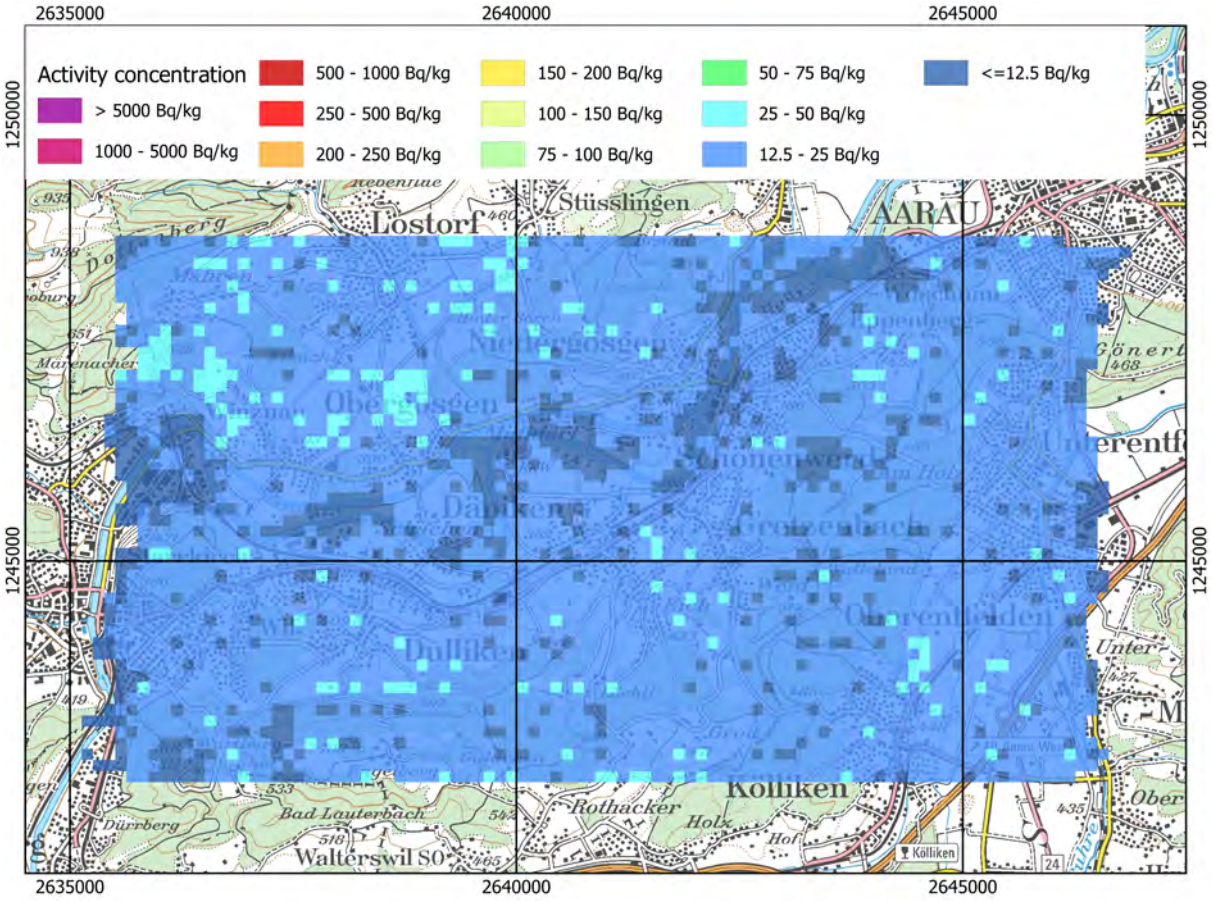

Figure 13: ^{232}Th activity concentration measured over the vicinity of nuclear power plant Gösgen (KKG). Geodaten©swisstopo.

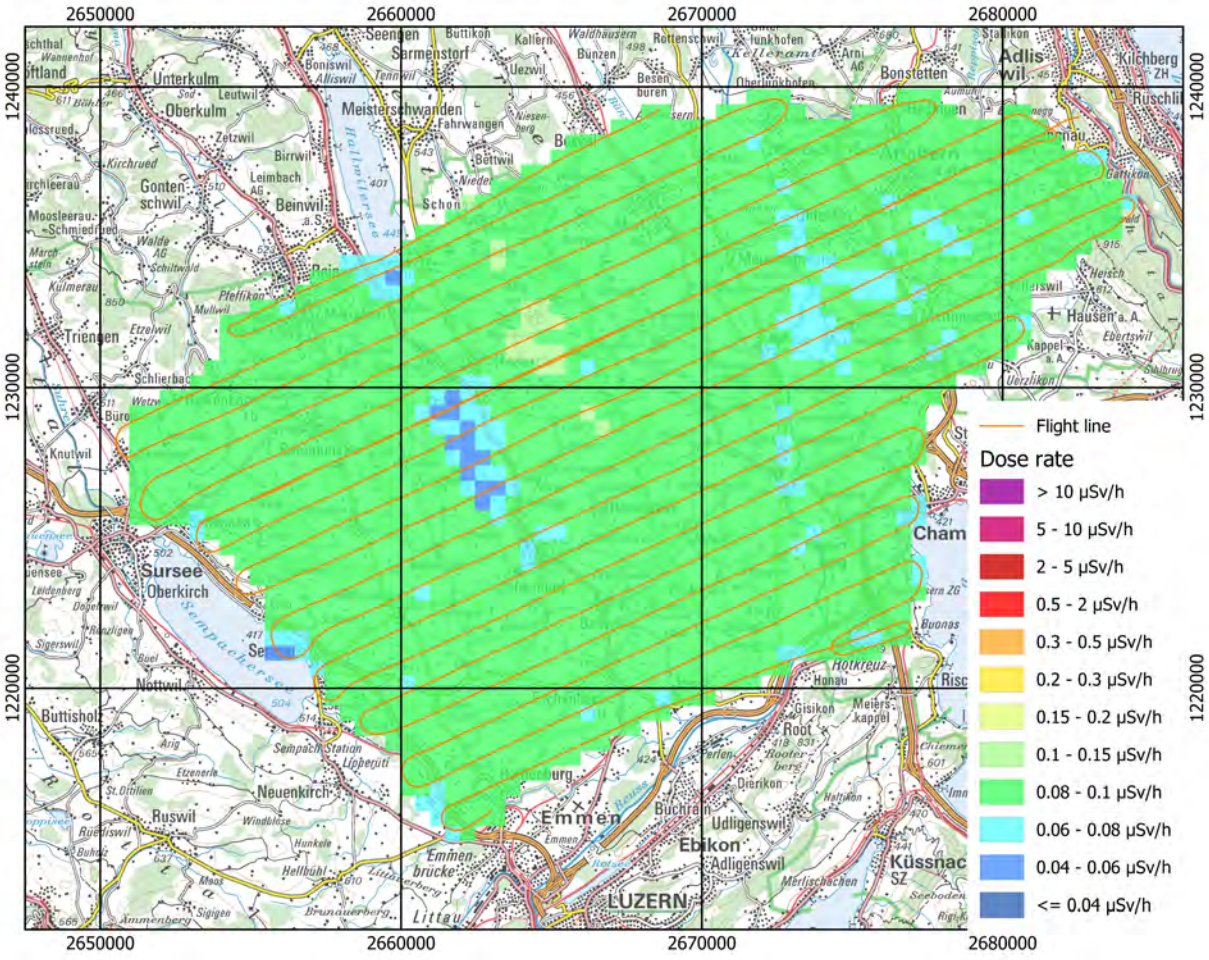

Figure 14: Dose rate over the extended vicinity of nuclear power plant Gösgen (KKG). Geodaten©swisstopo.

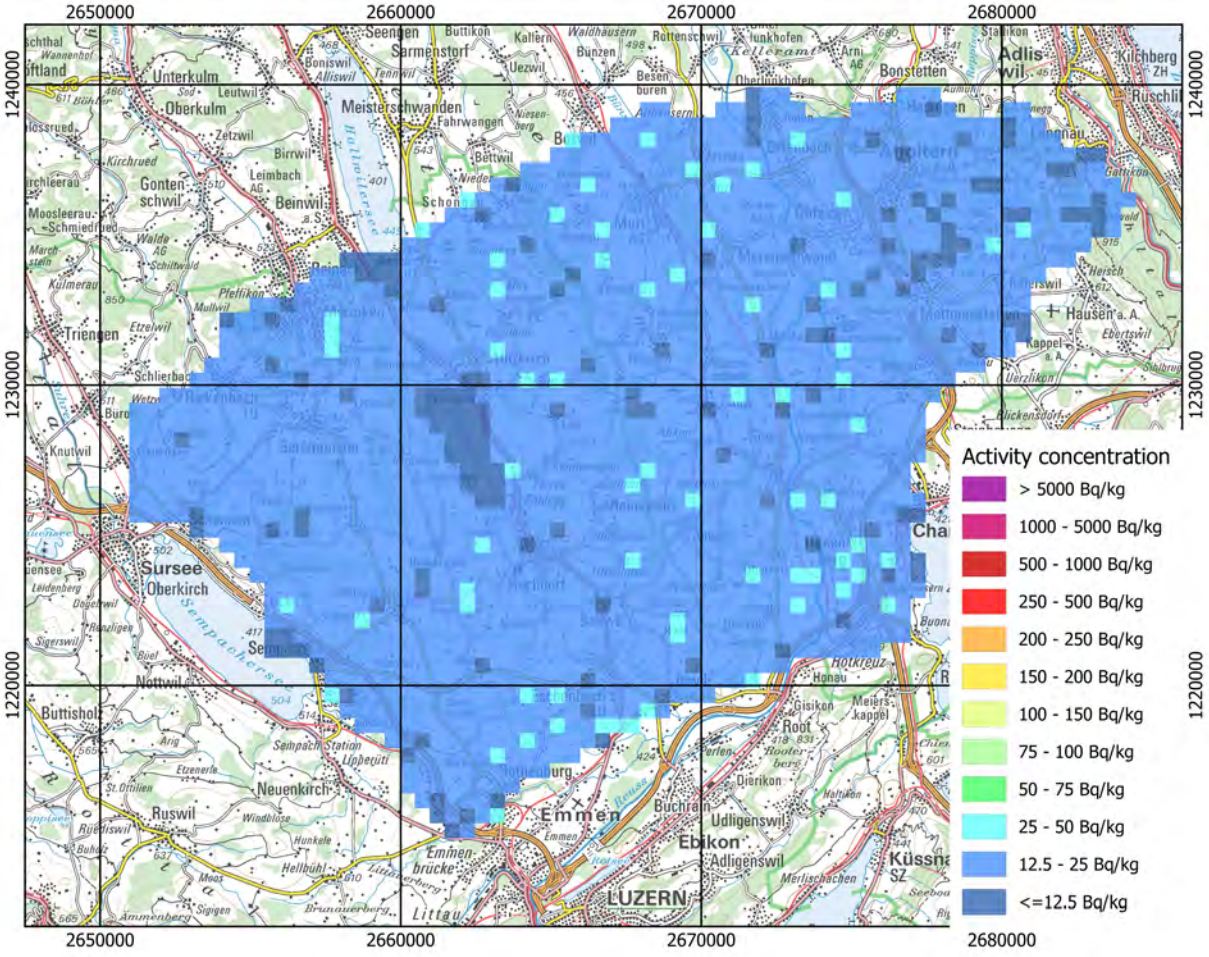

Figure 15: ^{232}Th activity concentration measured over the extended vicinity of nuclear power plant Gösgen (KKG). Geodaten©swisstopo.

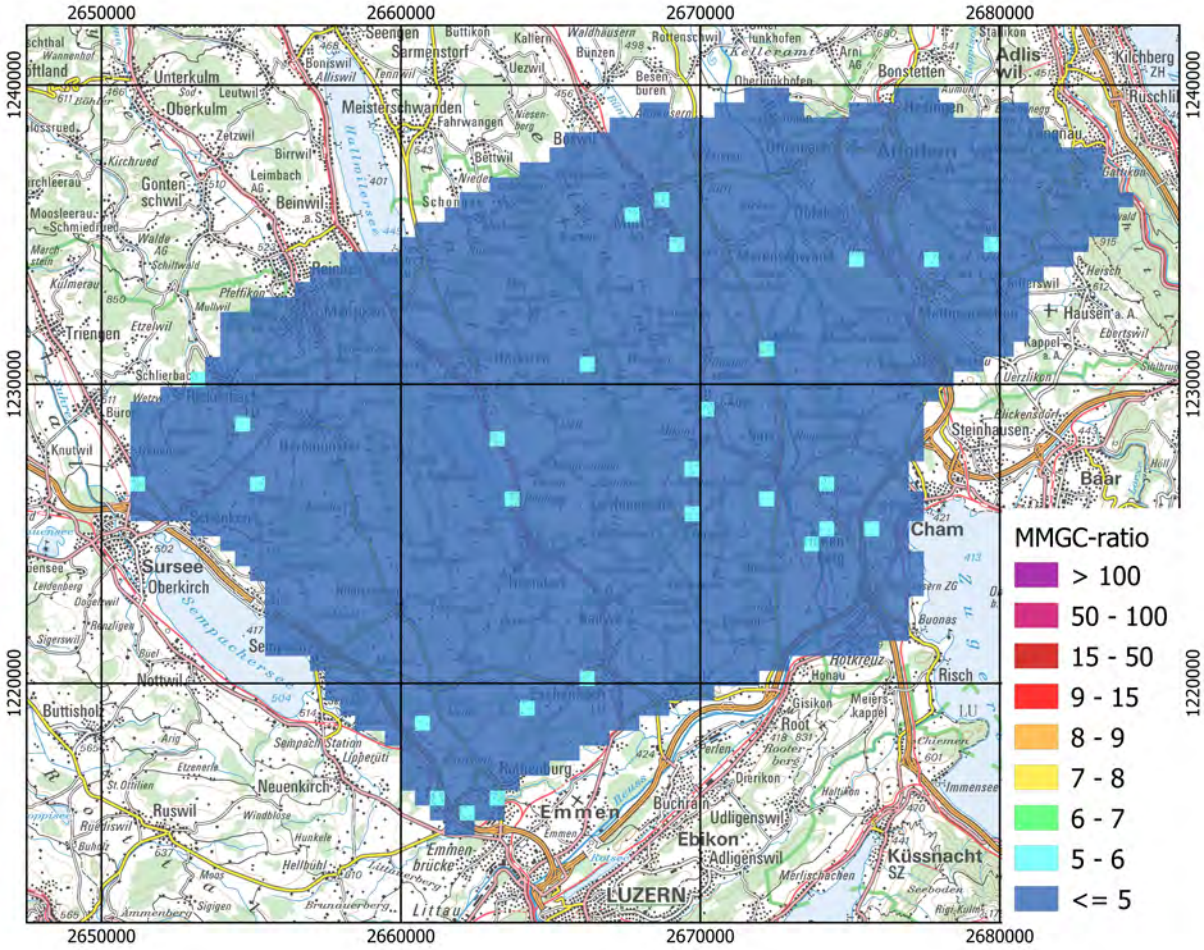

Figure 16: Man-made gross count (MMGC) ratio over the extended vicinity of nuclear power plant Gösgen (KKG). Geodaten©swisstopo.

2.3 Frauenfeld, Lugano, Nyon and Wil

The series of radiological background measurements over Swiss cities was complemented throughout Switzerland with measurements over Frauenfeld, Lugano, Nyon and Wil.
The maps of the dose rate around Frauenfeld and Wil (Figures 17 and 36) show typical values for northern Switzerland. The maps of the MMGC-ratio (Figures 18 and 37) as indicator for man-made radionuclides do not suggest the presence of man-made radionudlides in these areas. Some points with slightly elevated MMGC-ratios can be associated with low values of ^{232}Th activity concentration (Figures 19 and 38). Low ^{232}Th concentrations bias the man-made-gross-count (MMGC) ratio toward higher values indicated for example by few cells in the MMGC-ratio range between 6 and 7 (Figure 37).
The dose rate map over Lugano (Figure 20) depicts homogeneous values over the measurement area and lower values over Lake Lugano, where photons from terrestrial radionuclides are attenuated by the water layer. This apparent spatial homogeneity is partly associated with the discrete colour scale introduced in 2019 (Section 1.4). The total dose rate can be separated in a contribution from cosmic radiation (for this area rather constant) and a terrestrial component caused by natural radionuclides in soil and rock. Spatial structures undetected in the total dose rate become visible in the map of the terrestrial dose rate (Figure 21), as the lower average of terrestrial dose rate is depicted with smaller increments between colour changes. The map of the MMGC-ratio (Figure 22) yields no clear indication on man-made radionuclides. The map of the natural radionuclide ^{232}Th does not display distinctly higher values in the region of the elevated dose rate. As southern Switzerland had some deposition of Chernobyl ^{137}Cs, the according map was analysed (Figure 24). Elevated ^{137}Cs activity concentrations can be observed in forests to the north and south of the measuring area. Figure 27 shows a clear indication of the 662 keV photon peak of ^{137}Cs in the spectrum over the northern area with elevated activity concentrations. Nevertheless, this area does not coincide with the area of elevated terrestrial dose rates (Figure 21). The activity concentration map of the natural radionuclide ^{40}K (Figure 26) reveals that the elevated terrestrial dose rate is caused by a superposition of elevated Caesium and Potassium concentrations. As the concentrations of both man-made and natural radionuclides are elevated, the effect cancels out in the MMGC-ratio. The measured^{137}Cs activity concentration is depicted in Figure 24 and the baseline map (see section 2.4.1) drawn in Figure 25 as comparison.
The spatial distribution of total dose rate in the region between Nyon at Lake Geneva (Figure 28) and the border to France is similar uniform as observed over Lugano. The separation into cosmic (Figure 29) and terrestrial (Figure 30) components of the dose rate shows an increase of the altitude dependent cosmic dose rate towards the heights of the Jura Mountains and a slightly elevated terrestrial dose rate at the lakeside. The map of the MMGC-ratio (Figure 31) gives no indication of man-made radionuclides. Both the activity concentrations of the natural radionuclides ^{232}Th (Figure 32) and ^{40}K (Figure 33) depict elevated activity concentrations on the lakeside as reason for the observed values of the terrestrial dose rate. The elevated Potassium and Thorium concentrations are associated with glacial deposits (Figures 34 and 35).

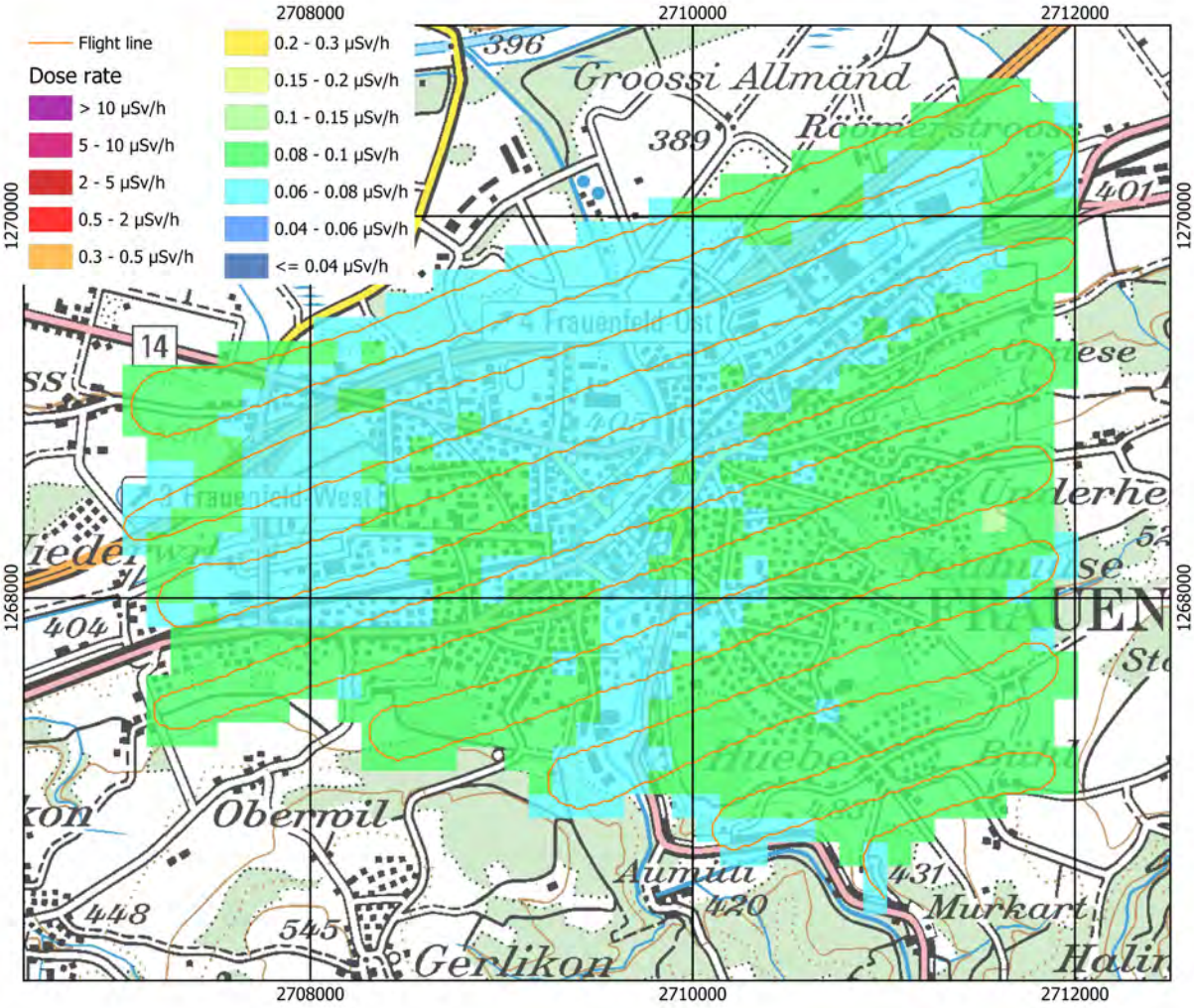

Figure 17: Dose rate over Frauenfeld. Geodaten©swisstopo.

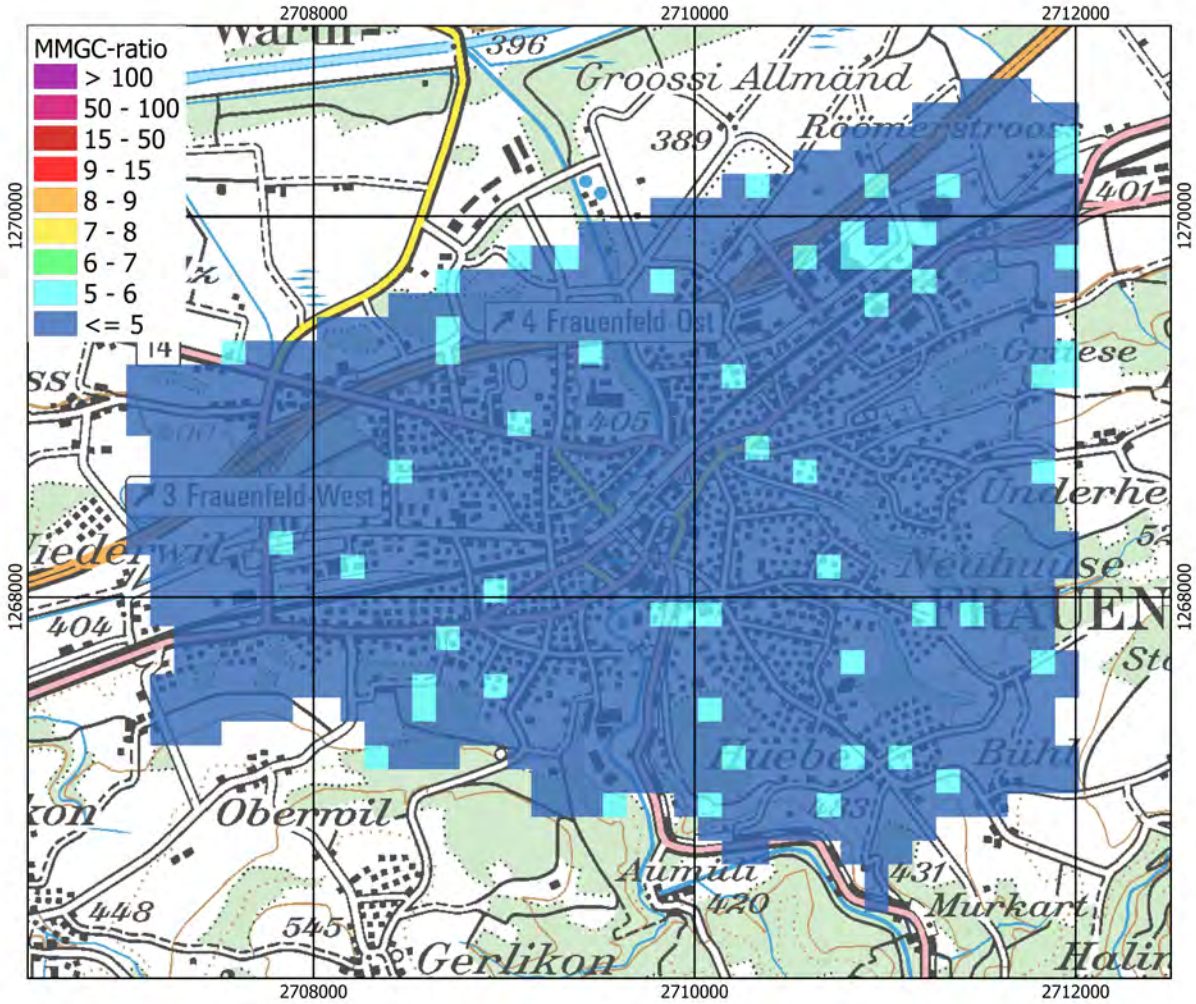

Figure 18: Man-made gross count (MMGC) ratio over Frauenfeld. Geodaten©swisstopo.

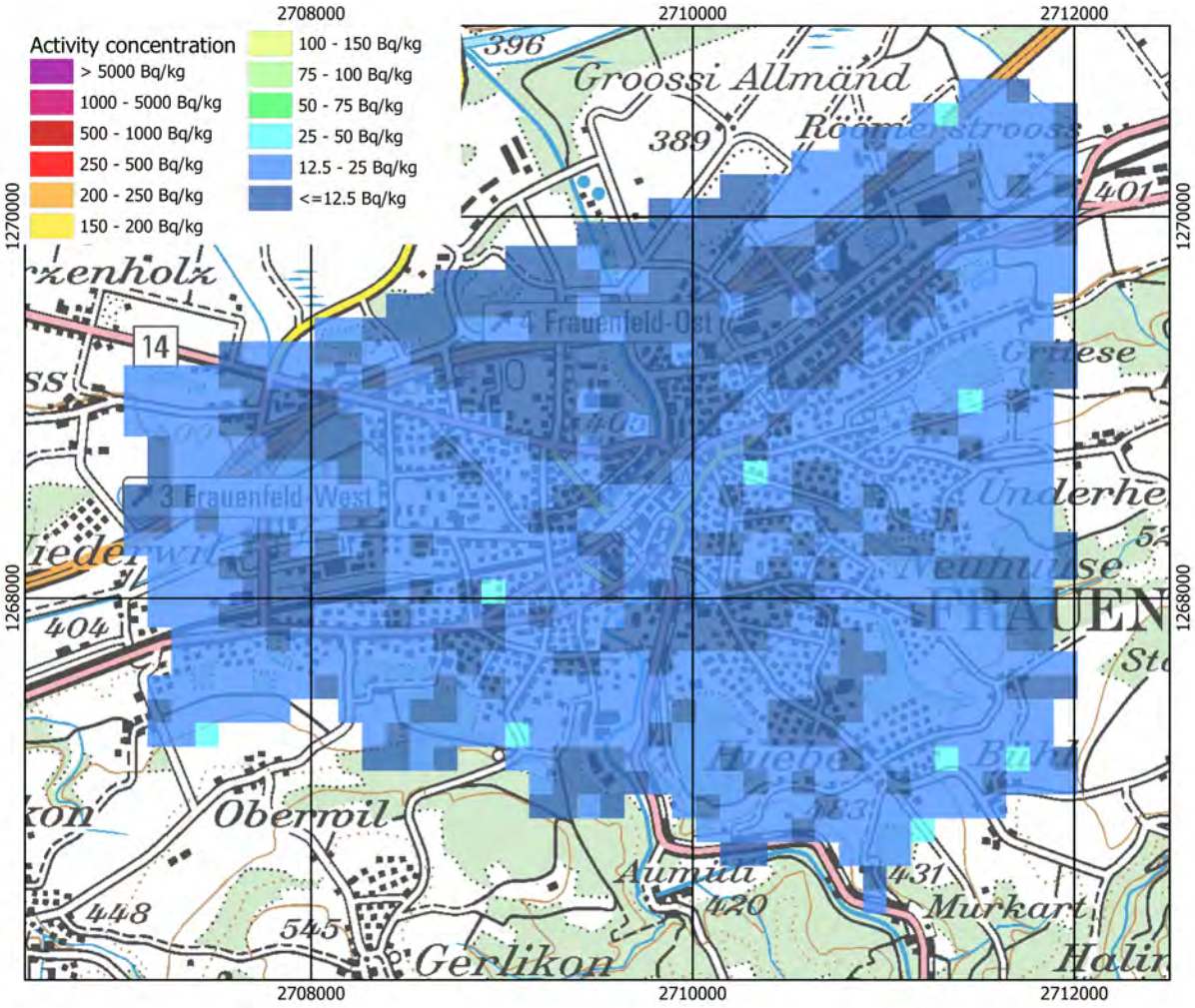

Figure 19: ^{232}Th activity concentration measured over Frauenfeld. Geodaten©swisstopo.

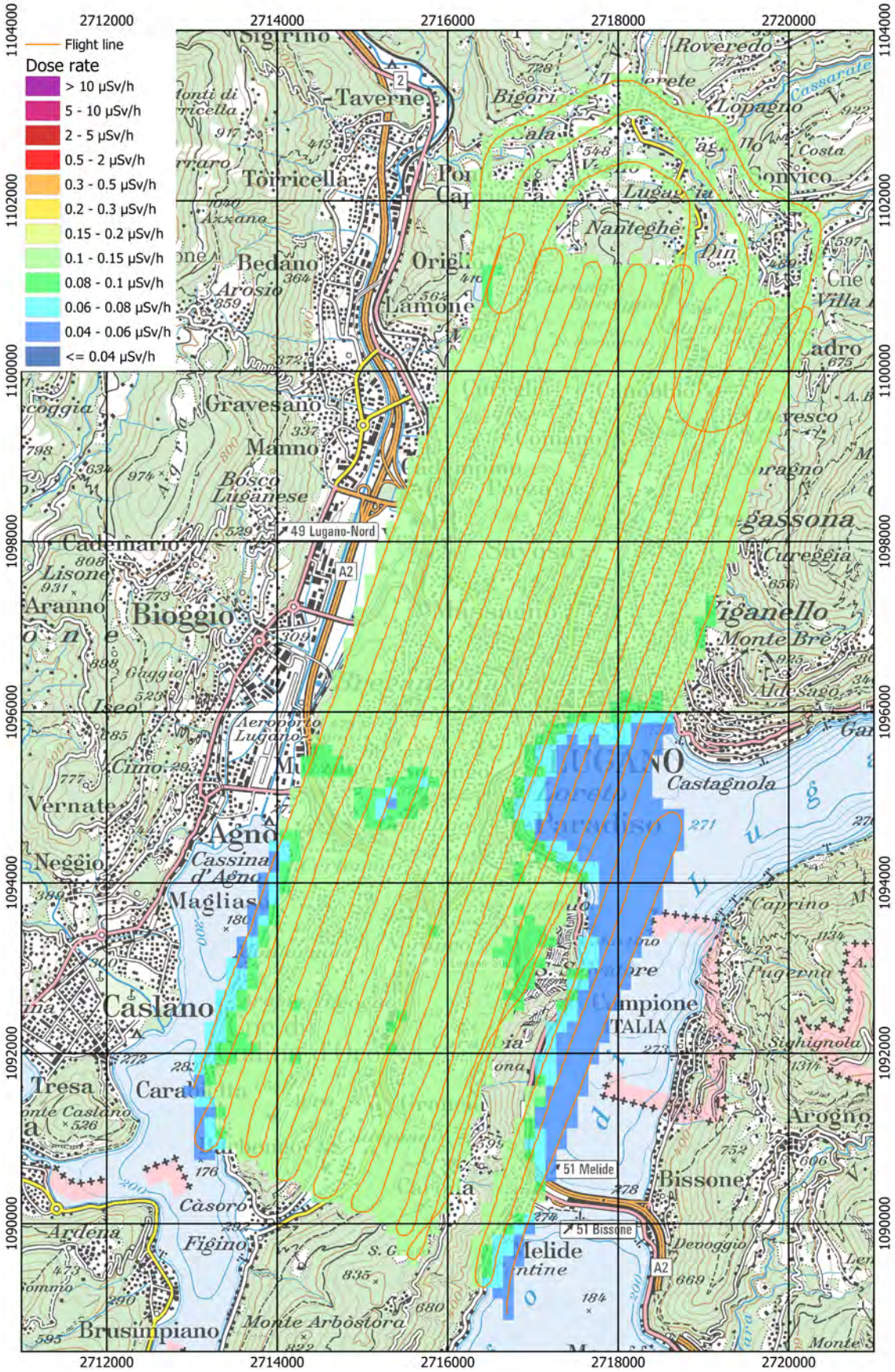

Figure 20: Dose rate over Lugano. Geodaten©swisstopo.

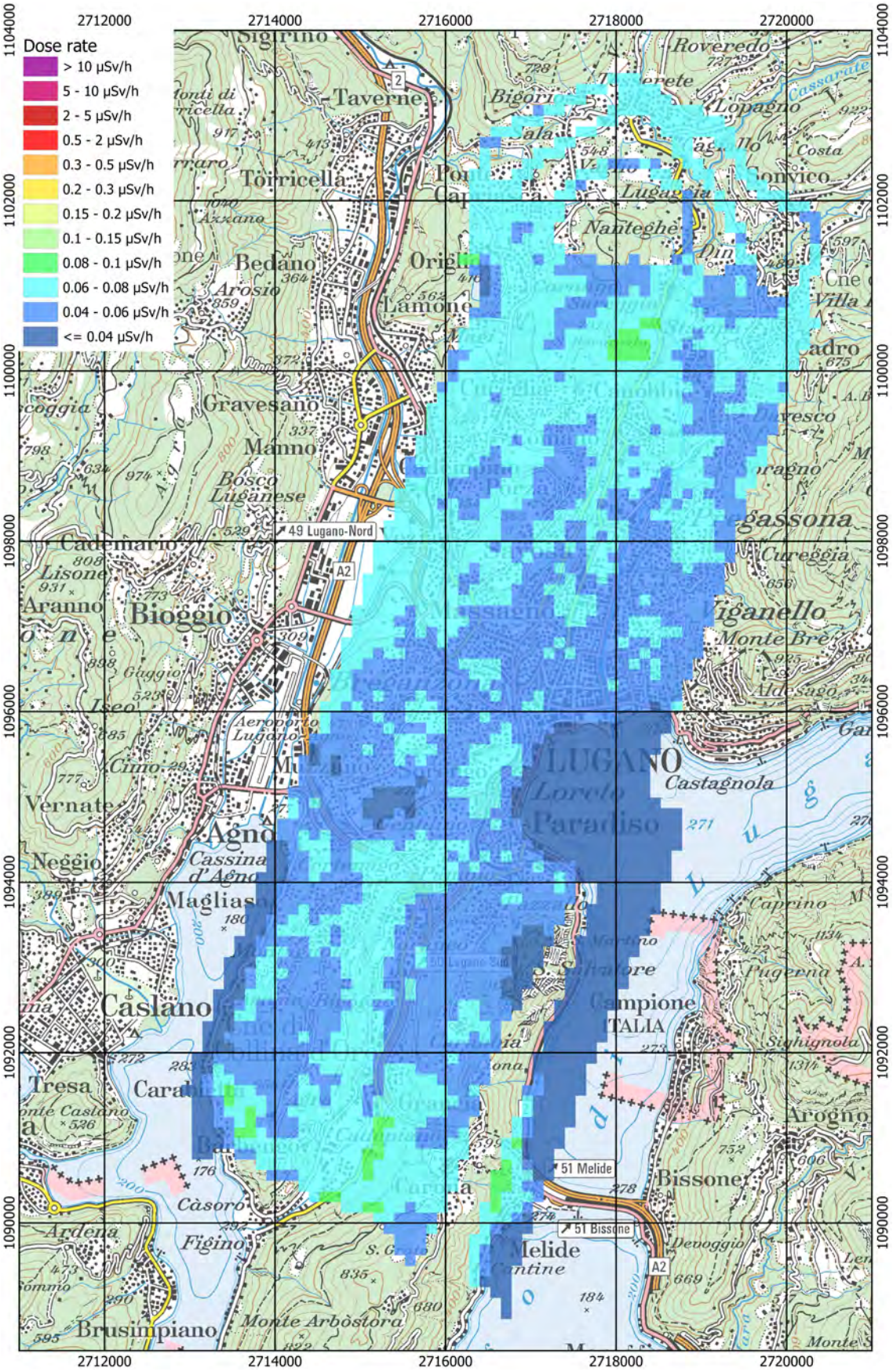

Figure 21: Terrestrial component of the dose rate over Lugano. Geodaten©swisstopo.

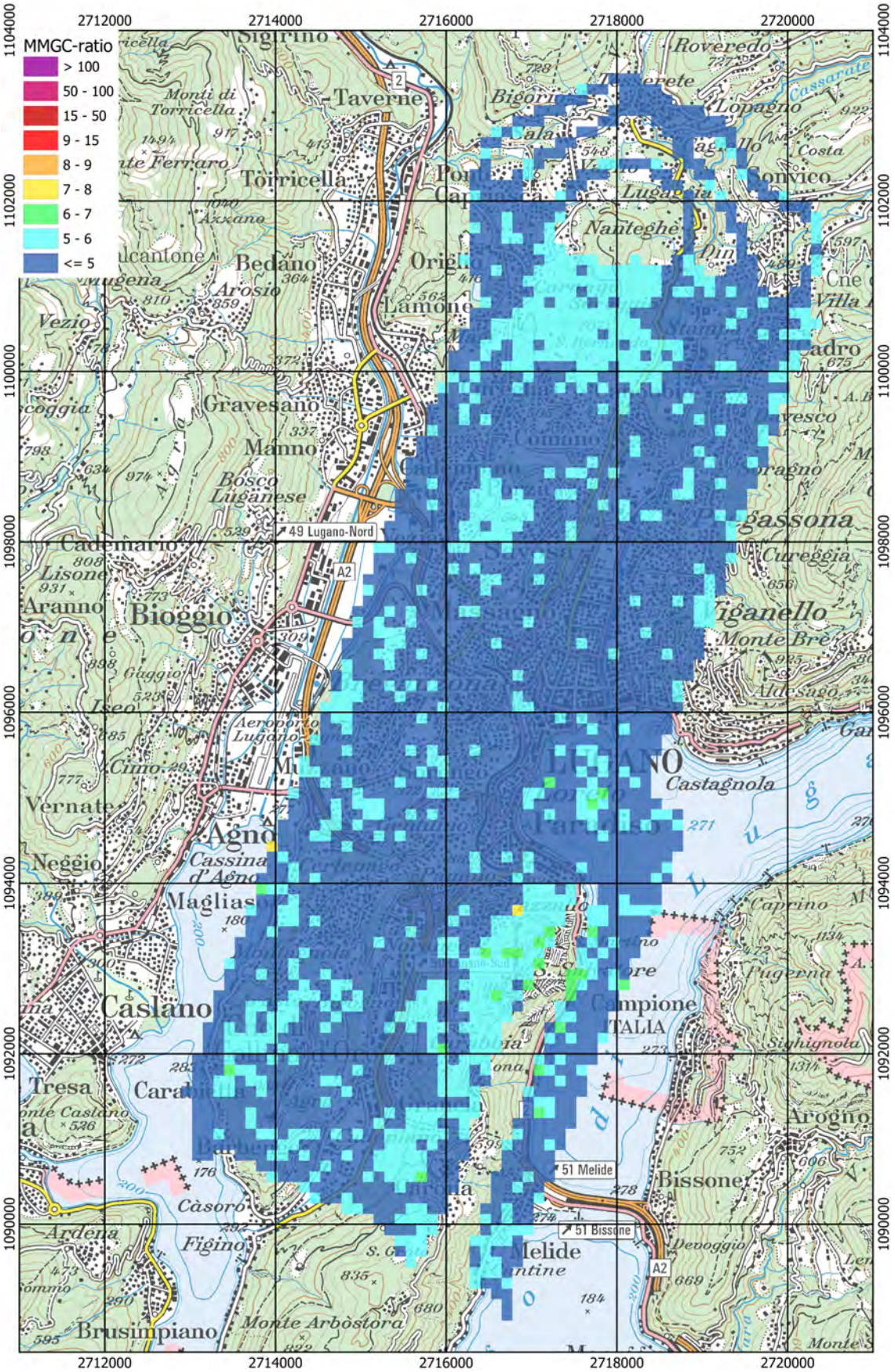

Figure 22: Man-made gross count (MMGC) ratio over Lugano. Geodaten©swisstopo.

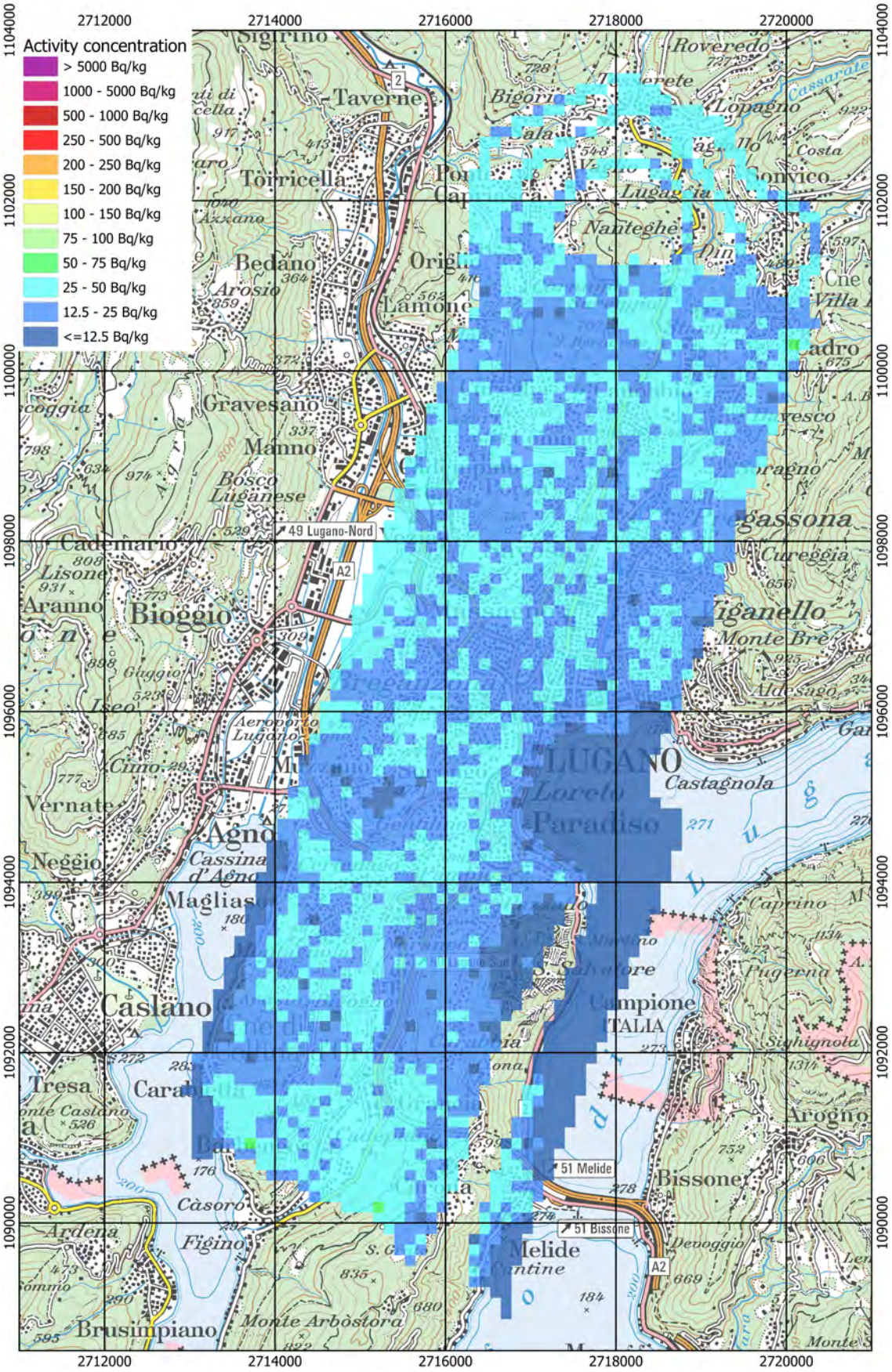

Figure 23: ^{232}Th activity concentration measured over Lugano. Geodaten©swisstopo.

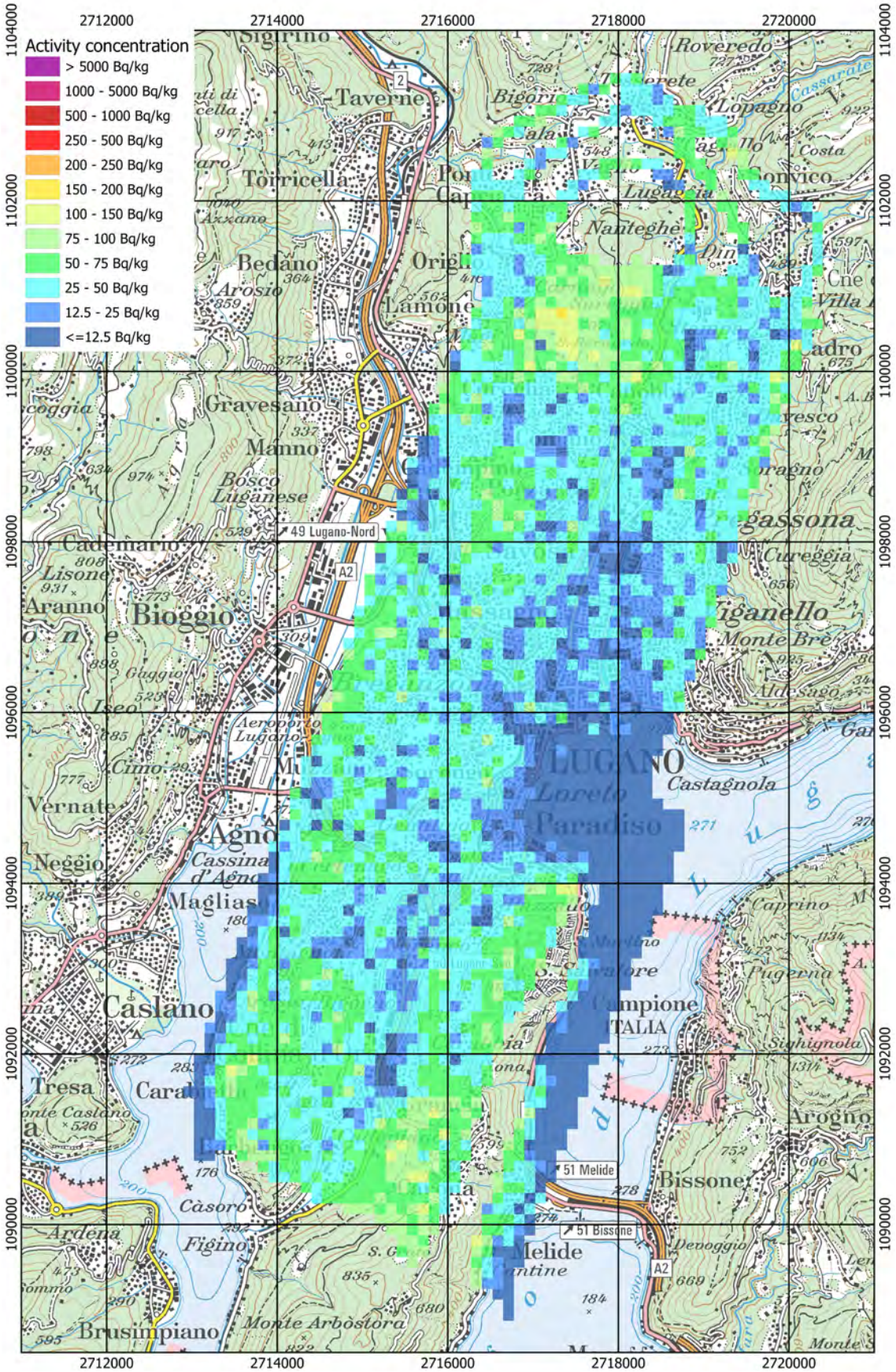

Figure 24: ^{137}Cs activity concentration measured over Lugano. Geodaten©swisstopo.

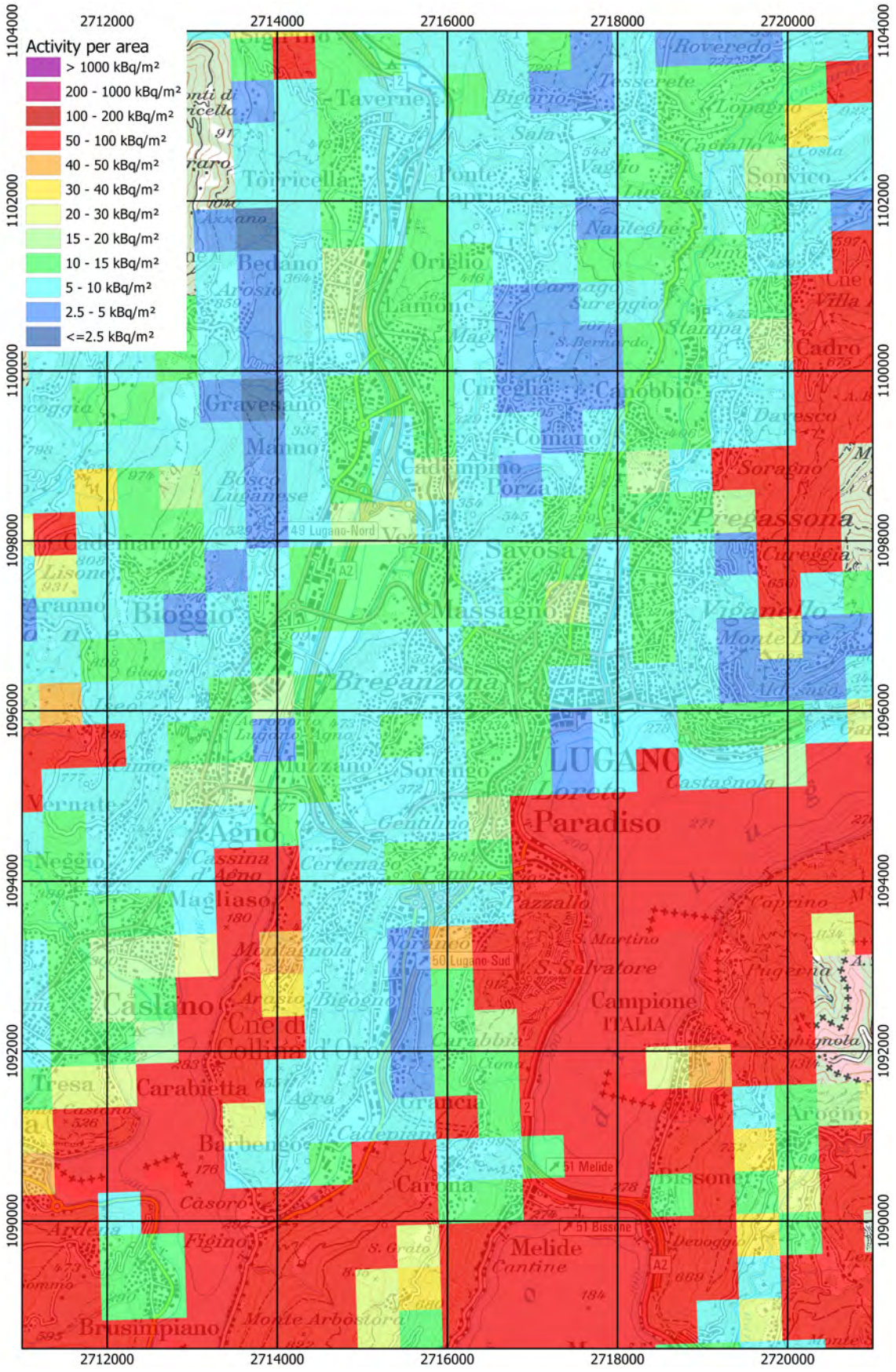

Figure 25: ^{137}Cs deposition over Lugano taken from baseline map (section 2.4.1). Geodaten©swisstopo, Caesium activity per area from Meusburger et al., 2020, provided electronically by ESDAC (Paganos et al. 2012).

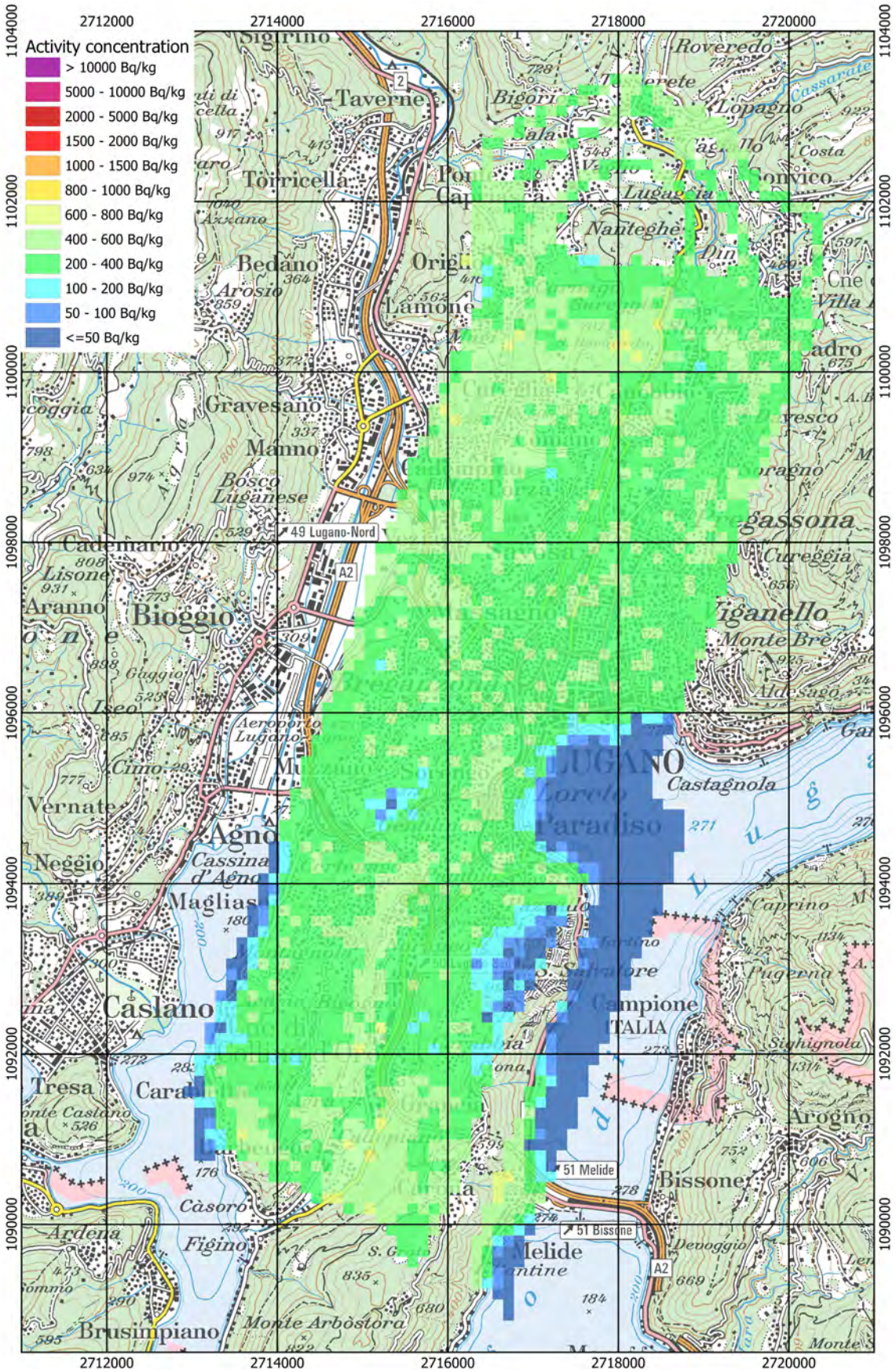

Figure 26: ^{40}K activity concentration measured over Lugano. Geodaten©swisstopo.

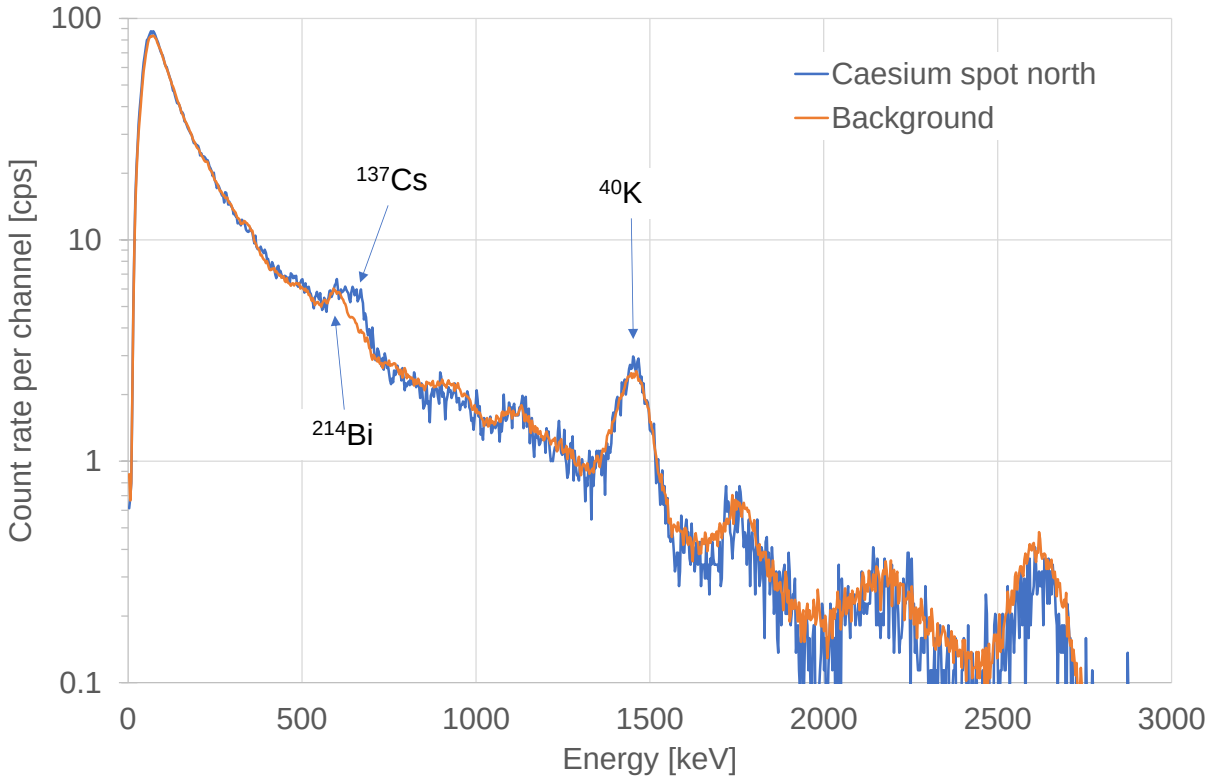

Figure 27: Photon spectrum over the area with elevated ^{137}Cs values north of Lugano in comparison to a background outside.

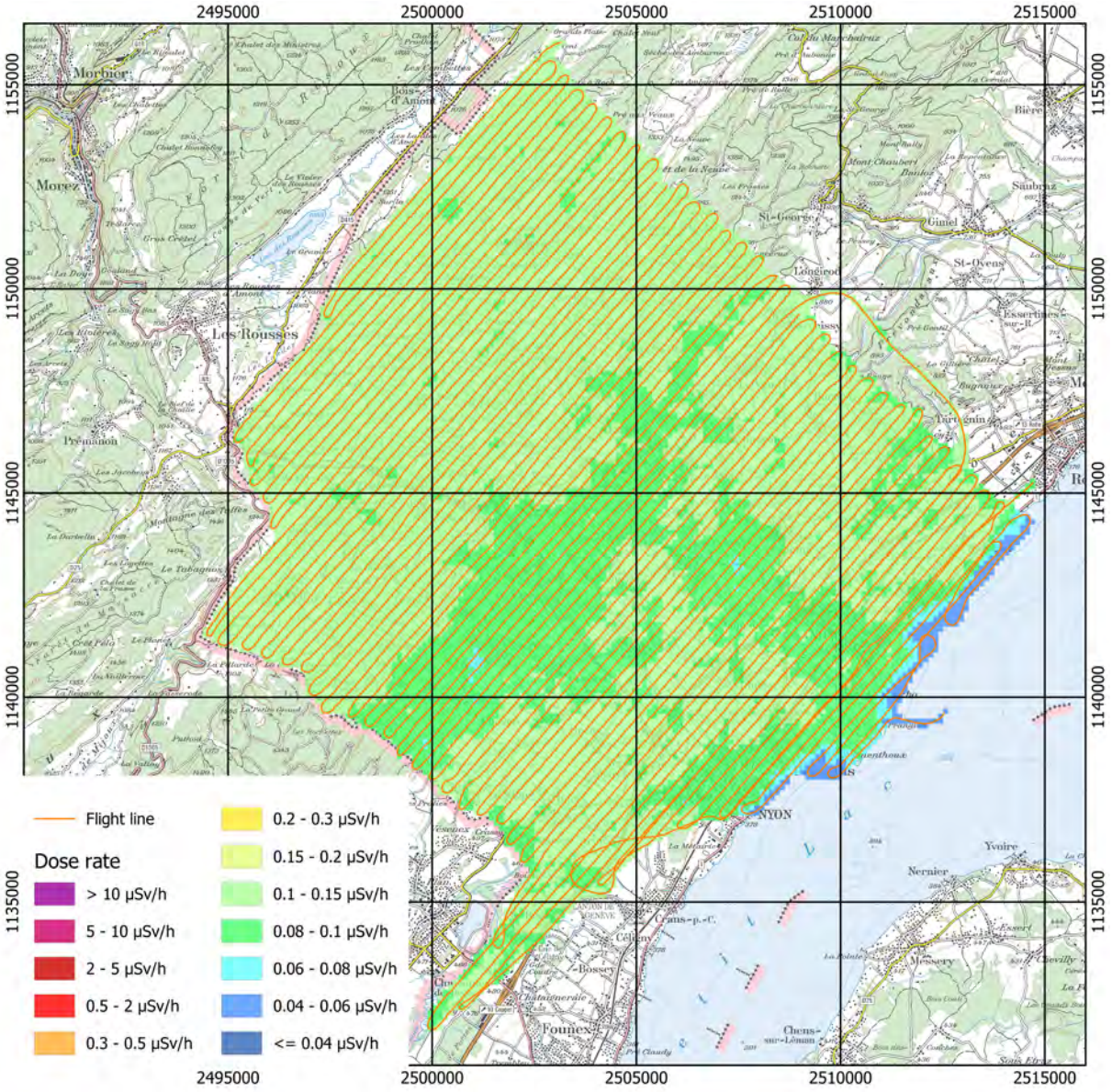

Figure 28: Dose rate over the vicinity of Nyon. Geodaten©swisstopo.

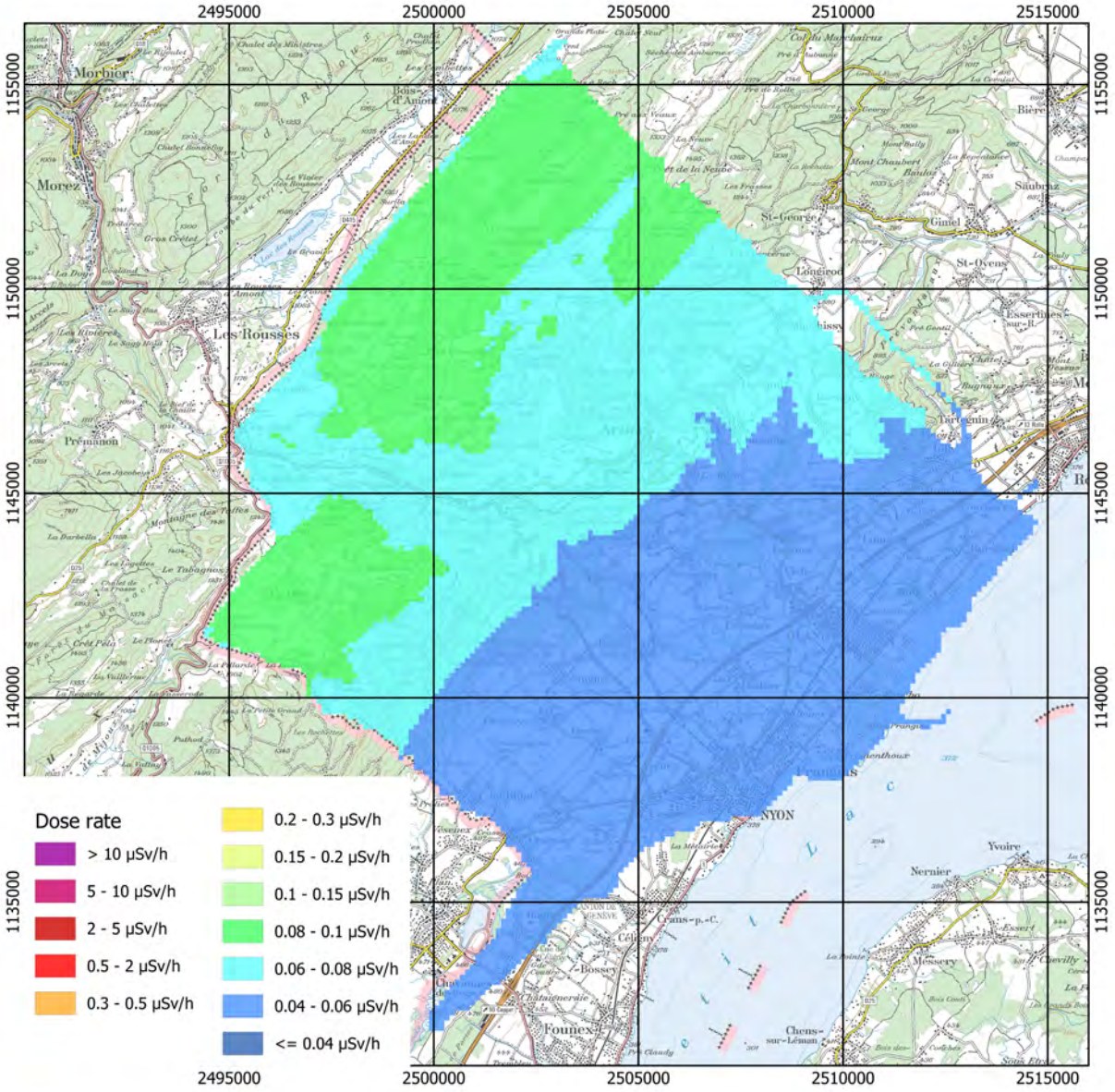

Figure 29: Cosmic component of the dose rate over the vicinity of Nyon. Geodaten©swisstopo.

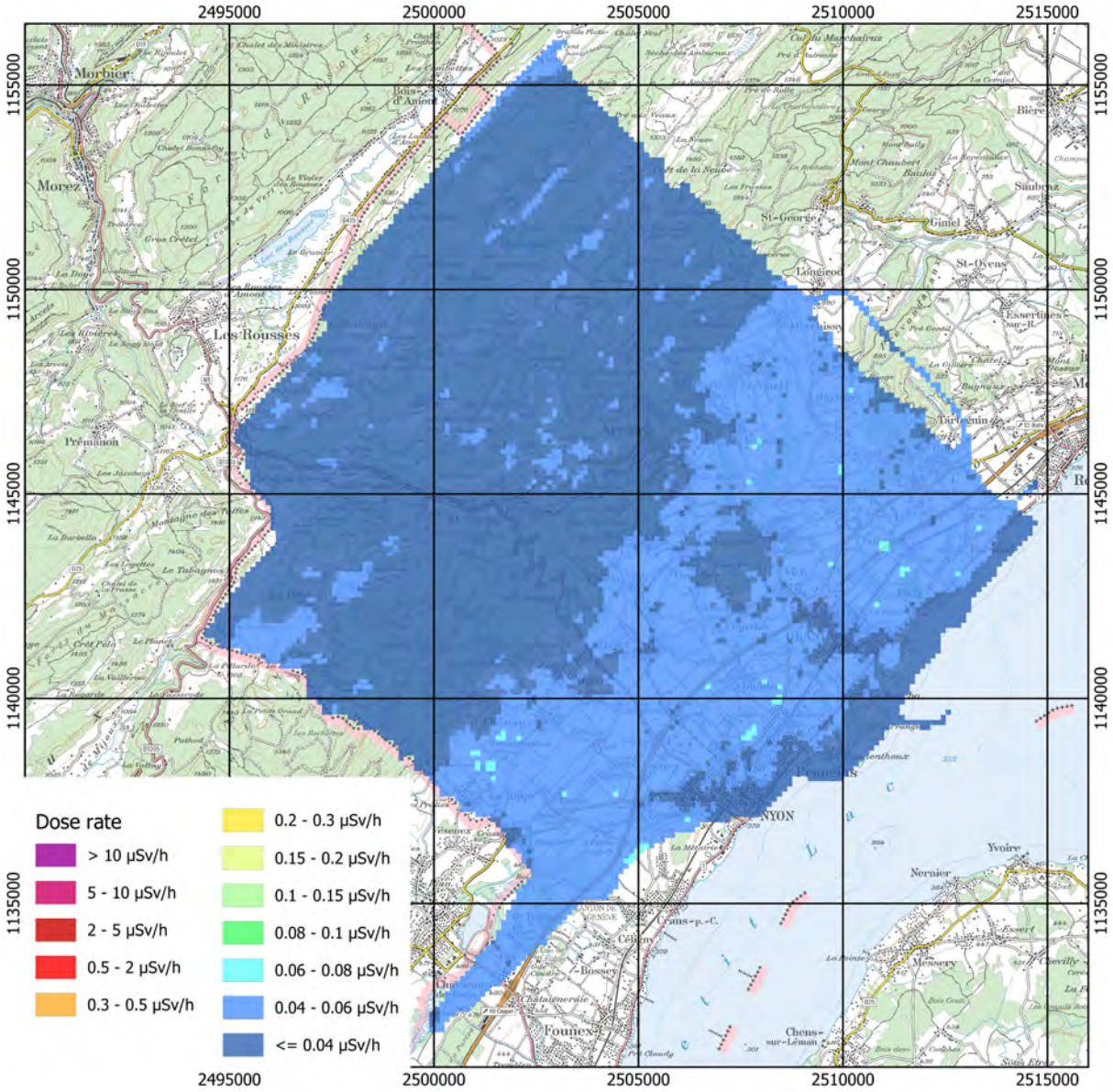

Figure 30: Terrestrial component of the dose rate over the vicinity of Nyon. Geodaten©swisstopo.

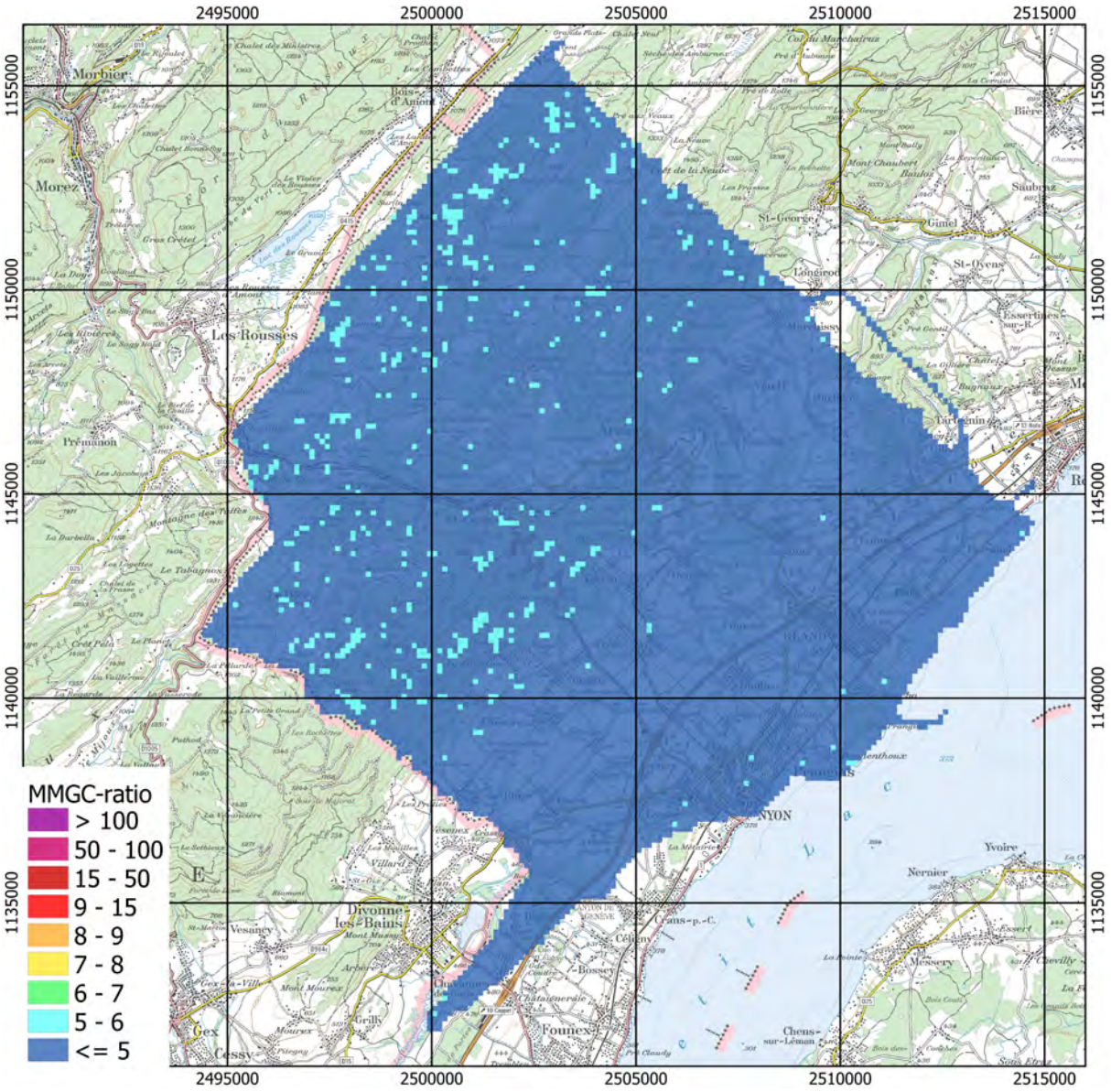

Figure 31: Man-made gross count (MMGC) ratio the vicinity of Nyon. Geodaten©swisstopo.

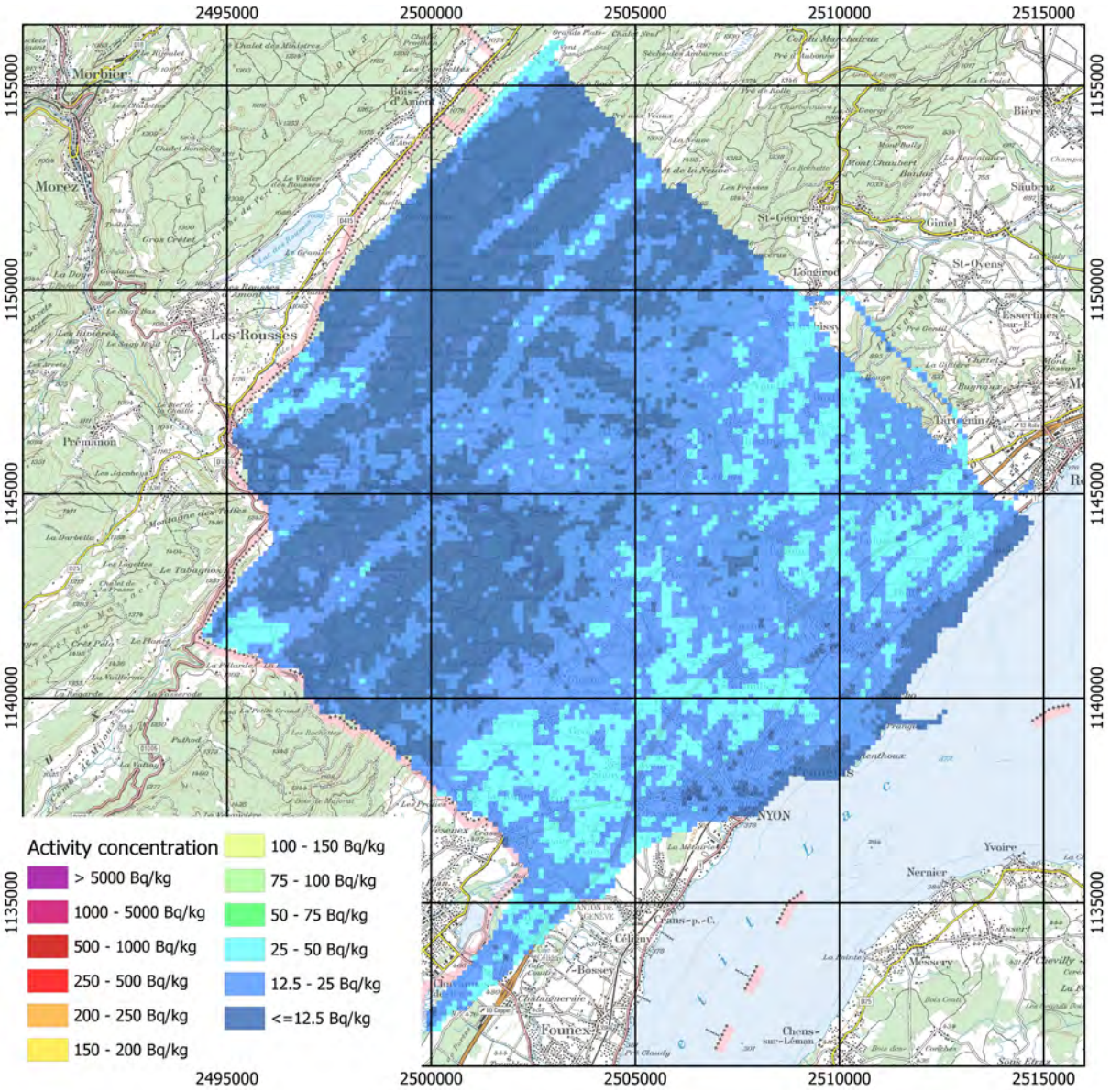

Figure 32: ^{232}Th activity concentration measured over the vicinity of Nyon. Geodaten©swisstopo.

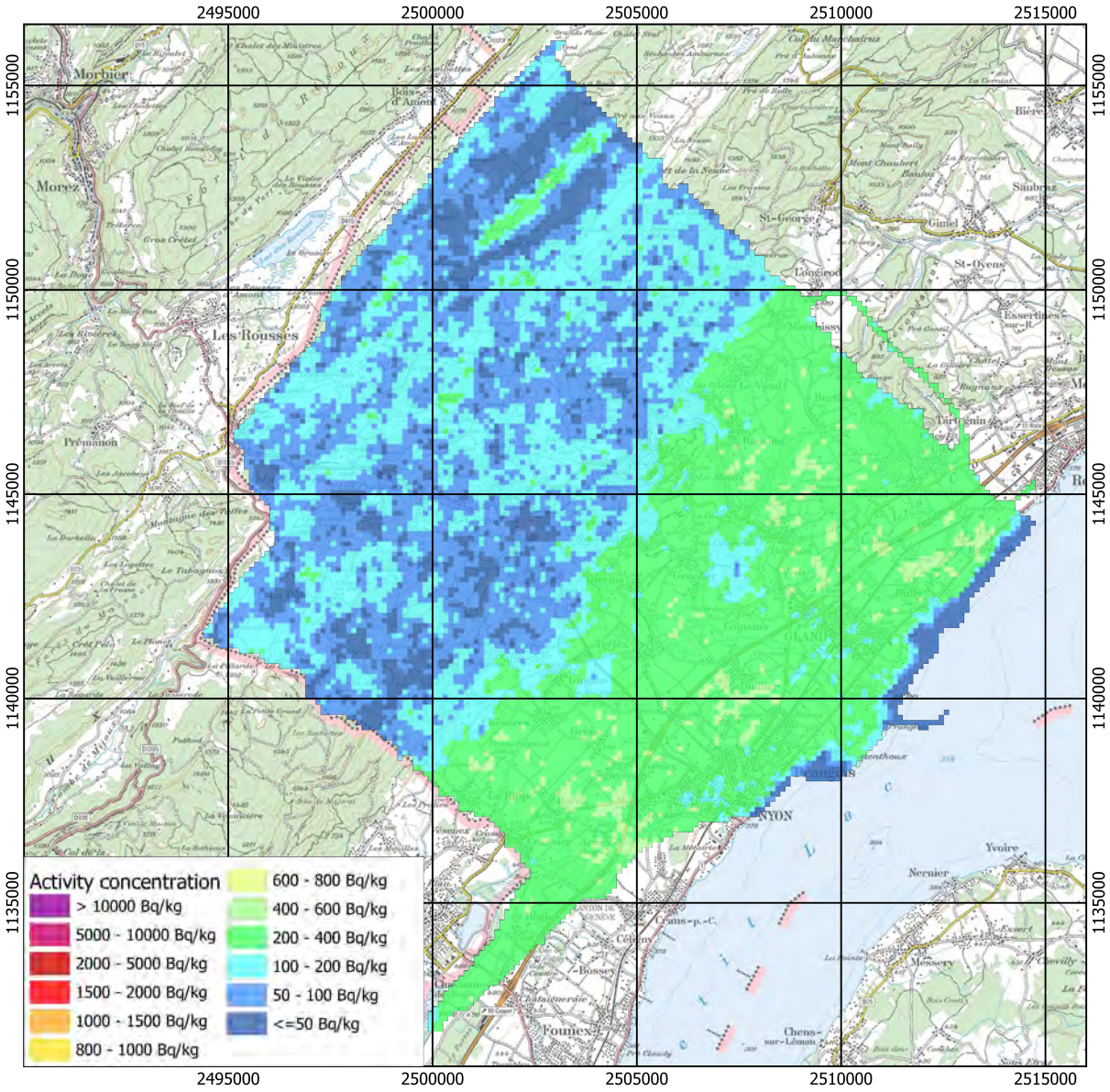

Figure 33: ^{40}K activity concentration measured over the vicinity of Nyon. Geodaten©swisstopo.

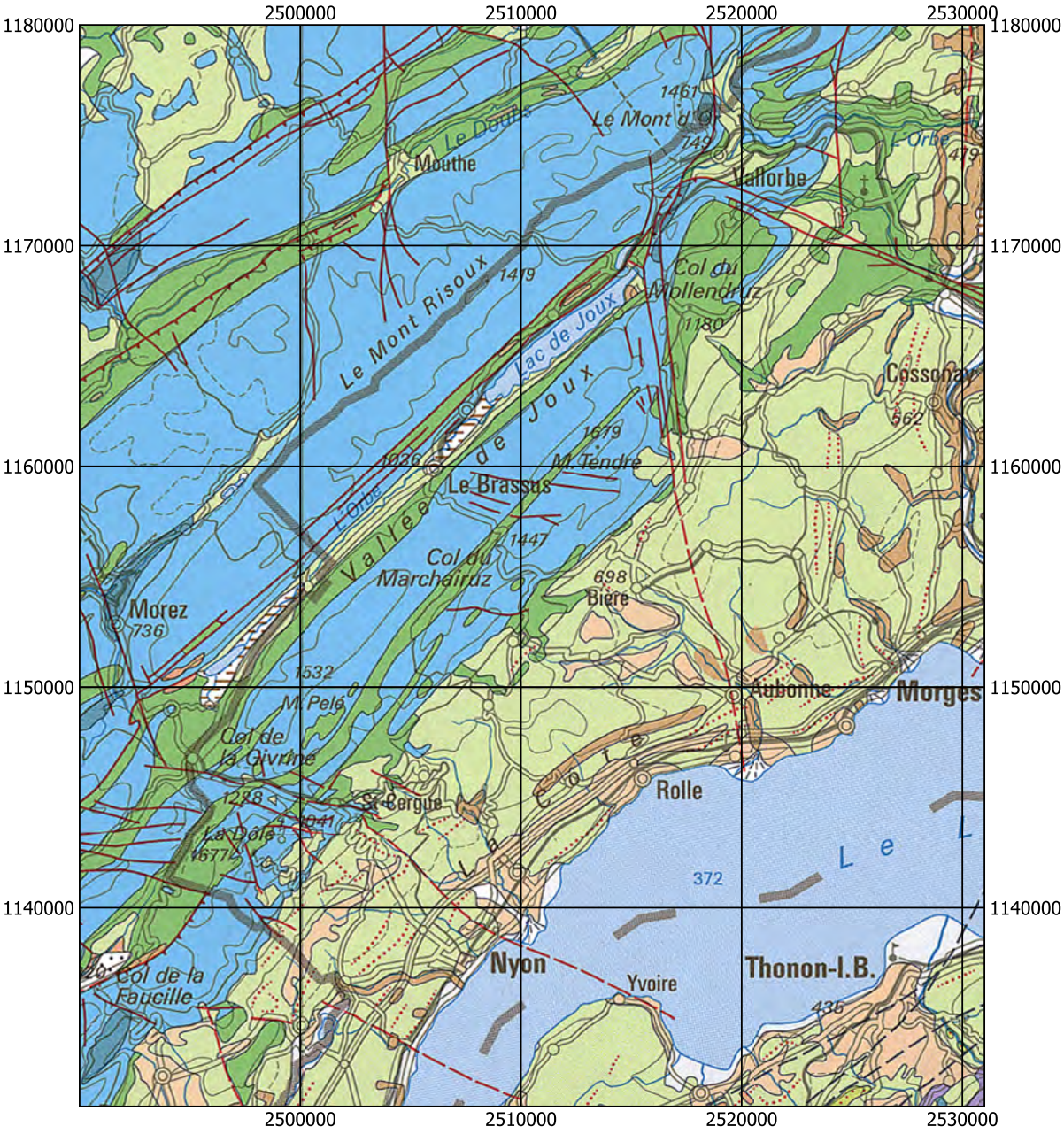

Figure 34: Geology in the vicinity of of Nyon and Lac de Joux. Geodaten©swisstopo.

Figure 35: Legend to geology in the vicinity of Nyon and Lac de Joux (in German). Geodaten©swisstopo.

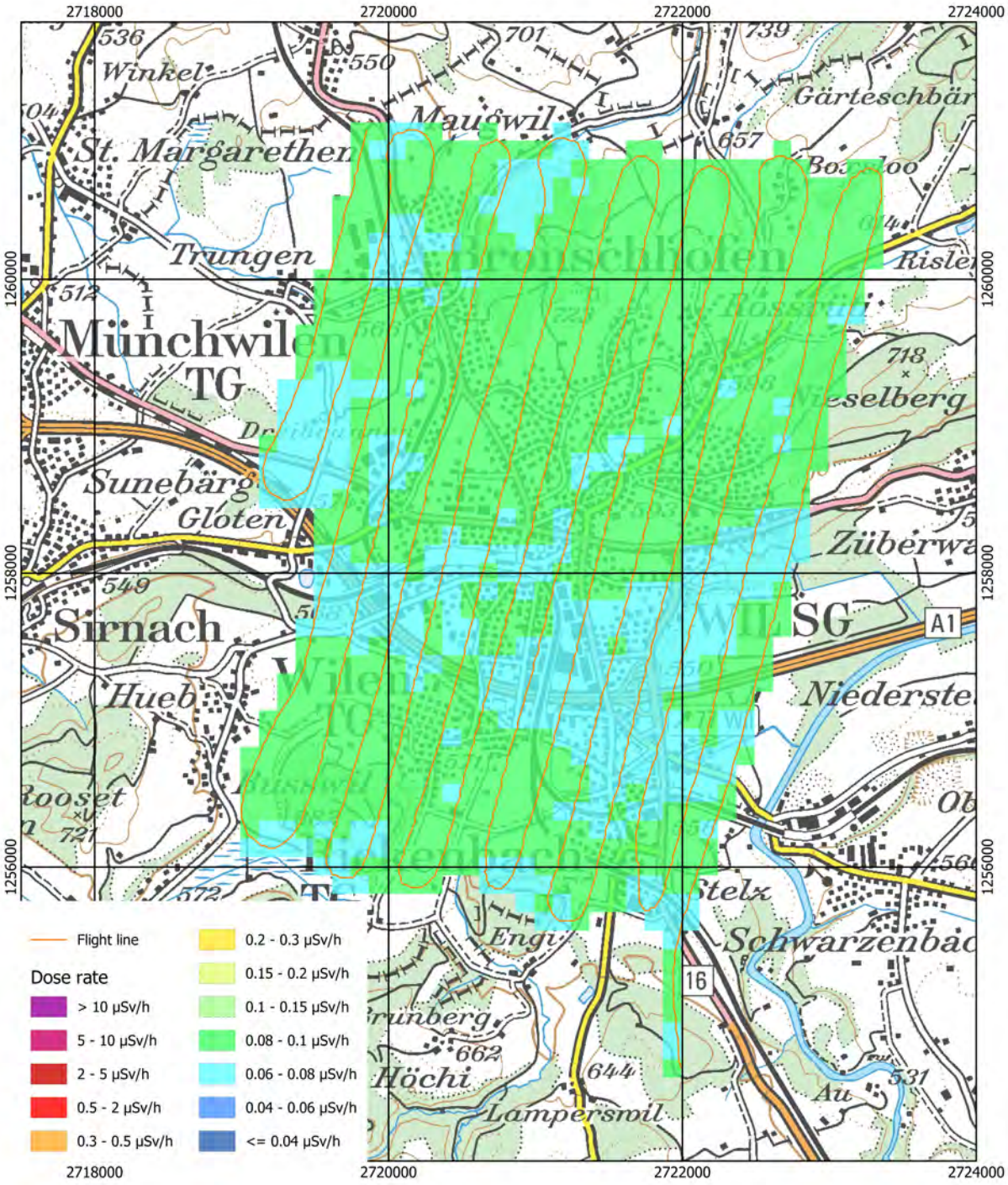

Figure 36: Dose rate over Wil. Geodaten©swisstopo.

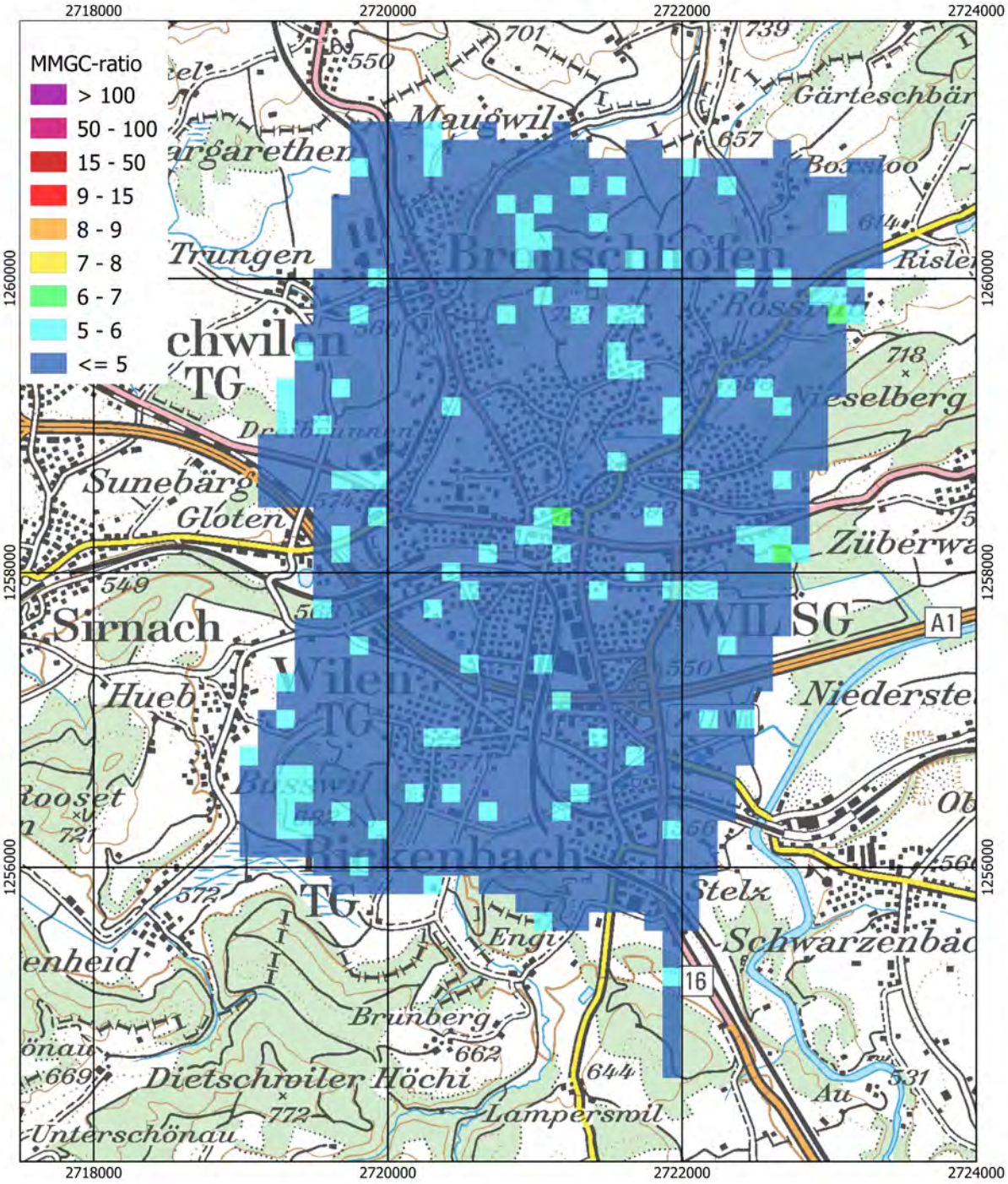

Figure 37: Man-made gross count (MMGC) ratio over Wil. Geodaten©swisstopo.

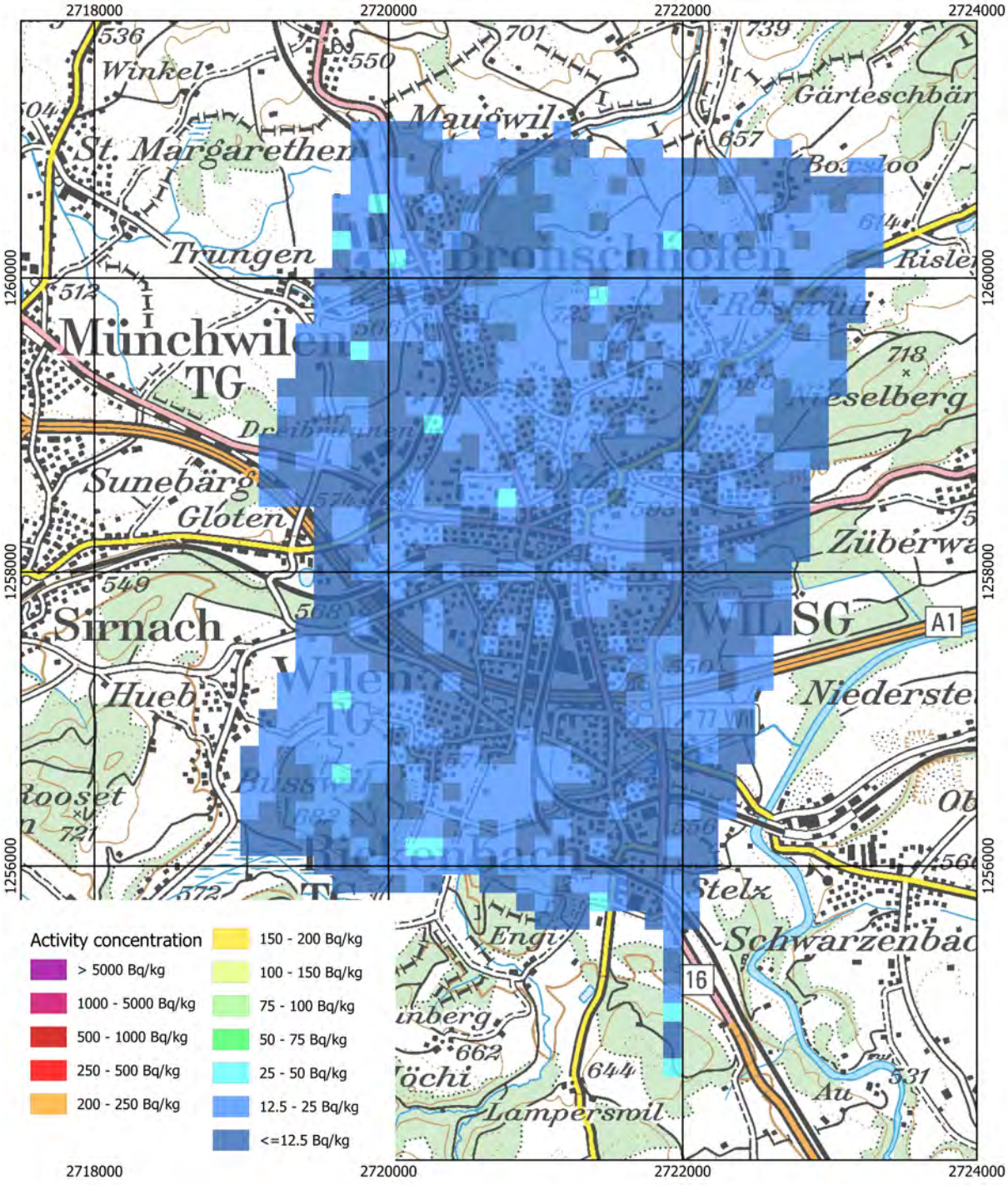

Figure 38: ^{232}Th activity concentration measured over Wil. Geodaten©swisstopo.

2.4 Chernobyl-follow-up

Radionuclides were deposited also in Switzerland in the wake of the Chernobyl accident. Measurements with airborne gamma-spectrometry over the afflicted regions started in 1991 with a calibration to in-situ ground measurements in the Magadino plain (Schwarz et al., 1992), followed with measurements over the Magadino plain in 1996 (Schwarz et al., 1997). Further measurements over regions in Canton Ticino were performed in 1999 (Bucher et al., 2000). Together with several areas in Canton Ticino, the point with the highest ^{137}Cs activity concentration measured in 1999 near Pizzo Ometto was re-inspected in 2011 (Bucher et al., 2012), leading to the conclusion that the reported ^{137}Cs activity concentration of 1860 Bq/kg was an artefact caused by an insufficient compensation of alpine terrain.
Some of the afflicted regions in western and southern Switzerland were inspected during ARM21 to compare remaining ^{137}Cs on the ground with the original depositions.

2.4.1 Reference values

Several references were used to compare the measured data with values published in the literature. Baseline maps of the total ^{137}Cs activity deposition (Figure 39) and the ^{137}Cs activity deposition originating from the Chernobyl accident (Figure 40) were published by Meusburger et al. in 2020. The data were decay corrected to first of August 2009. Digital representations of the published maps were obtained from the European Soil Data Centre (ESDAC, Paganos et al., 2012) in GEOTIFF format. The data was masked by the authors to exclude values at locations with elevations larger than 1000 m, which unfortunately involves large parts of Switzerland. The colour scale used for the baseline map of ^{137}Cs activity per square meter was aligned to the coulour scale used for the map of ^{137}Cs activity per wet mass (Section 1.4), to render direct comparability of the different maps.
A coarser gridded map of ^{137}Cs activity deposition caused by the Chernobyl accident, published by Evangeliou et al. (2016), was electronically available at the Norwegian Institute for Air Research (NILU) in plain text format (Figure 41). The values were decay corrected to first of May, 1986.
Another reference source for ^{137}Cs activity deposition is the Atlas of Caesium deposition on Europe after the Chernoby accident, published by the European Commission in 1998. The digital copy of a scanned version of this atlas including all maps found online had a coarse resolution, making reading of values in the map zoomed to Switzerland (Figure 42) difficult.
Deposition of radionuclides from the Chernobyl accident in Switzerland were immediately analysed by the Swiss Federal Nuclear Safety Inspectorate (ENSI, former Hauptabteilung für die Sicherheit der Kernanlagen HSK) and published in November 1986. The according ^{137}Cs activity deposition map is shown in Figure 43.
The spatial distribution of the results of soil sample analysis throughout Switzerland was published by Riesen et al. in 1999 (Figure 44). The data were decay corrected to the first of July 1993.
Table 9 of the radioactive decay of ^{137}Cs from the reference date of the respective map to the first of August 2021, defined as reference date of ARM21, facilitates the comparison of the different maps.

Map	Reference date	Remaining ^{137}Cs activity fraction
39, 40	1.8.2009	76 %
41, 42, 43	1.5.1986	44 %
44	1.7.1993	52 %

Table 9: Remaining ^{137}Cs activity fraction since map reference date.

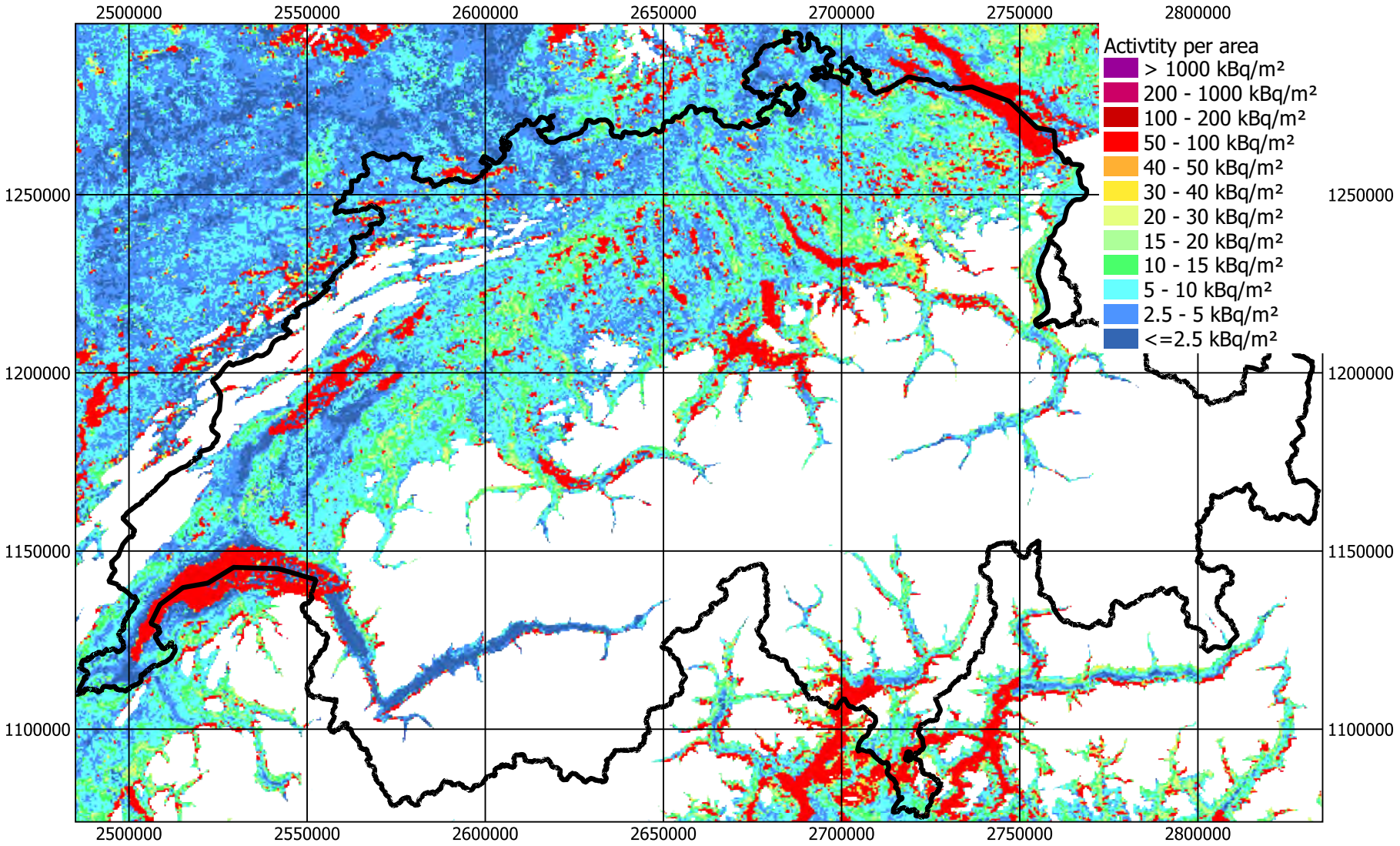

Figure 39: Total ^{137}Cs activity per area in Switzerland 2009 taken from baseline map. Geodaten©swisstopo, Caesium activity per area from Meusburger et al., 2020, provided electronically by ESDAC (Paganos et al. 2012).

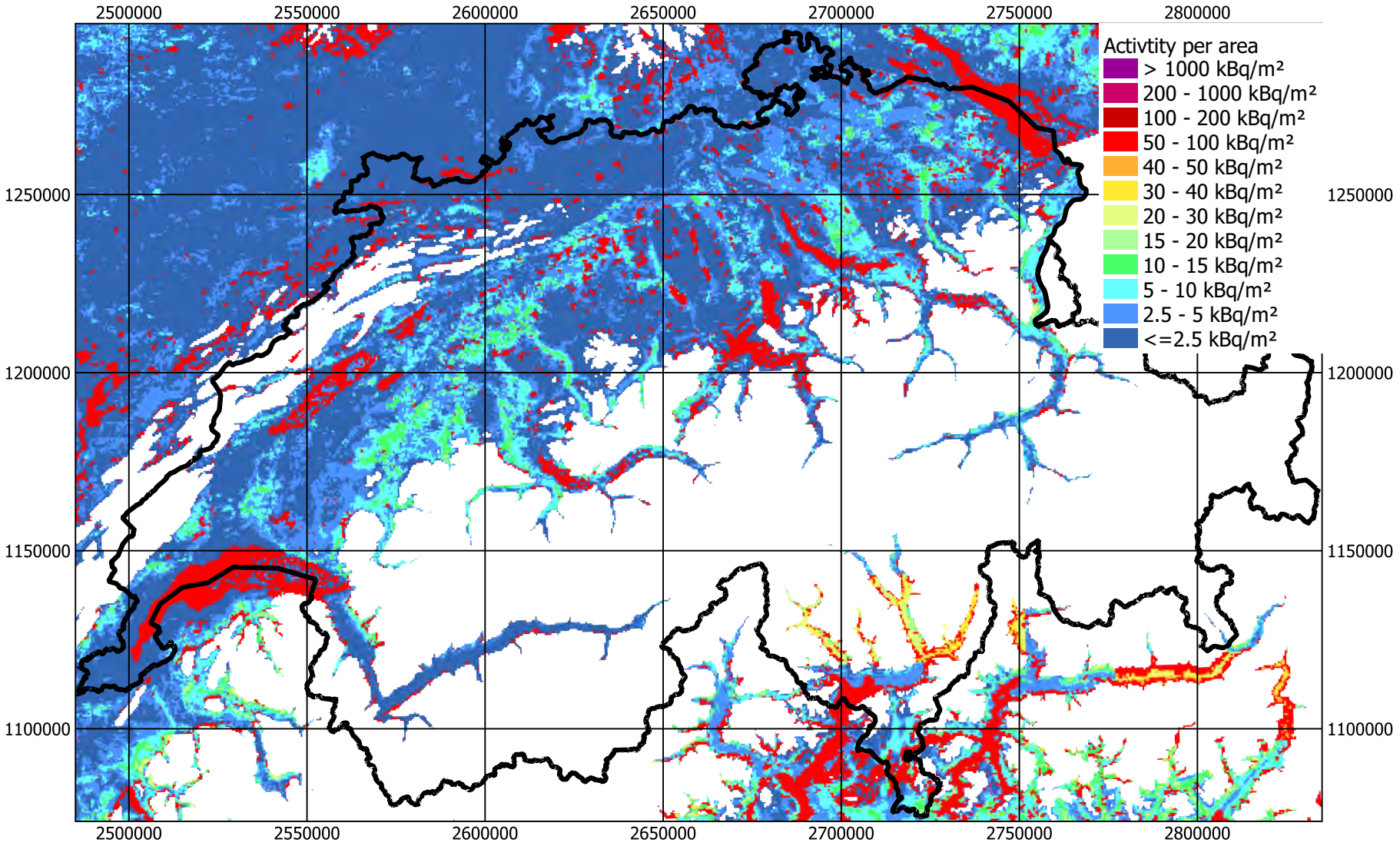

Figure 40: ^{137}Cs deposition originating from Chernobyl in Switzerland 2009 taken from baseline map. Geodaten©swisstopo, Caesium activity per area from Meusburger et al., 2020, provided electronically by ESDAC (Paganos et al. 2012).

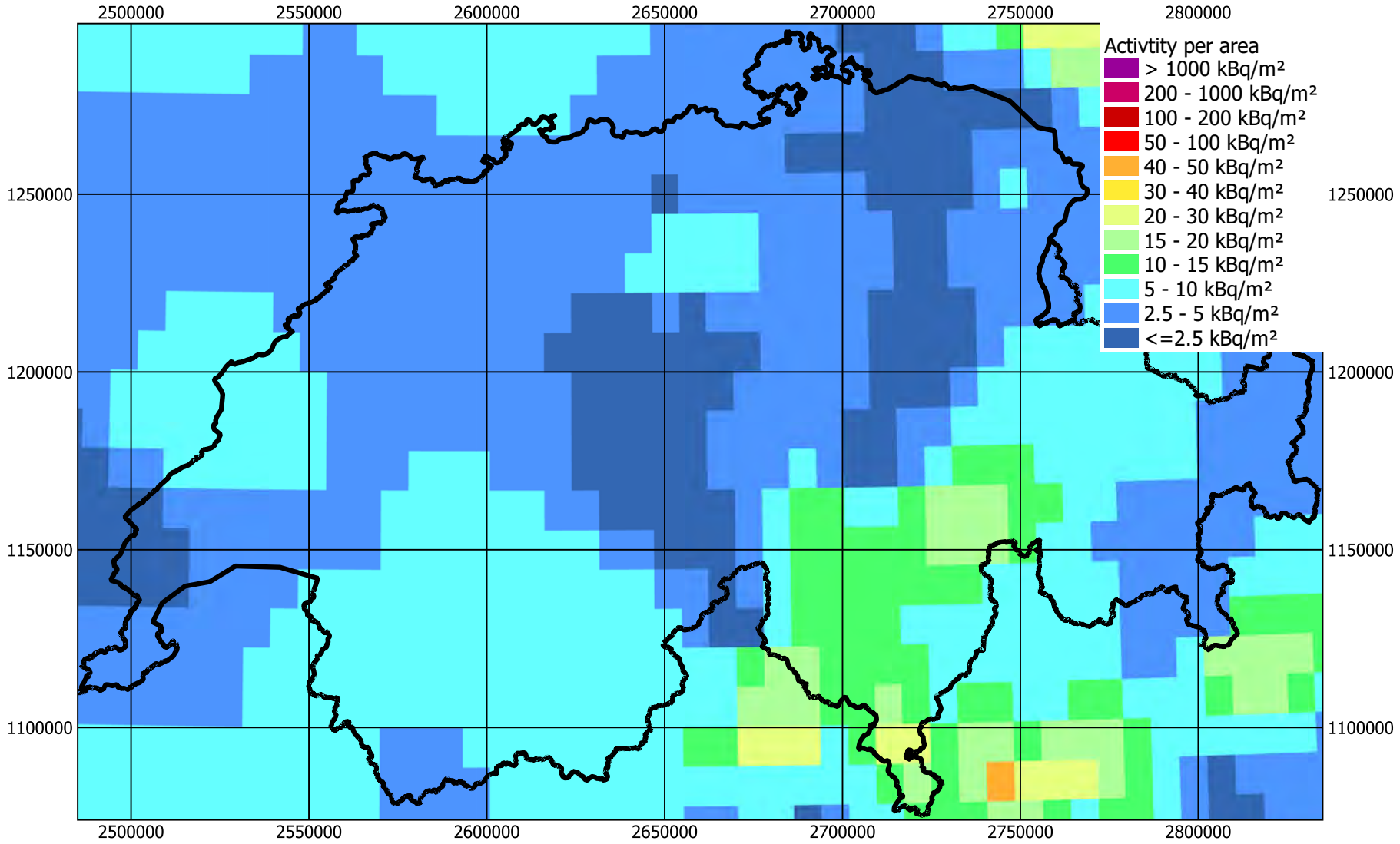

Figure 41: ^{137}Cs deposition originating from Chernobyl in Switzerland 1986 taken from Evangeliou et al., 2016. Geodaten©swisstopo, Caesium activity per area from Evangeliou et al., 2016, provided electronically at http://radio. nilu.no/Chernobyl/Griddeddata.aspx.

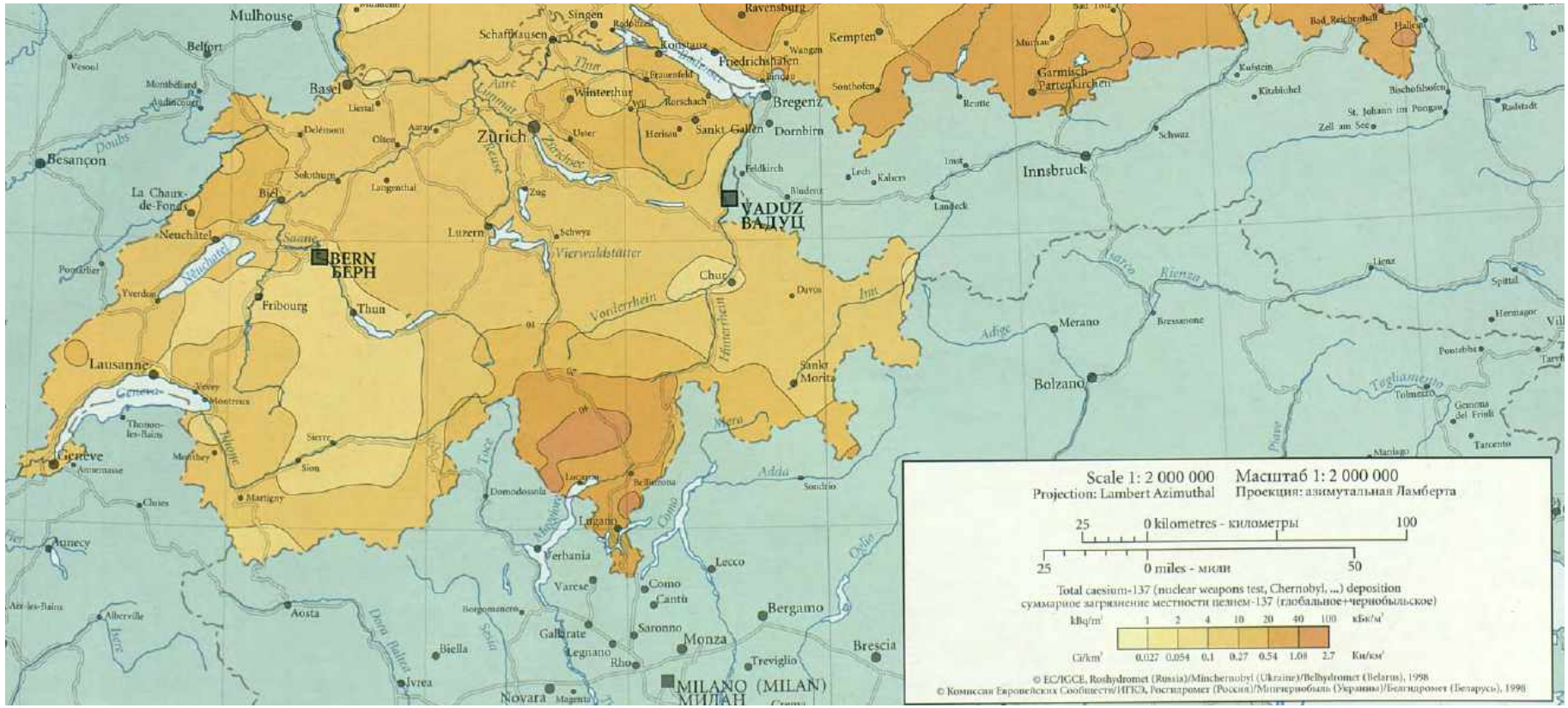

Figure 42: Total ^{137}Cs deposition in Switzerland taken from the Atlas of the European Commission (European commission, 1998).

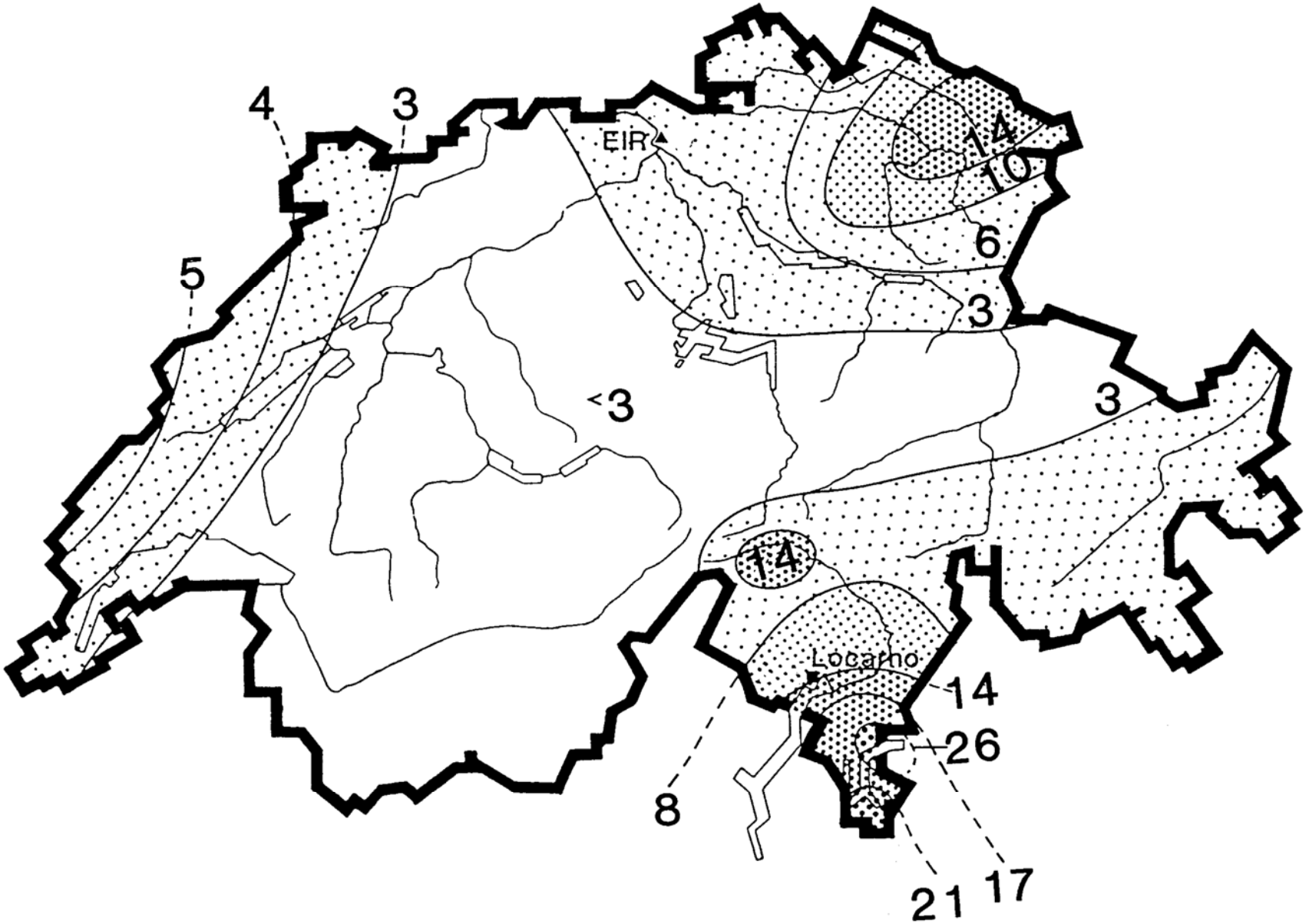

Figure 43: ^{137}Cs deposition originating from Chernobyl in Switzerland taken from HSK-report HSK-AN-1816, 1986. Values are given in kBq/m^2.

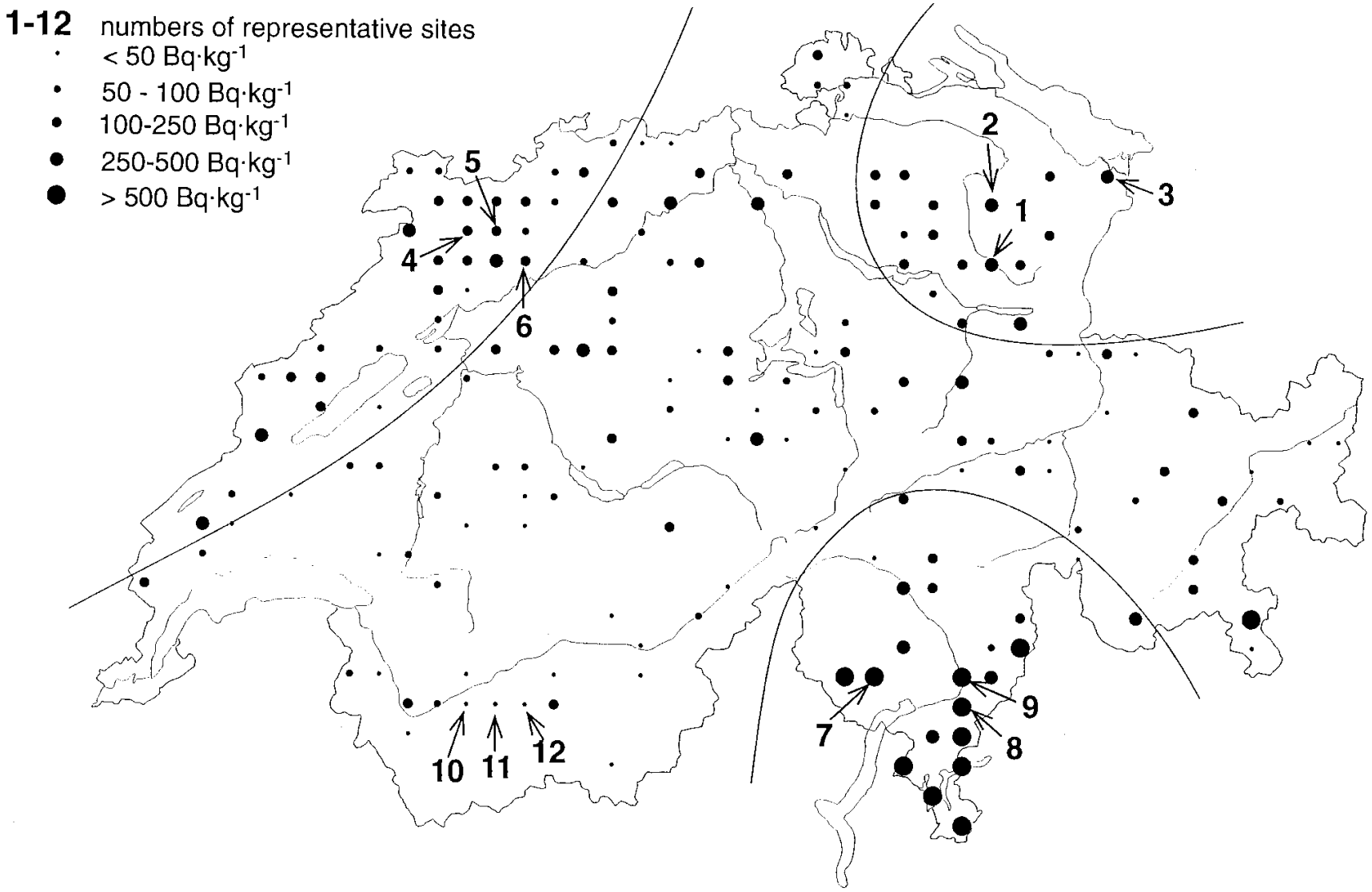

Figure 44: Samples of total ^{137}Cs activity concentration originating from Chernobyl in Switzerland taken from Riesen et al., 1999.

2.4.2 Joux

The region around Lac de Joux in the Jura mountains near the border to France was afflicted from some radionuclide deposition in the wake of the Chernobyl accident. Besides the effect of attenuation of photons in the water layer of Lac de Joux, no distinctive elevation of dose rate is observed (Figure 45). Similar to the pattern of naturally occurring radionuclides in the adjacent region between Nyon and the French border, the activity concentrations of ^{232}Th and ^{40}K are higher leaving the Jura mountains to the south-west (Figures 46 and 47) due to glacial deposits (Figure 48). The values of the MMGC-ratio do not yield a clear indication of the presence of man-made radionuclides (Figure 49). The map of ^{137}Cs activity concentration (Figure 50) shows a scant residual of Chernobyl deposition in the forest of the Jura mountains matching the pattern visible in the map of the MMGC-ratio (Figure 49). Unfortunately, the baseline map of ^{137}Cs activity deposition (Figure 51) does not provide values in most of the measuring area.
Seven points in the measuring area were inspected with in-situ gamma-spectrometry by staff of the NBC-EOD Centre of Competence (NBC-EOD) on September 6th and 9th, 2021. The location of the measurement points are marked in the map of ^{137}Cs activity concentration (Figure 50). All activity concentrations (Table 10) were determined under the assumption of a vertically homogeneous activity profile.

Point	Coordinates [m]		Activity concentration [Bq/kg]			
	East	North	^{40}K	^{232}Th	^{238}U	^{137}Cs
1	2514160	1161452	145 ± 18	9 ± 2	35 ± 3	30 ± 4
2	2514523	1161537	223 ± 26	16 ± 3	37 ± 3	43 ± 5
3	2511908	1158944	238 ± 27	19 ± 2	65 ± 5	30 ± 4
4	2511892	1158840	259 ± 30	20 ± 3	65 ± 5	42 ± 5
5	2511873	1158856	309 ± 34	24 ± 3	83 ± 6	157 ± 16
6	2511963	1158835	322 ± 35	24 ± 3	96 ± 7	34 ± 4
7	2511705	1157873	297 ± 33	23 ± 3	83 ± 6	30 ± 4
Average	-	-	256 ± 61	19 ± 6	66 ± 23	52 ± 46

Table 10: Activity concentrations measured with in-situ gamma-spectrometry and estimated uncertainty (k=1).

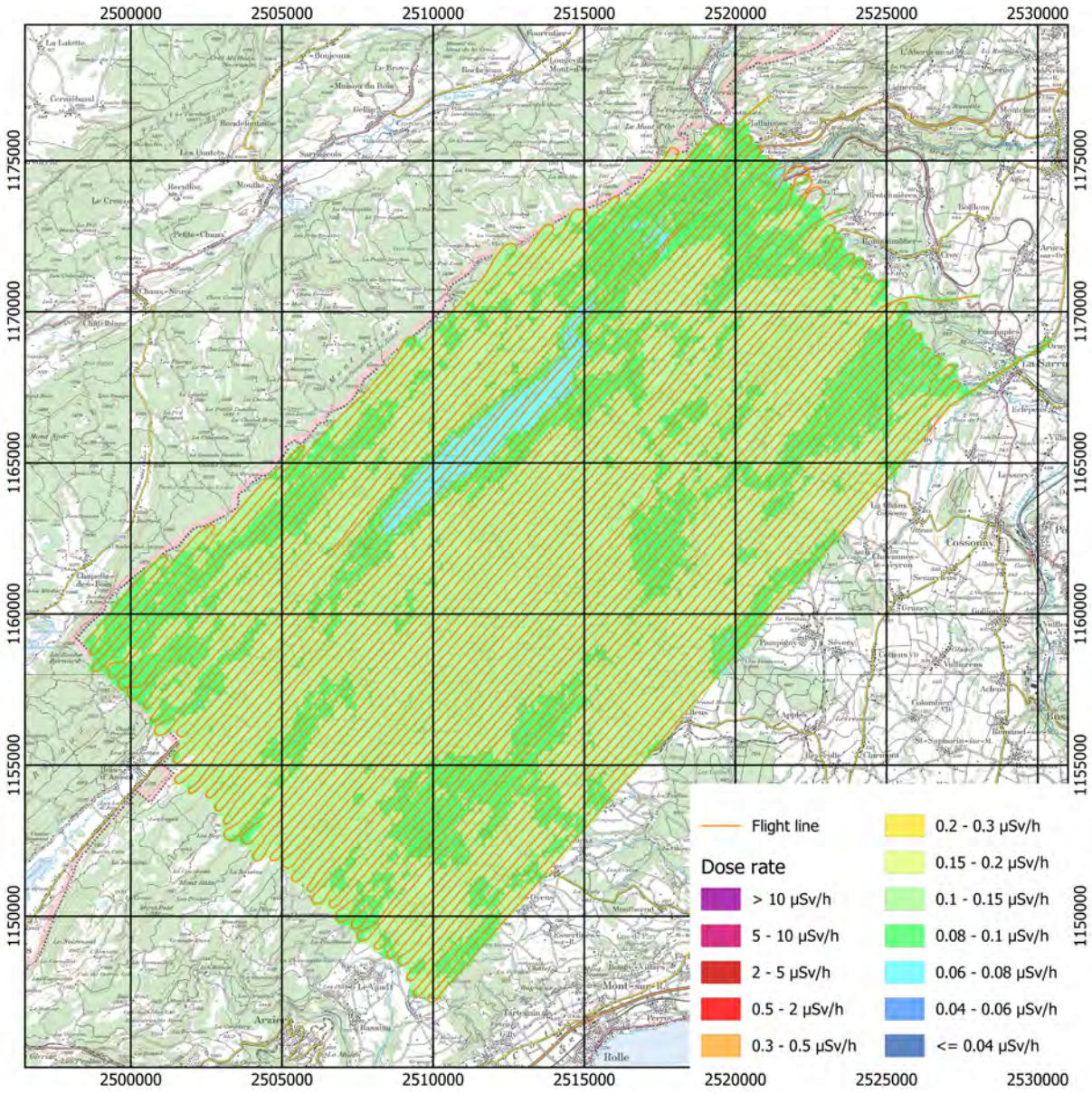

Figure 45: Dose rate over the region around Lac de Joux. Geodaten©swisstopo.

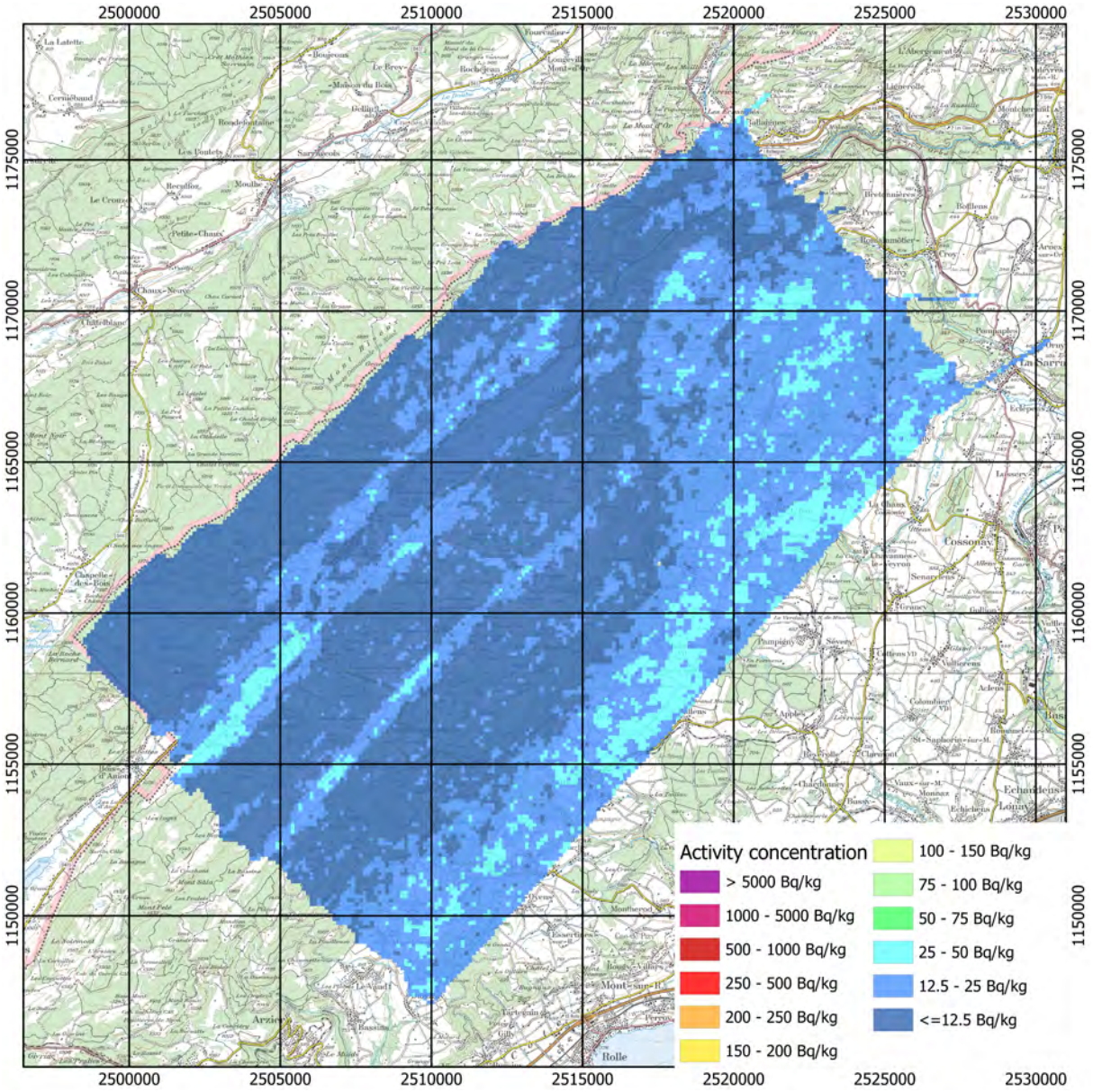

Figure 46: ^{232}Th activity concentration measured over the region around Lac de Joux. Geodaten©swisstopo.

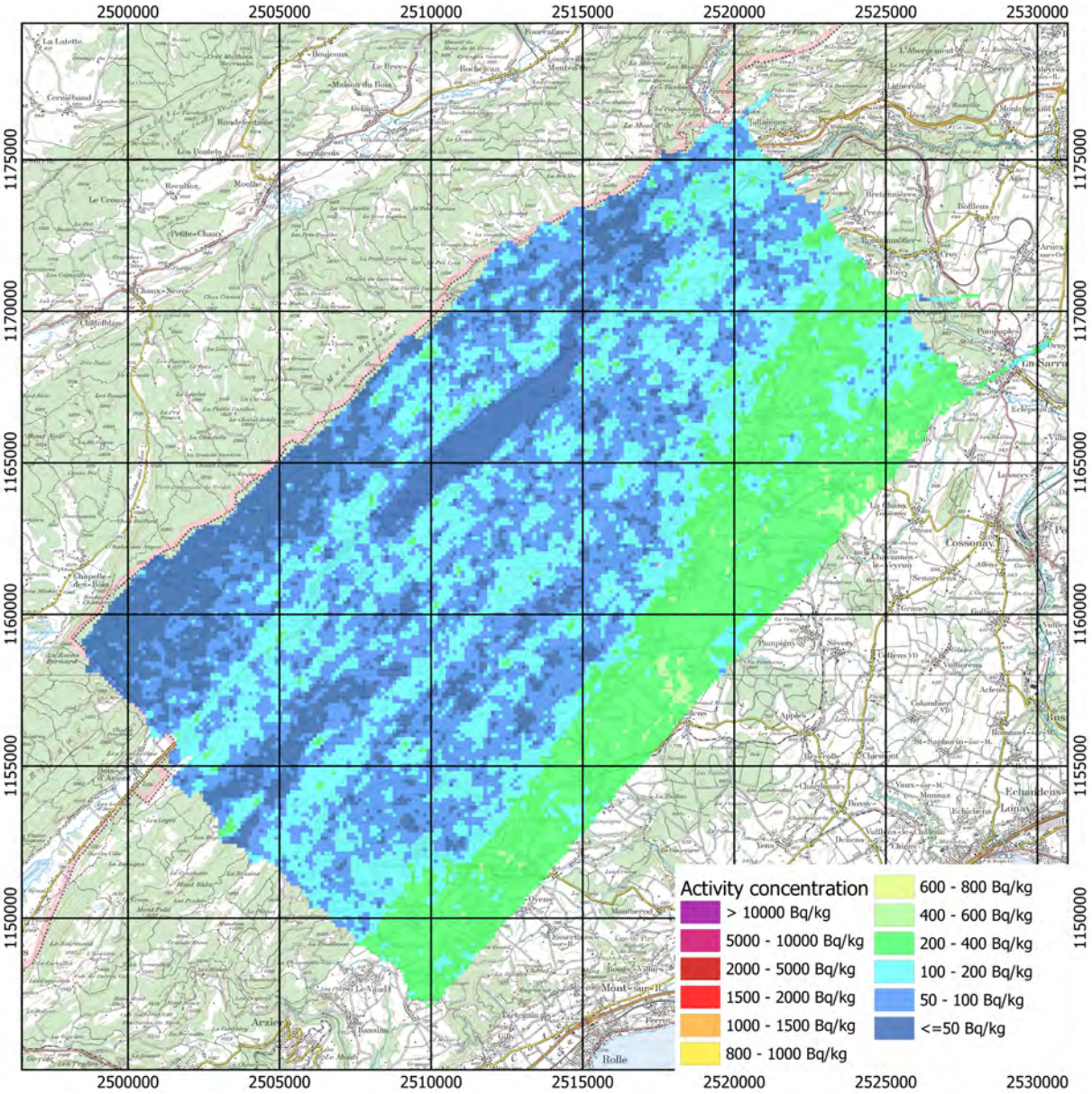

Figure 47: ^{40}K activity concentration measured over the region around Lac de Joux. Geodaten©swisstopo.

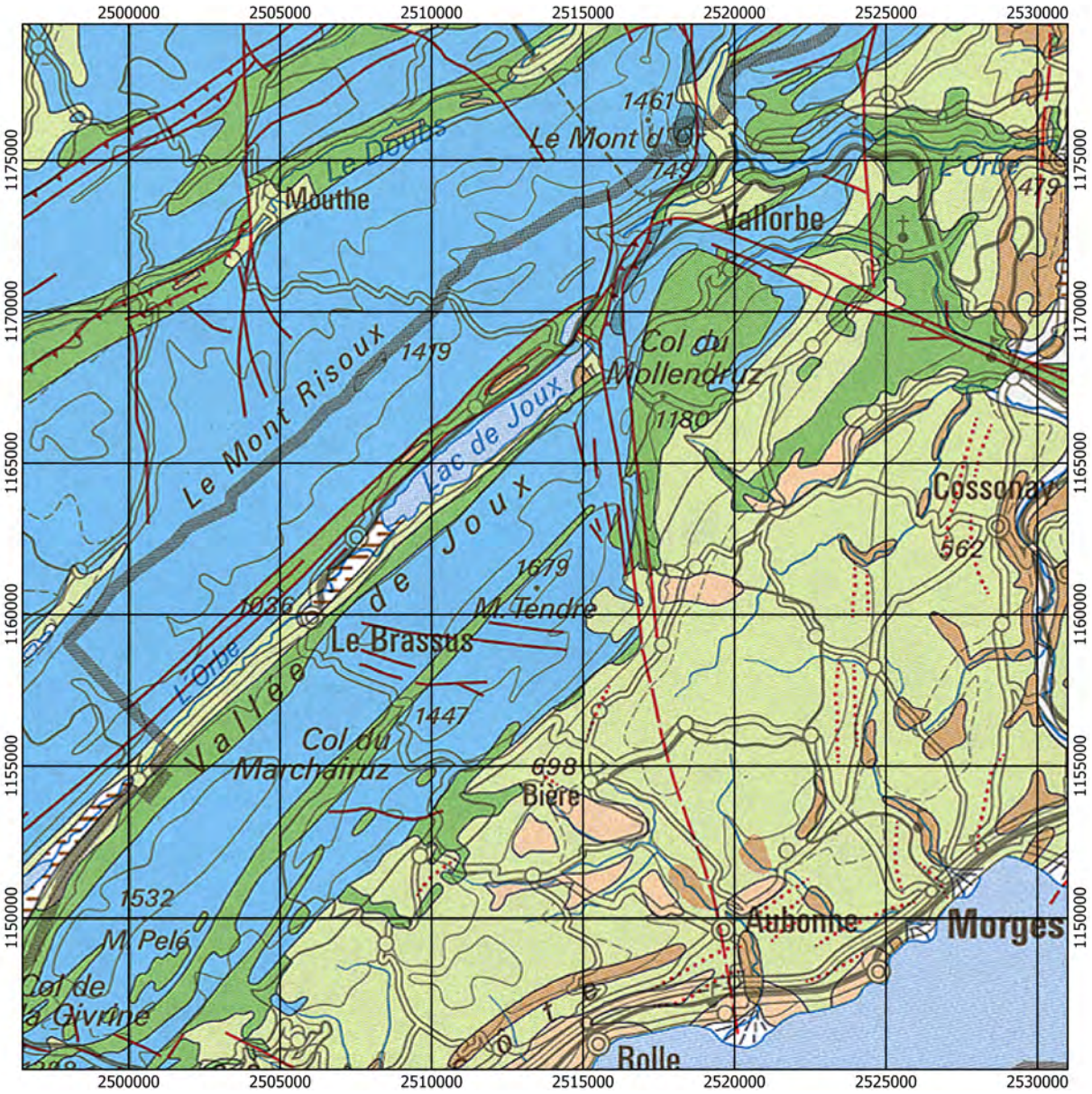

Figure 48: Geology of the region around Lac de Joux. The legend to the map is identical to the legend for the region around Nyon depicted in Figure 35. Geodaten©swisstopo.

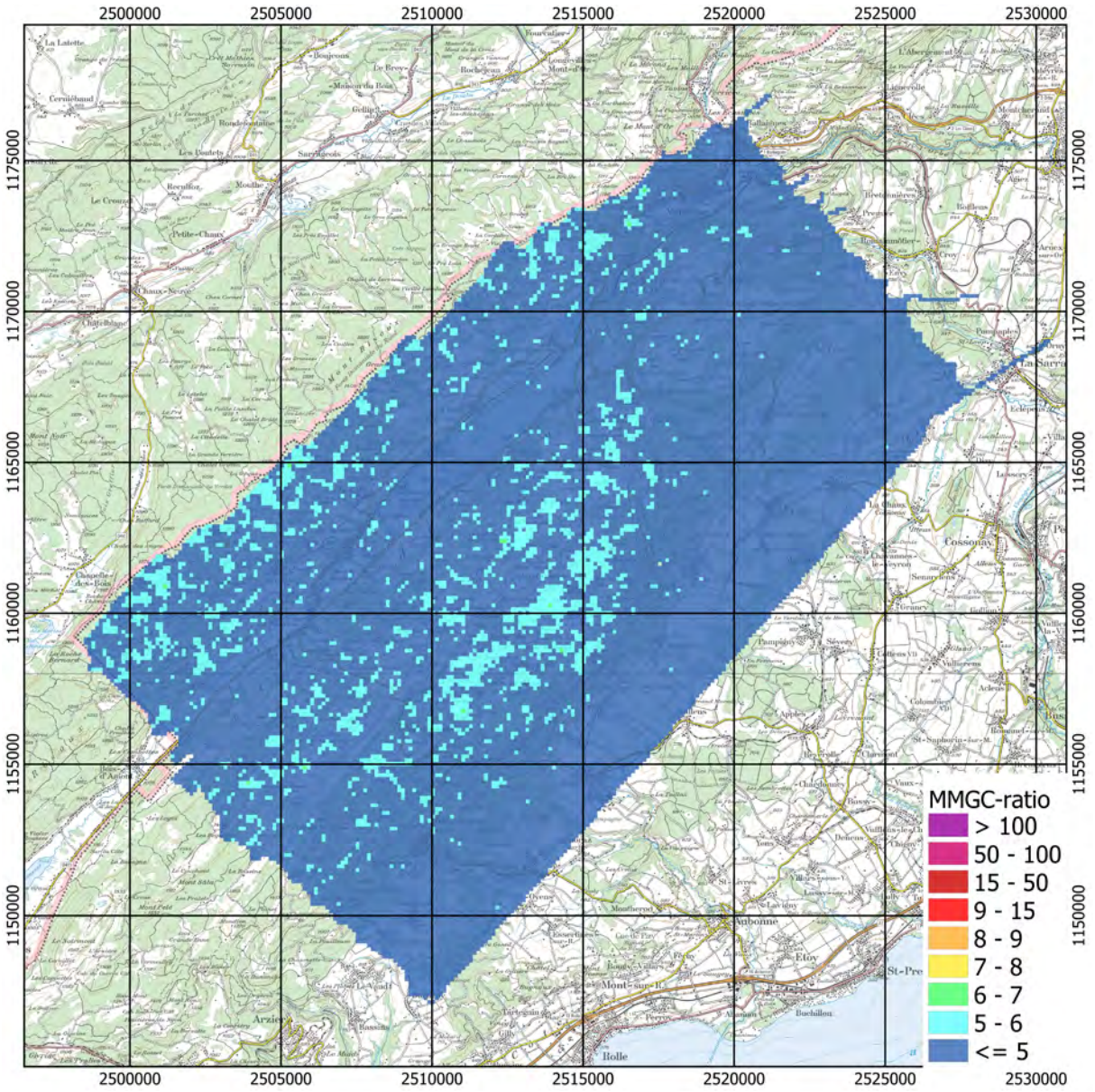

Figure 49: Man-made gross count (MMGC) ratio over the region around Lac de Joux. Geodaten©swisstopo.

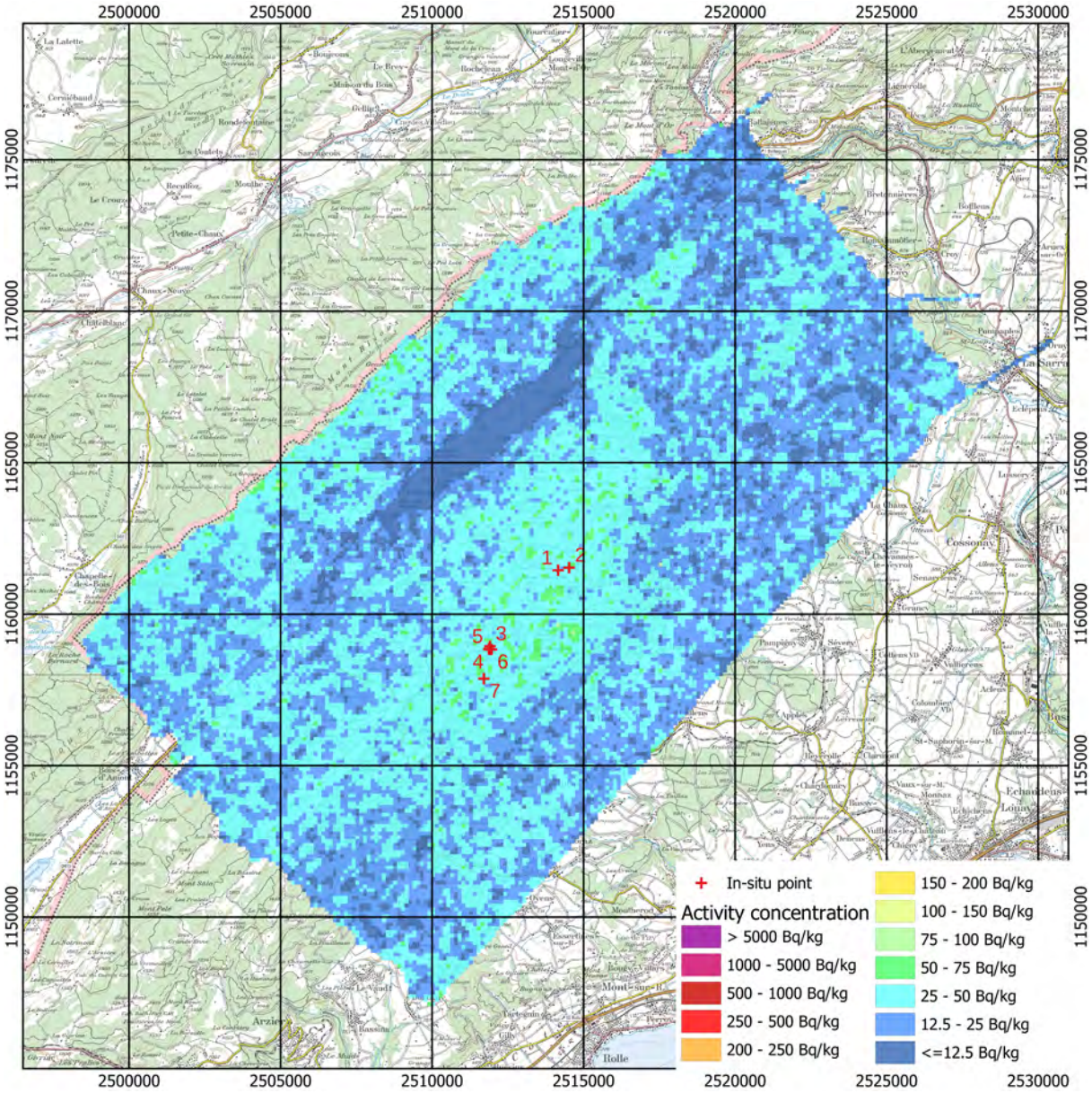

Figure 50: ^{137}Cs activity concentration measured over the region around Lac de Joux. Locations of in-situ gamma-spectrometric measurements are marked with red crosses. Geodaten©swisstopo.

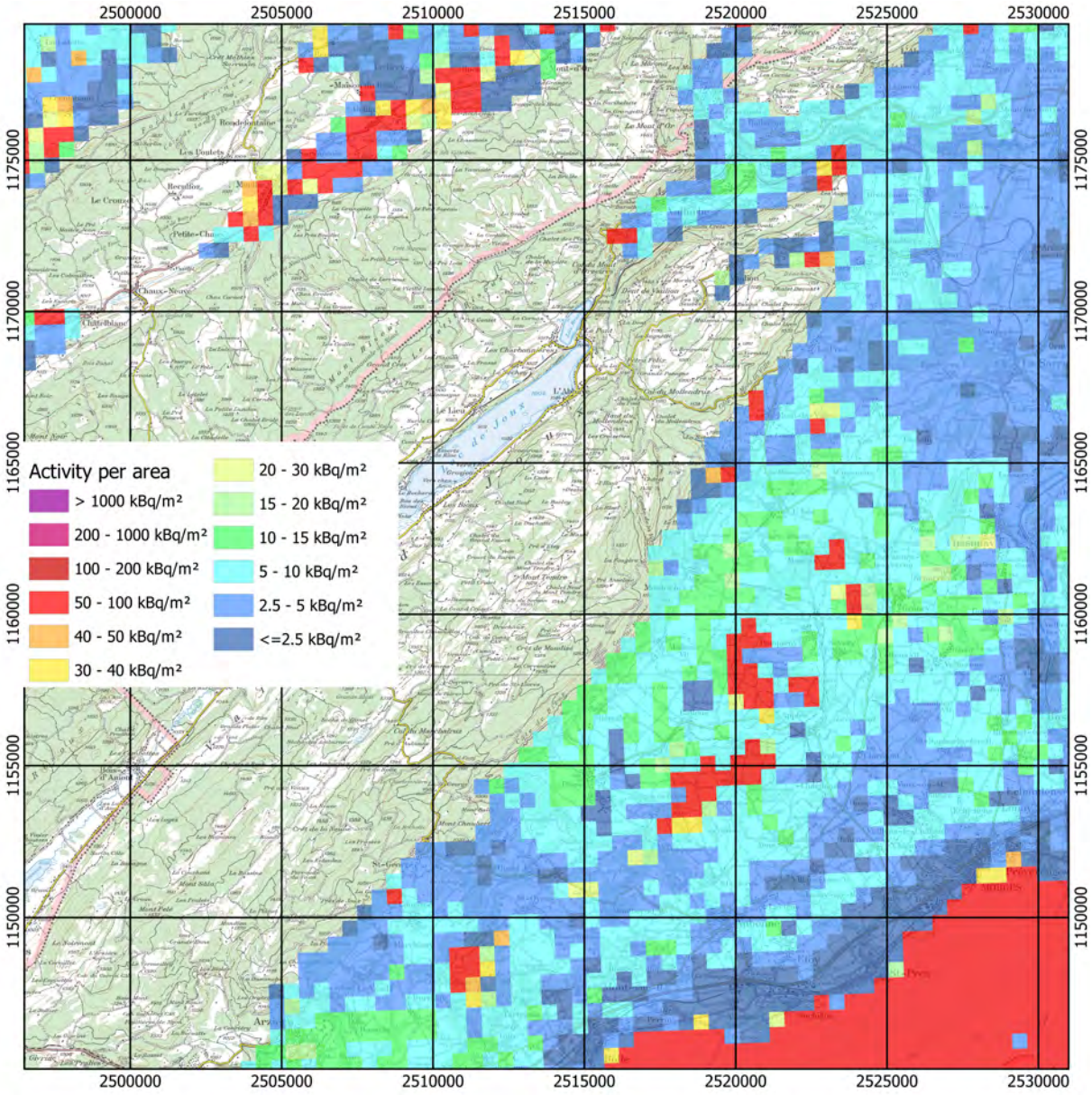

Figure 51: Total ^{137}Cs activity per area in the region around Lac de Joux 2009 taken from baseline map. Geodaten©swisstopo, Caesium activity per area from Meusburger et al., 2020, provided electronically by ESDAC (Paganos et al. 2012).

2.4.3 Canton Ticino

Several small areas in Swiss Canton Ticino with elevated ^{137}Cs activity concentrations were inspected in southern Switzerland. The maps of total dose rate (Figures 52, 57, 62, 67, 72 and 77) show values which are influenced by the elevation of the measuring areas due to the altitude dependent cosmic dose rate contribution. The maps of the ^{232}Th activity concentration depict typical values for Swiss soils (Figures 53, 58, 63, 68, 73 and 78). Whereas no obvious signal in the MMGC-ratio can be observed in the measuring areas (Figures 54, 61, 64, 71, 74 and 79), maps of the ^{137}Cs activity concentration indicate some elevated concentrations (Figures 55, 59, 65, 69, 75 and 80). These elevated ^{137}Cs activity concentrations are chiefly found in forested sectors of the measurement areas. Excerpts of the baseline map of Meusburger et al., 2020 (Figures 56, 60, 66, 70, 76 and 81) are displayed for comparison in all inspected areas.

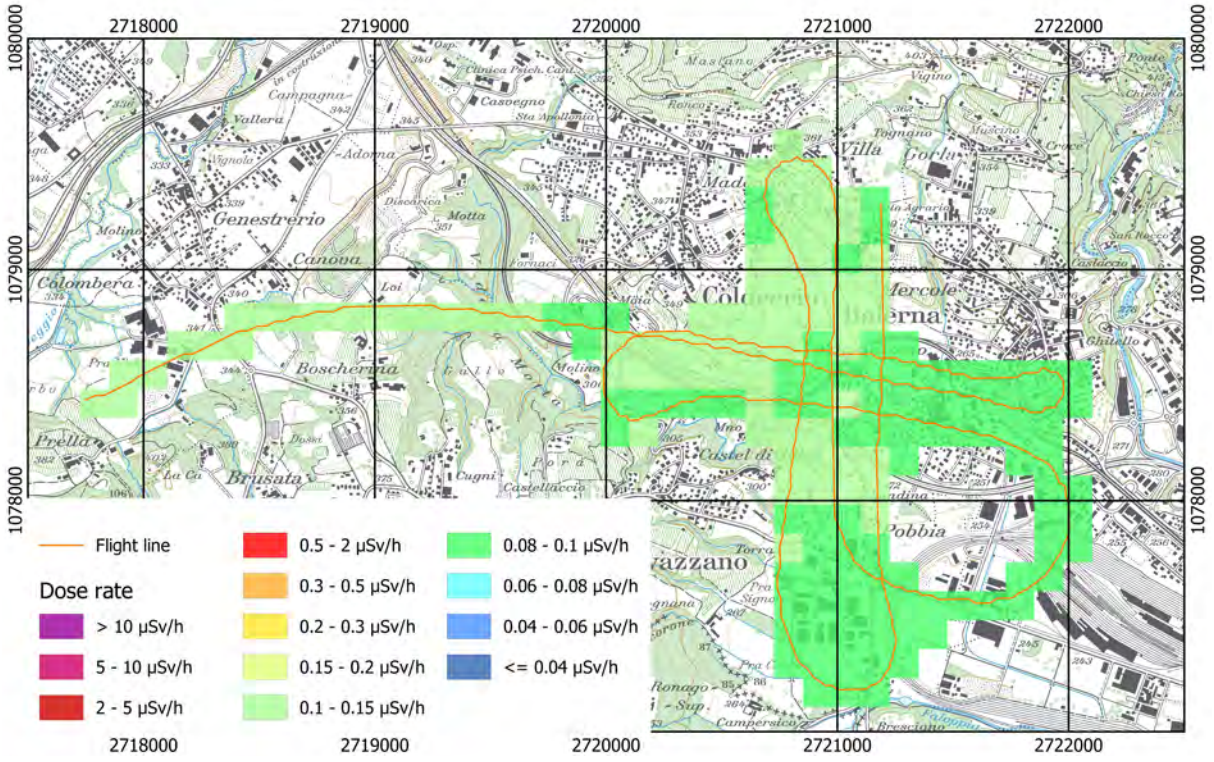

Figure 52: Dose rate over Balerna. Geodaten©swisstopo.

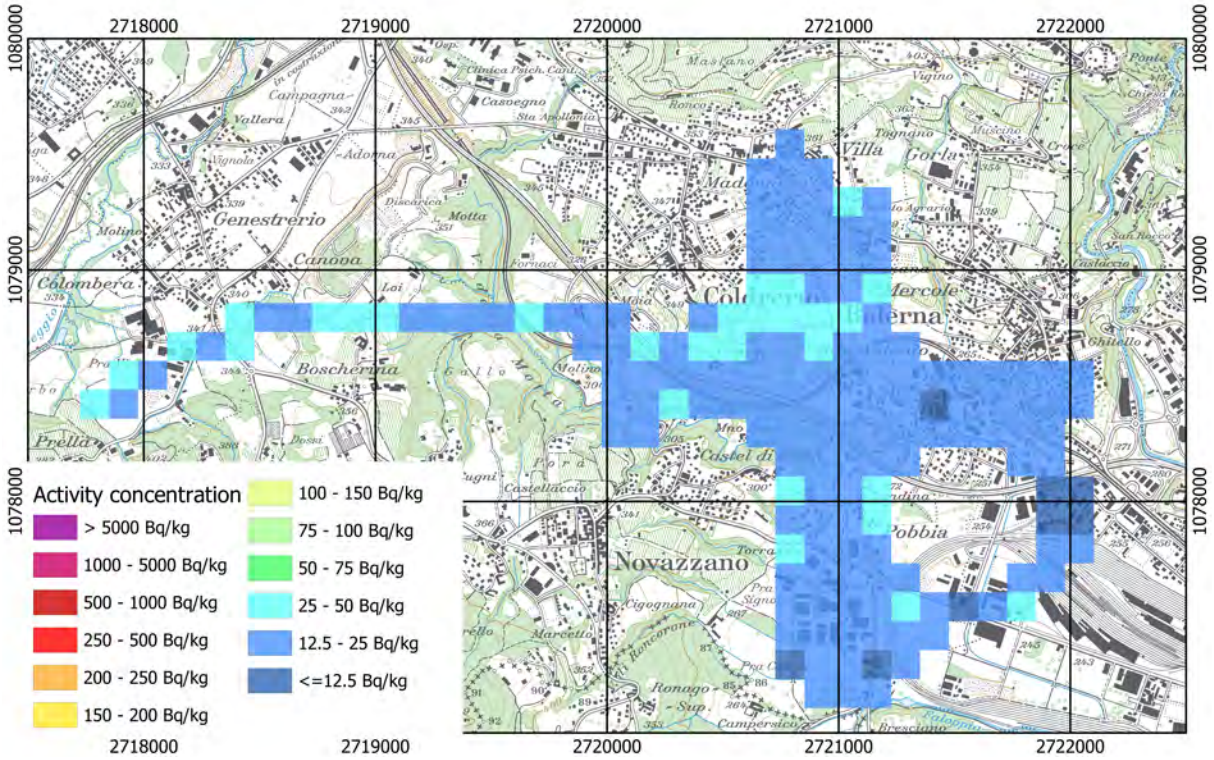

Figure 53: ^{232}Th activity concentration measured over Balerna. Geodaten©swisstopo.

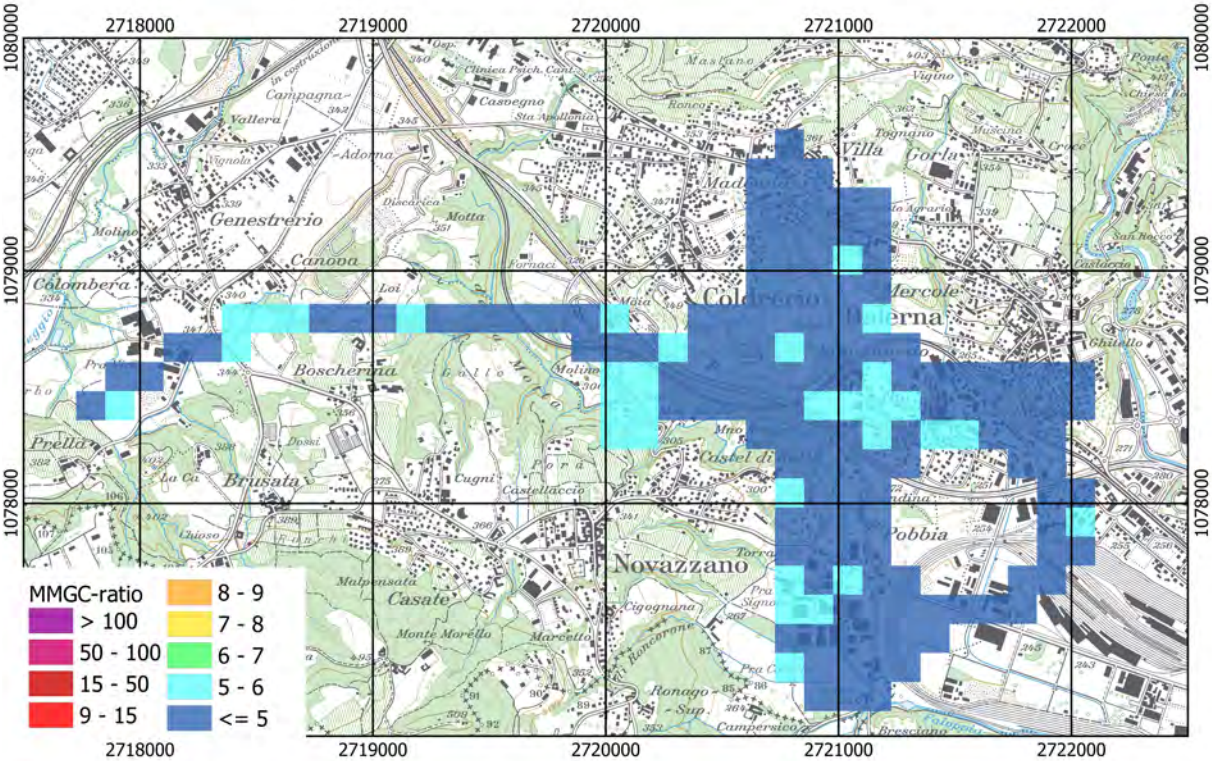

Figure 54: Man-made gross count (MMGC) ratio over Balerna. Geodaten©swisstopo.

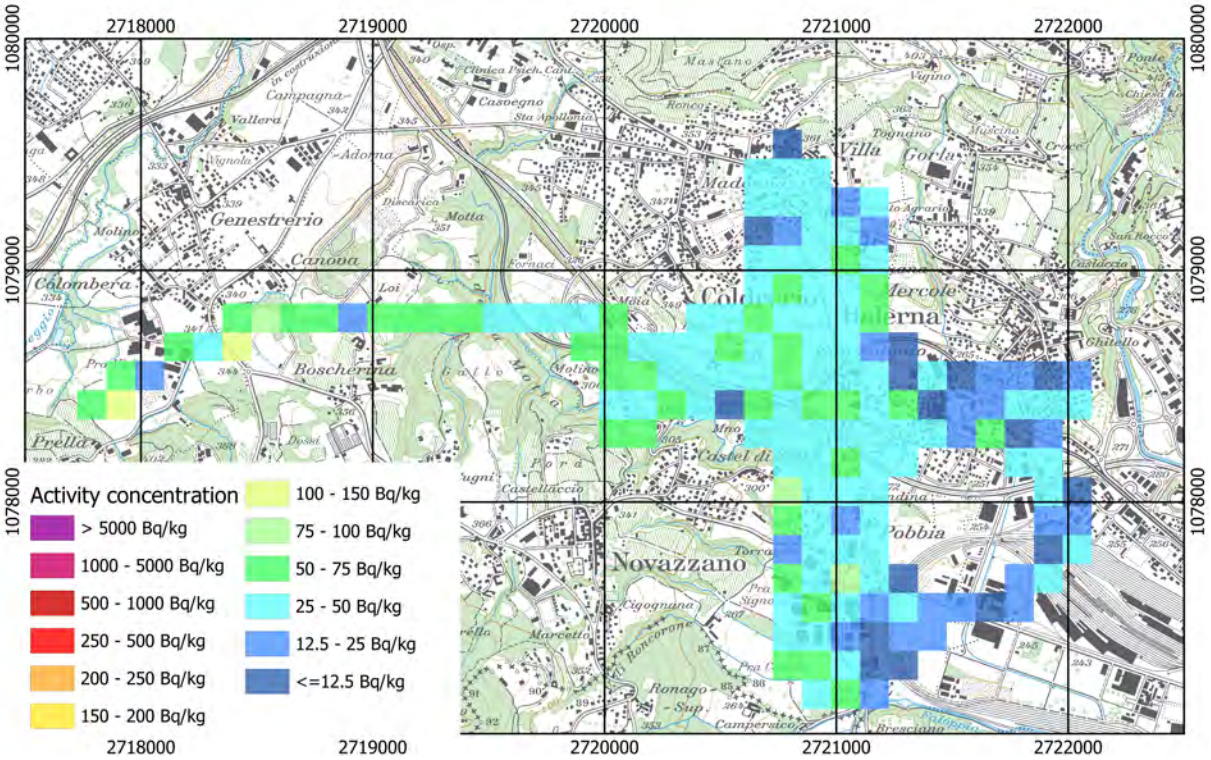

Figure 55: ^{137}Cs activity concentration measured over Balerna. Geodaten©swisstopo.

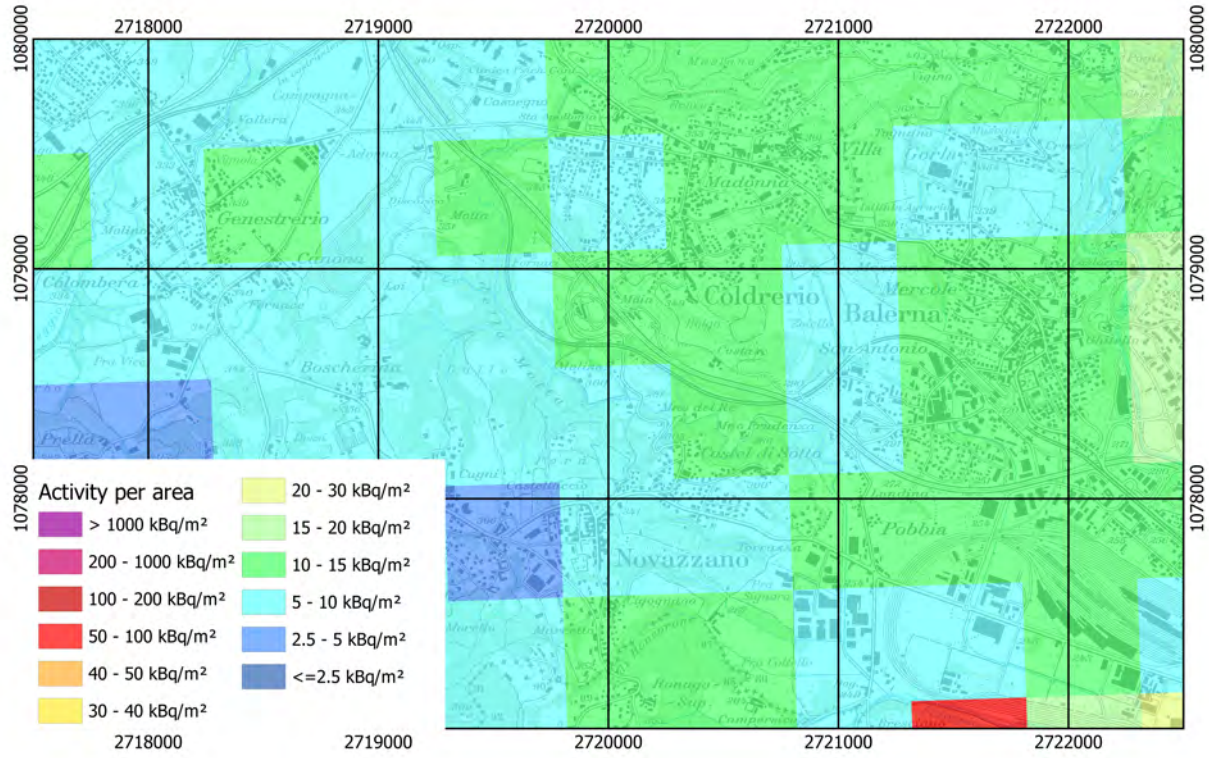

Figure 56: ^{137}Cs activity per area over Balerna 2009 taken from baseline map. Geodaten©swisstopo, Caesium activity per area from Meusburger et al., 2020, provided electronically by ESDAC (Paganos et al. 2012).

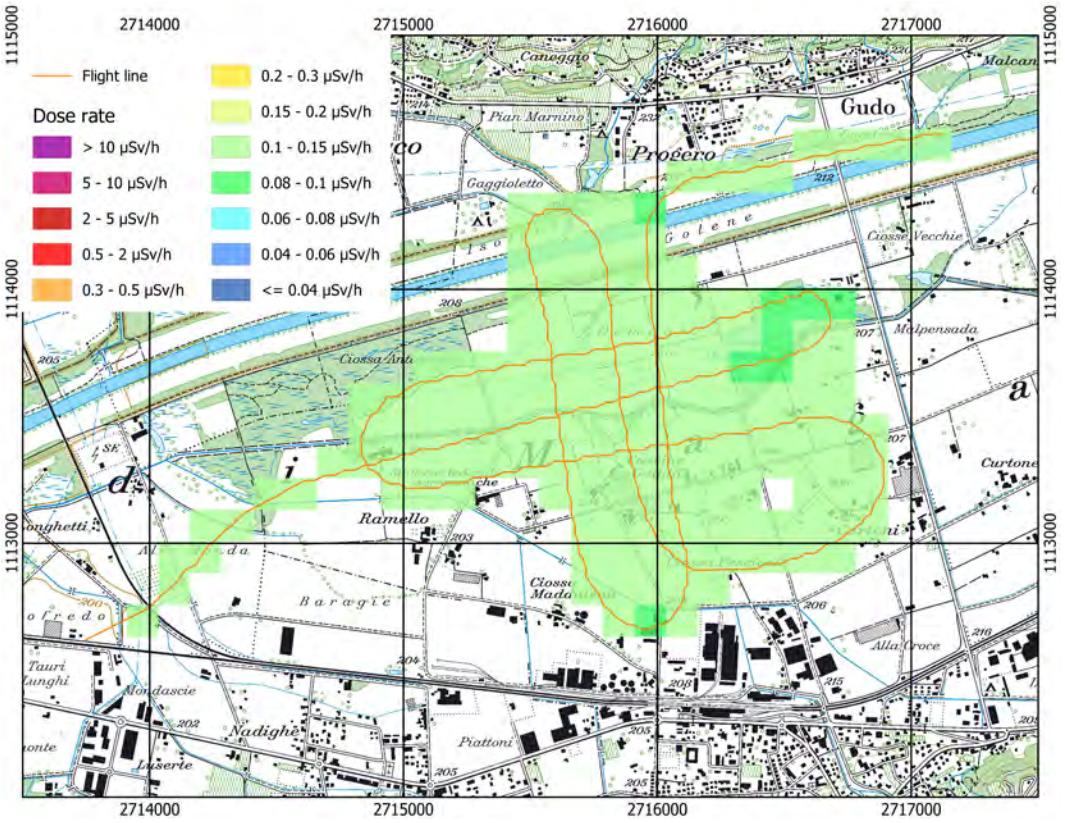

Figure 57: Dose rate over Demanio. Geodaten©swisstopo.

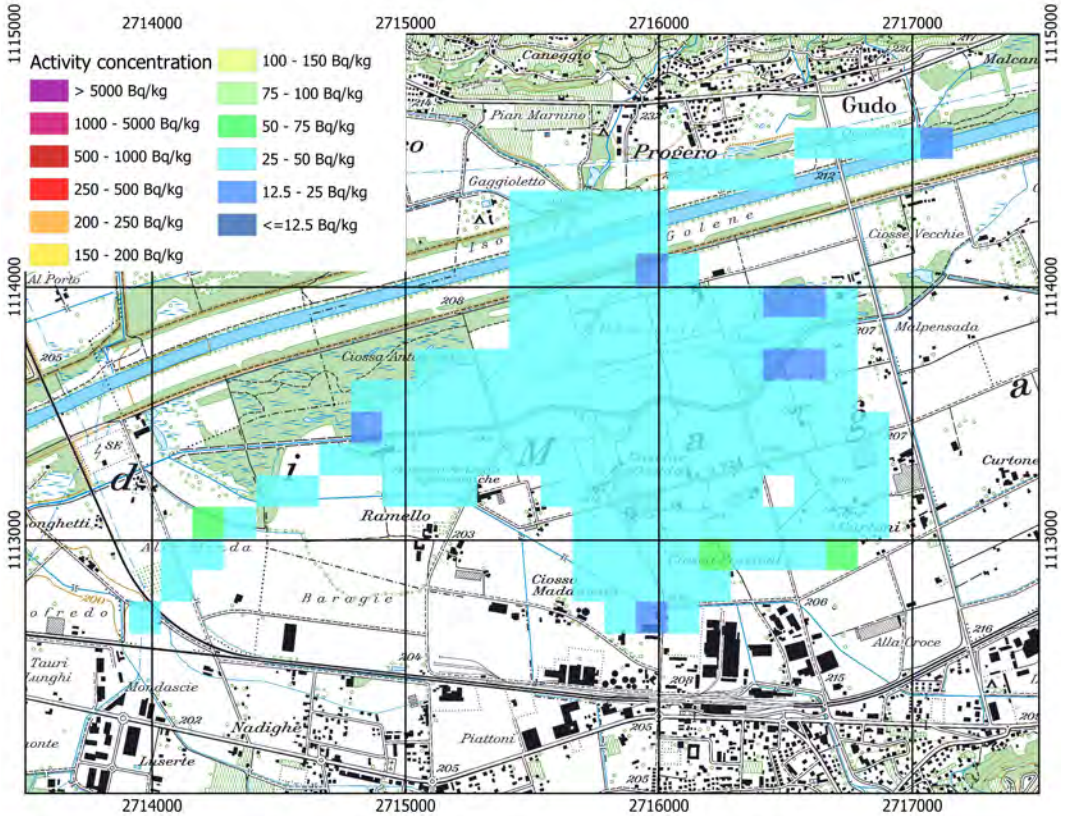

Figure 58: ^{232}Th activity concentration measured over Demanio. Geodaten©swisstopo.

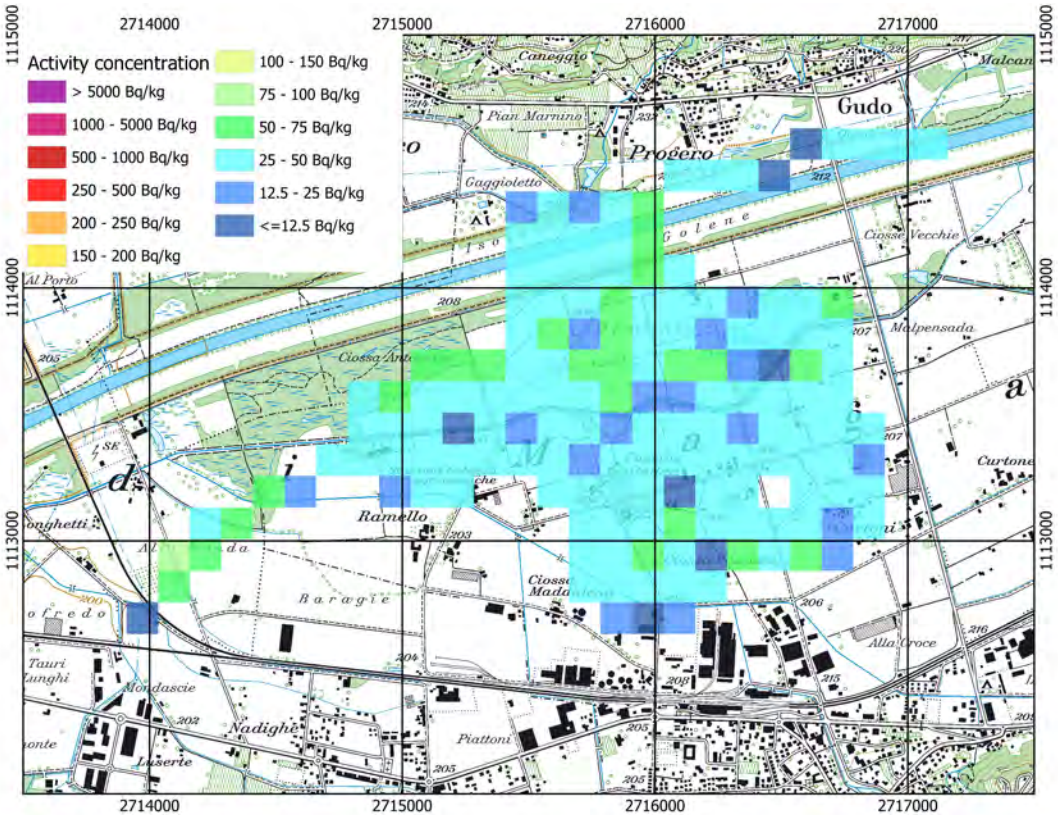

Figure 59: ^{137}Cs activity concentration measured over Demanio. Geodaten©swisstopo.

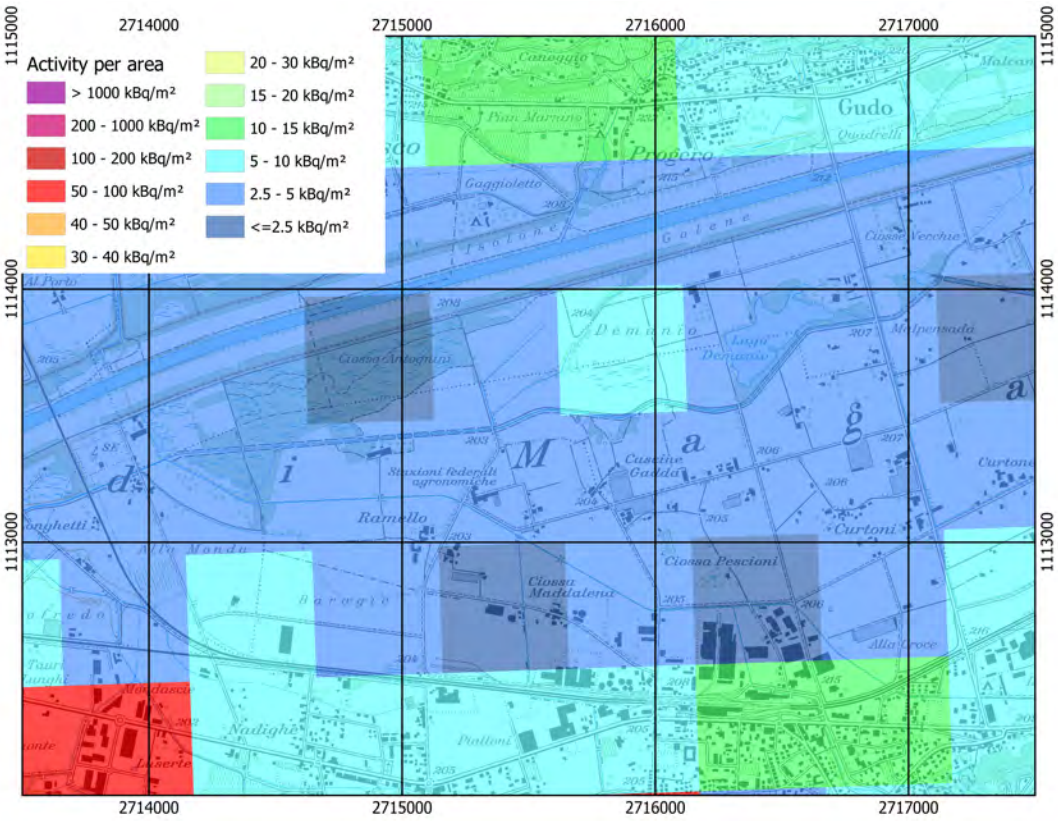

Figure 60: ^{137}Cs activity per area over Demanio 2009 taken from baseline map. Geodaten©swisstopo, Caesium activity per area from Meusburger et al., 2020, provided electronically by ESDAC (Paganos et al. 2012).

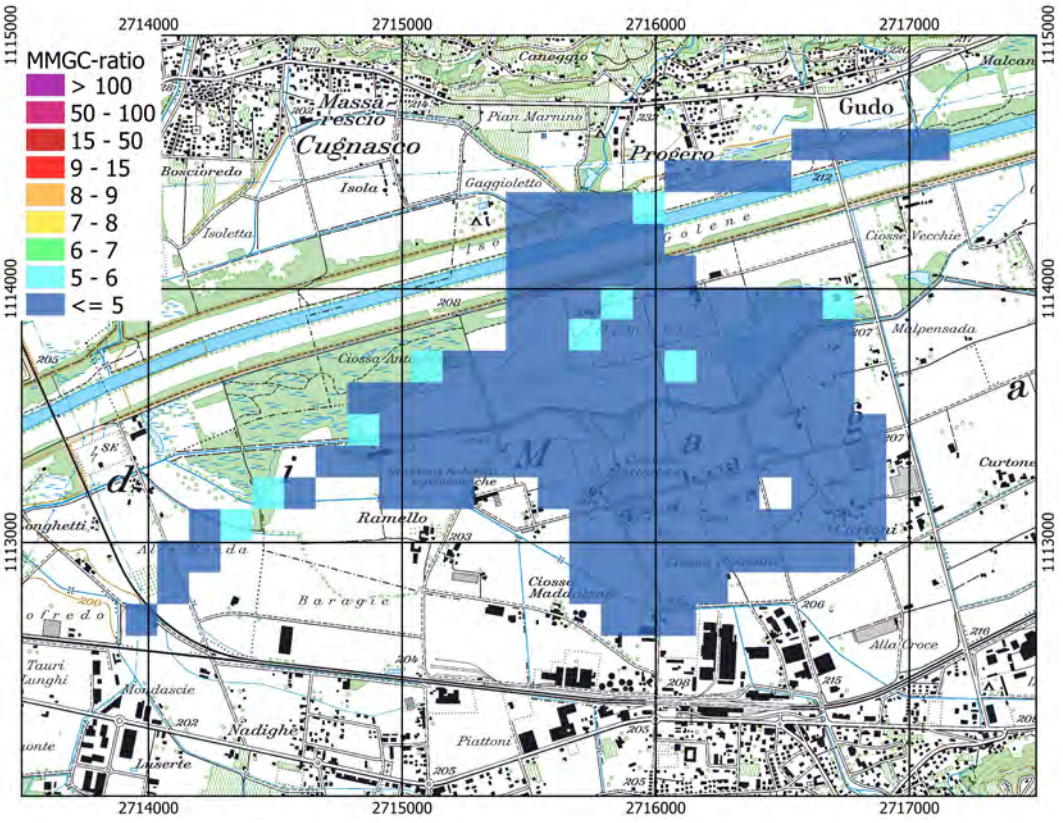

Figure 61: Man-made gross count (MMGC) ratio over Demanio. Geodaten©swisstopo.

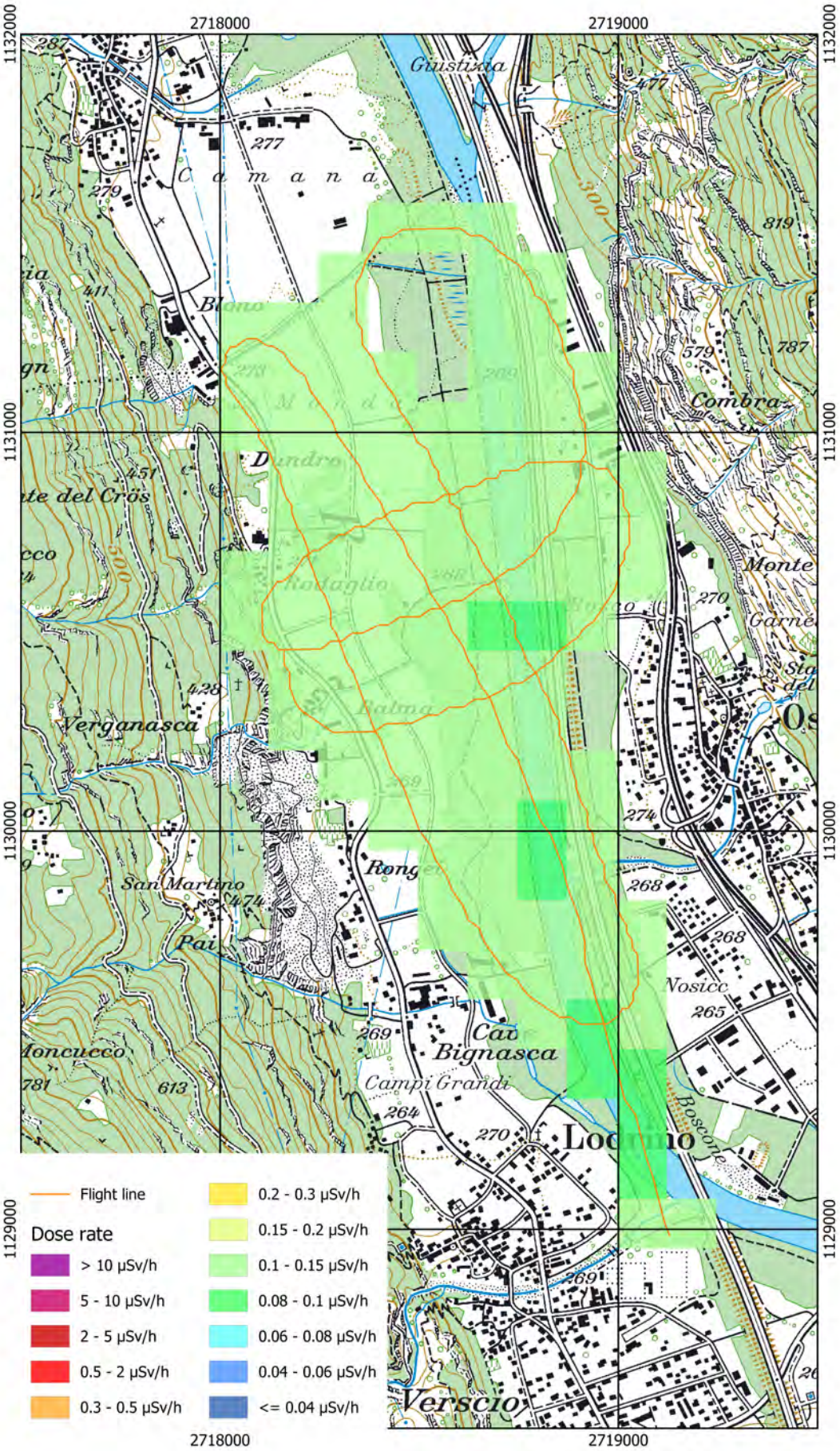

Figure 62: Dose rate near Lodrino. Geodaten©swisstopo.

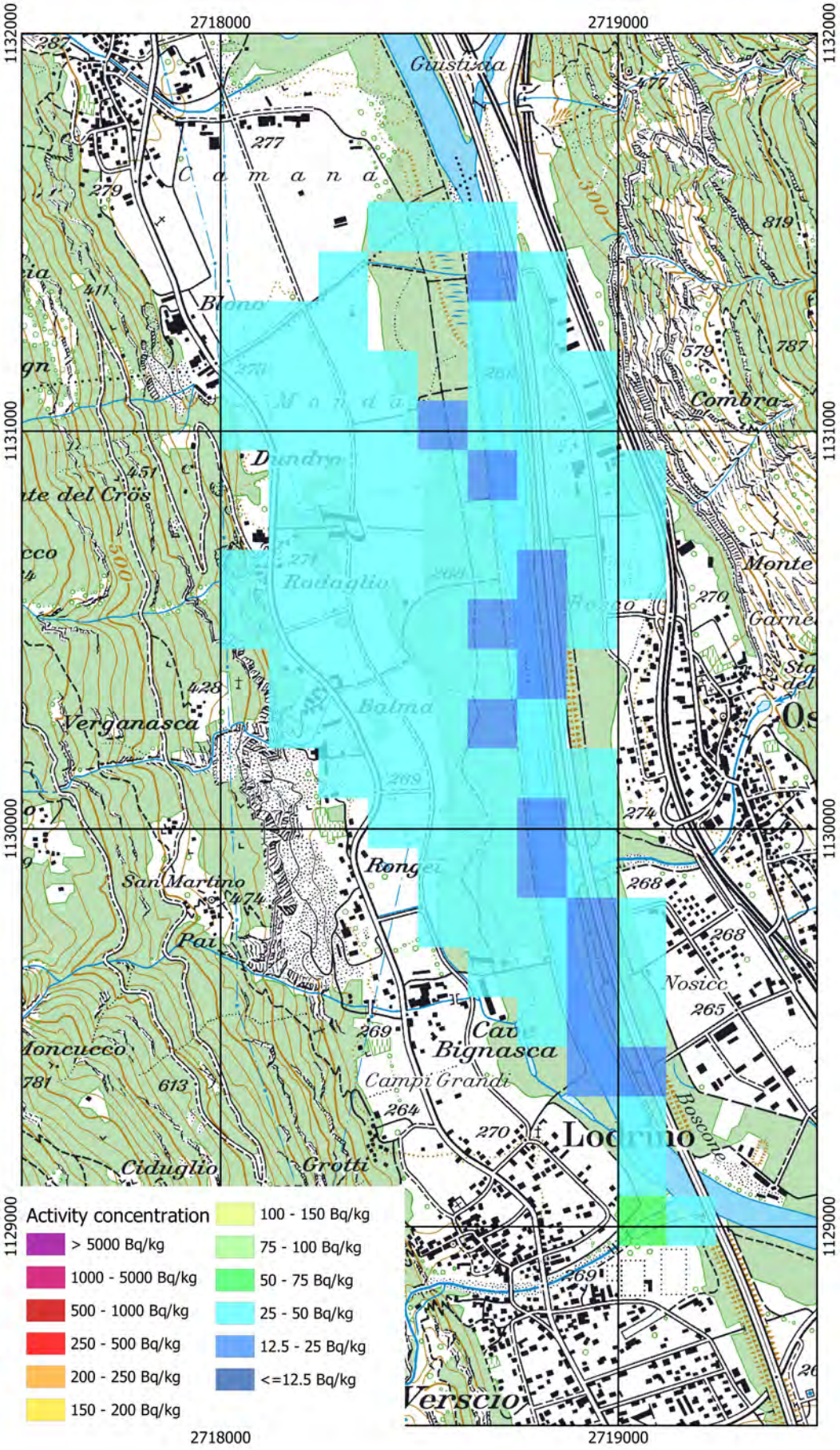

Figure 63: ^{232}Th activity concentration measured near Lodrino. Geodaten©swisstopo.

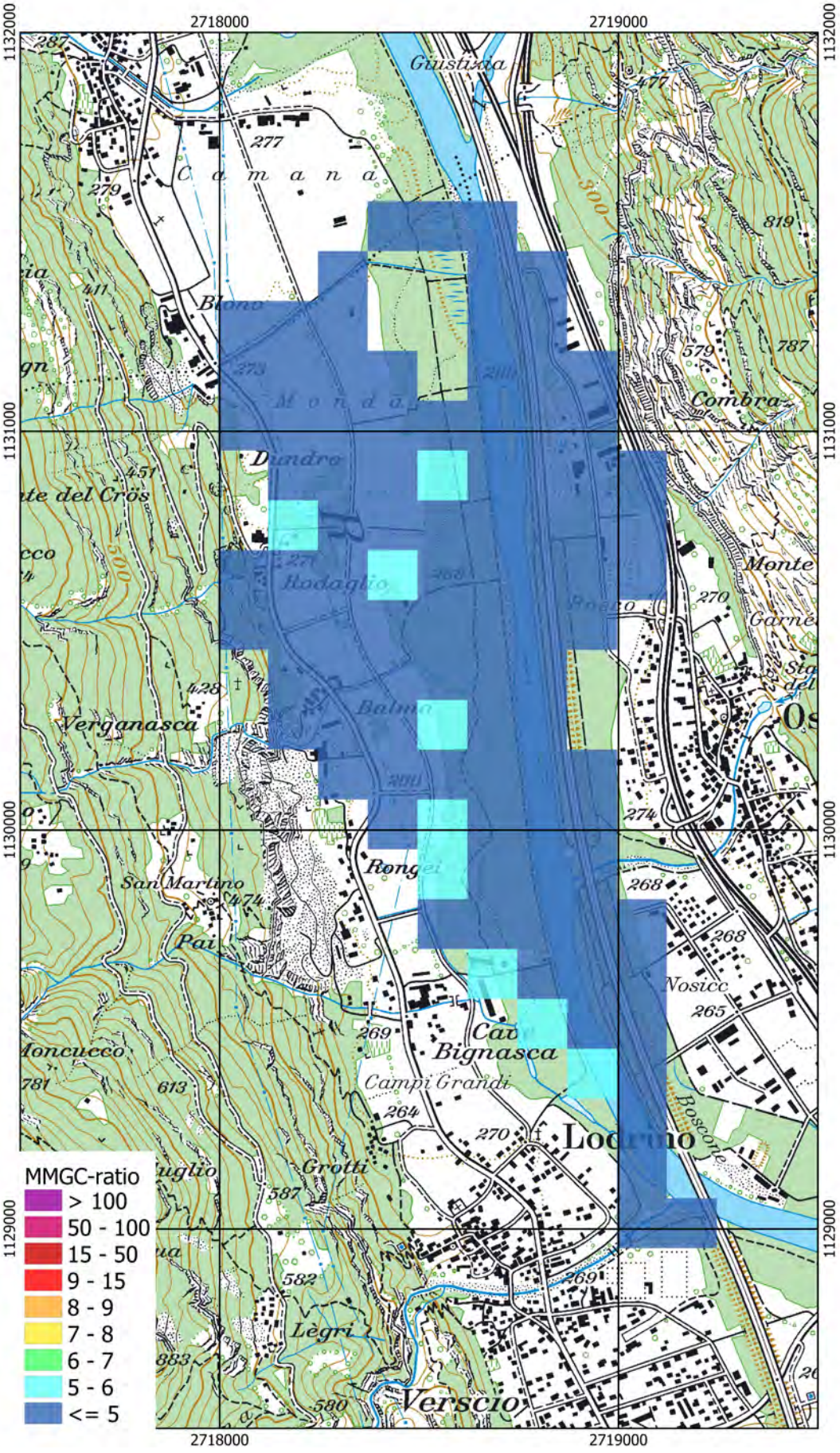

Figure 64: Man-made gross count (MMGC) ratio near Lodrino. Geodaten©swisstopo.

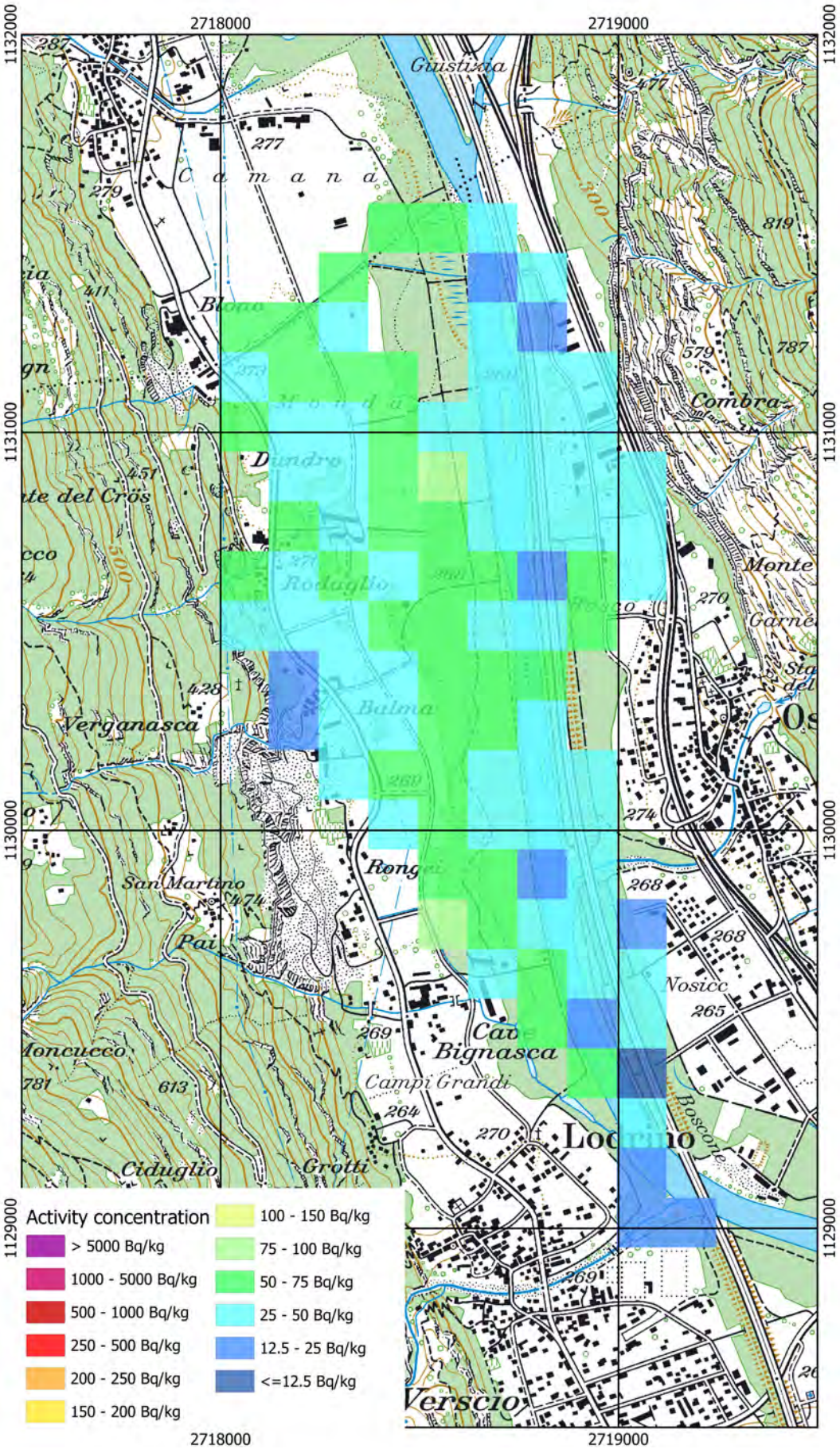

Figure 65: ^{137}Cs activity concentration measured near Lodrino. Geodaten©swisstopo.

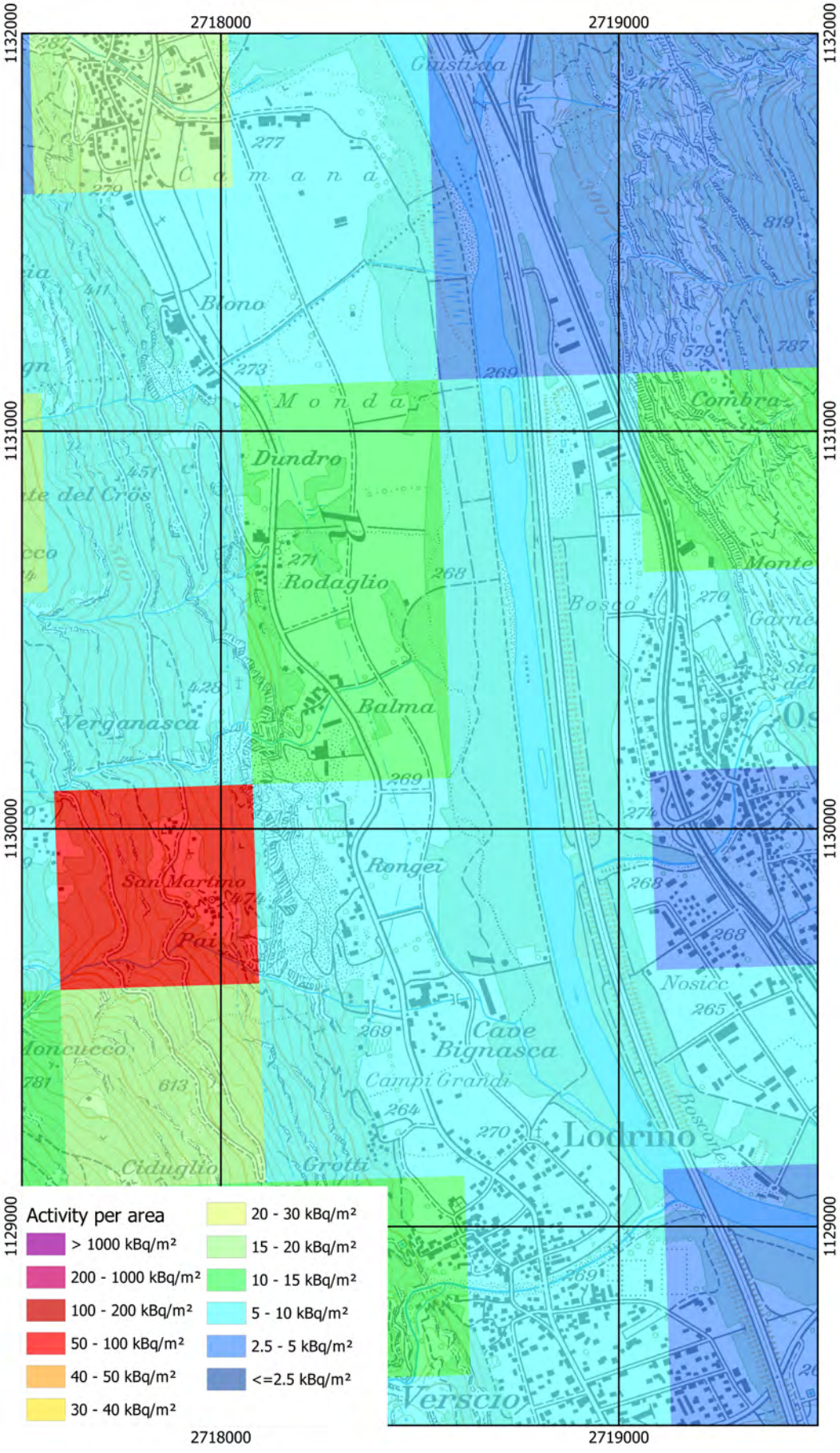

Figure 66: ^{137}Cs activity per area over Lodrino 2009 taken from baseline map. Geodaten©swisstopo, Caesium activity per area from Meusburger et al., 2020, provided electronically by ESDAC (Paganos et al. 2012).

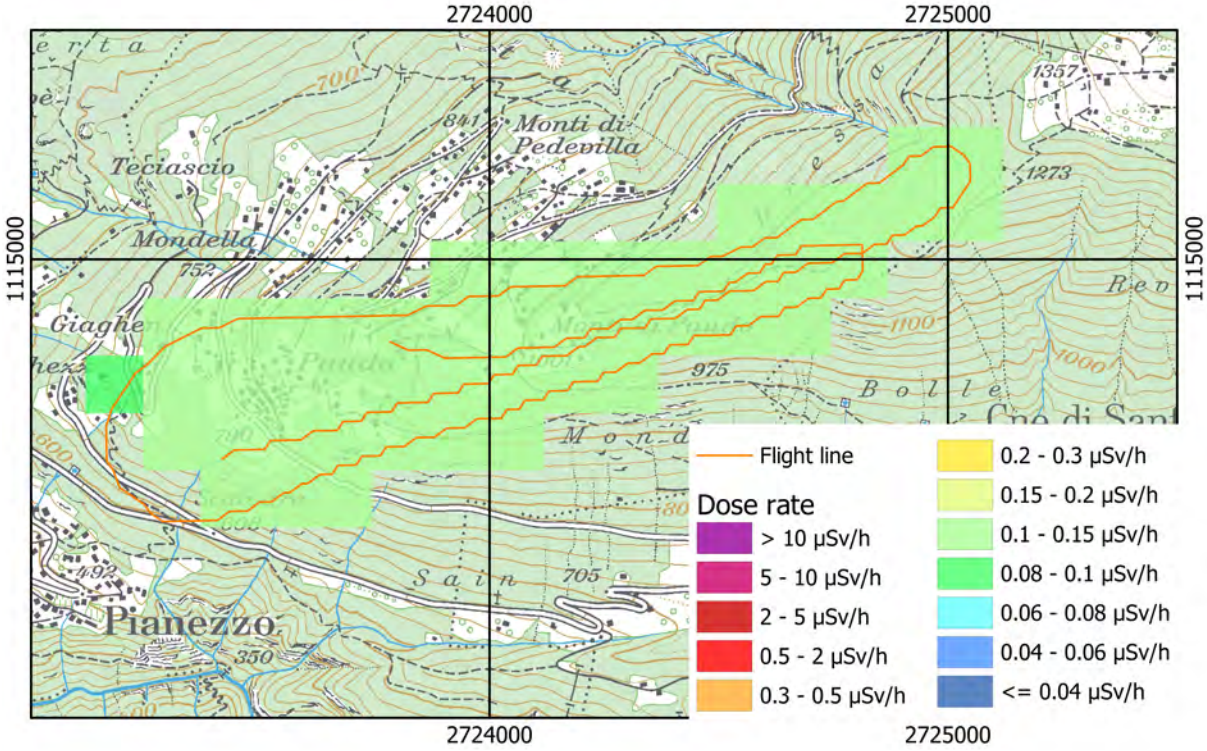

Figure 67: Dose rate at the Monti di Paudo. Geodaten©swisstopo.

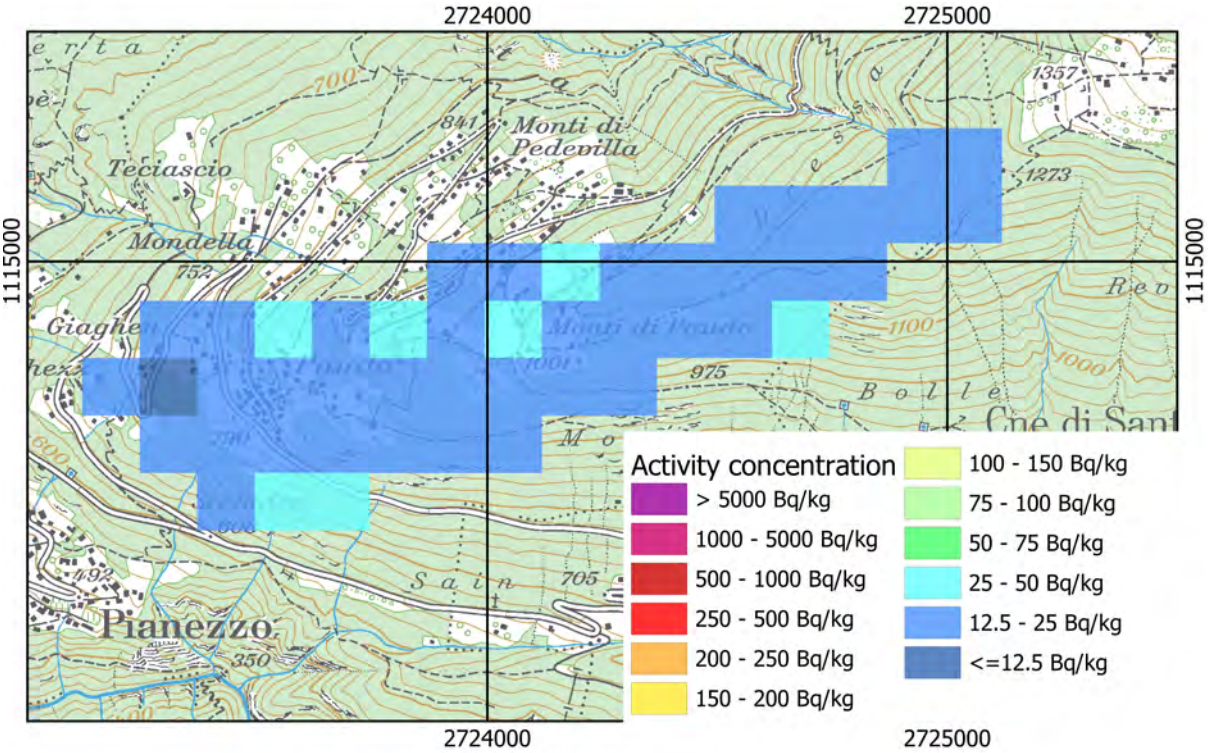

Figure 68: ^{232}Th activity concentration measured at the Monti di Paudo. Geodaten©swisstopo.

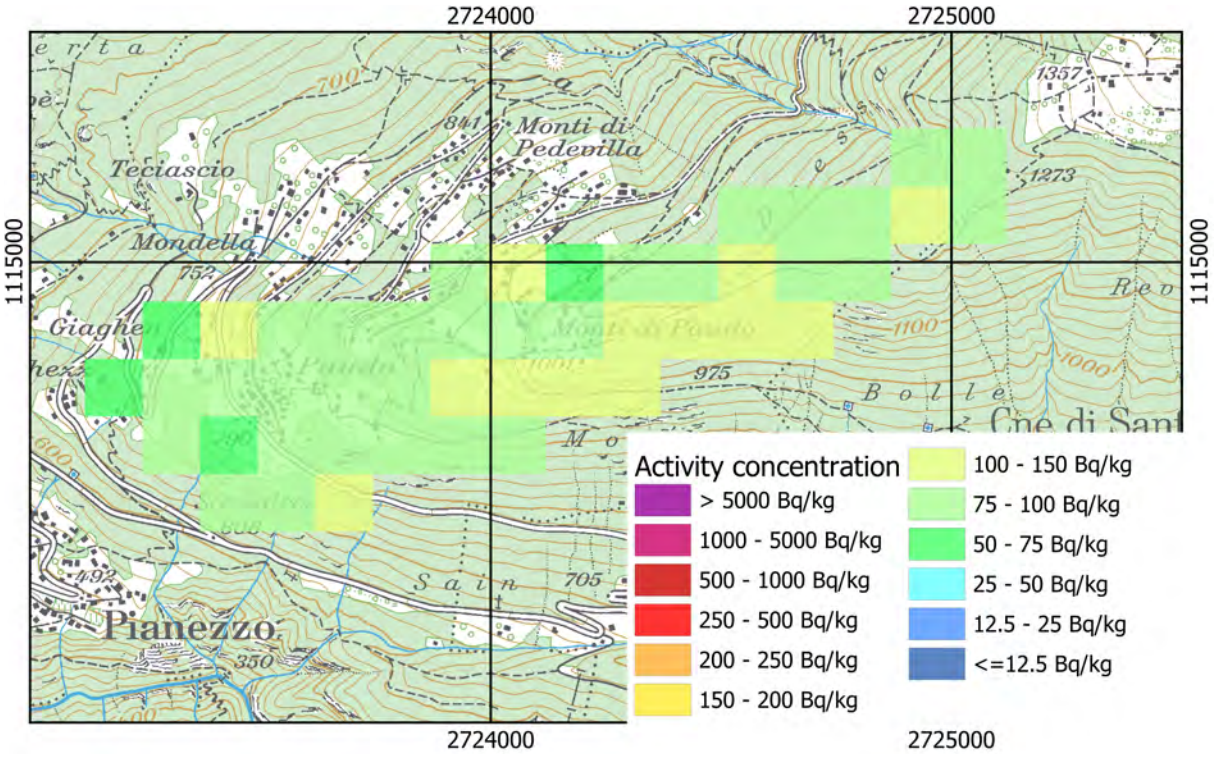

Figure 69: ^{137}Cs activity concentration measured at the Monti di Paudo. Geodaten©swisstopo.

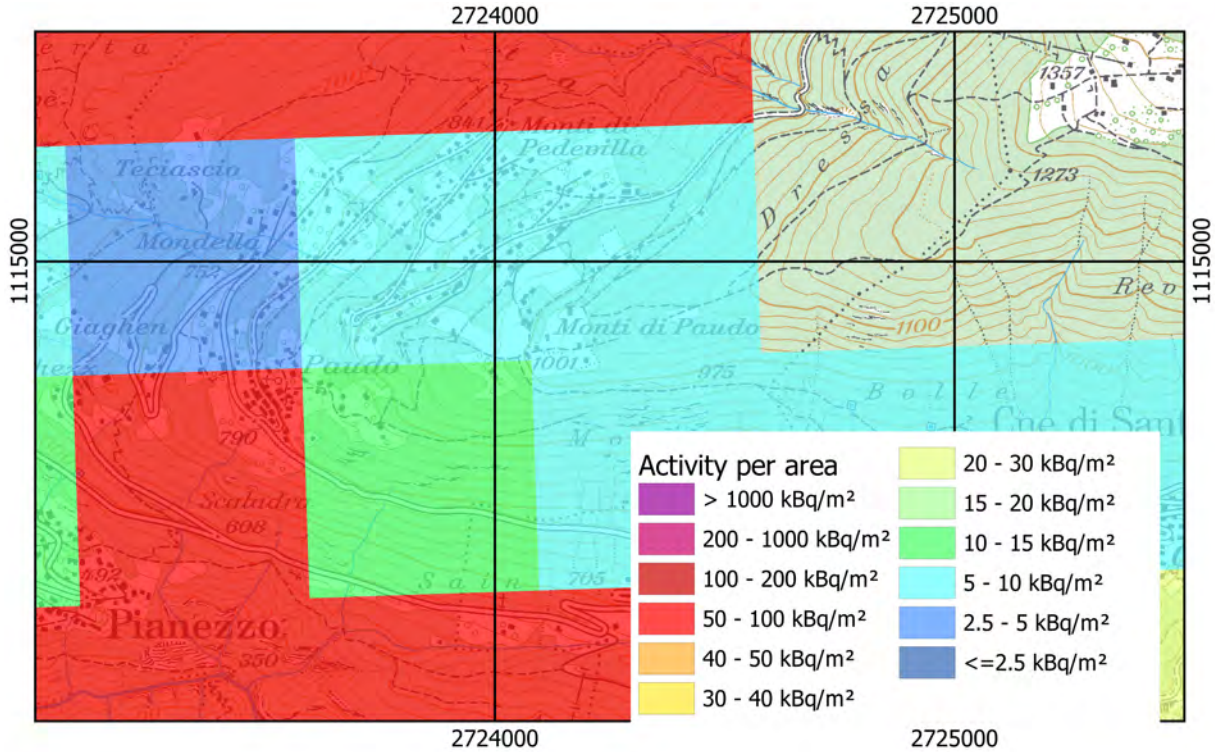

Figure 70: ^{137}Cs activity per area at the Monti di Paudo 2009 taken from baseline map. Geodaten©swisstopo, Caesium activity per area from Meusburger et al., 2020, provided electronically by ESDAC (Paganos et al. 2012).

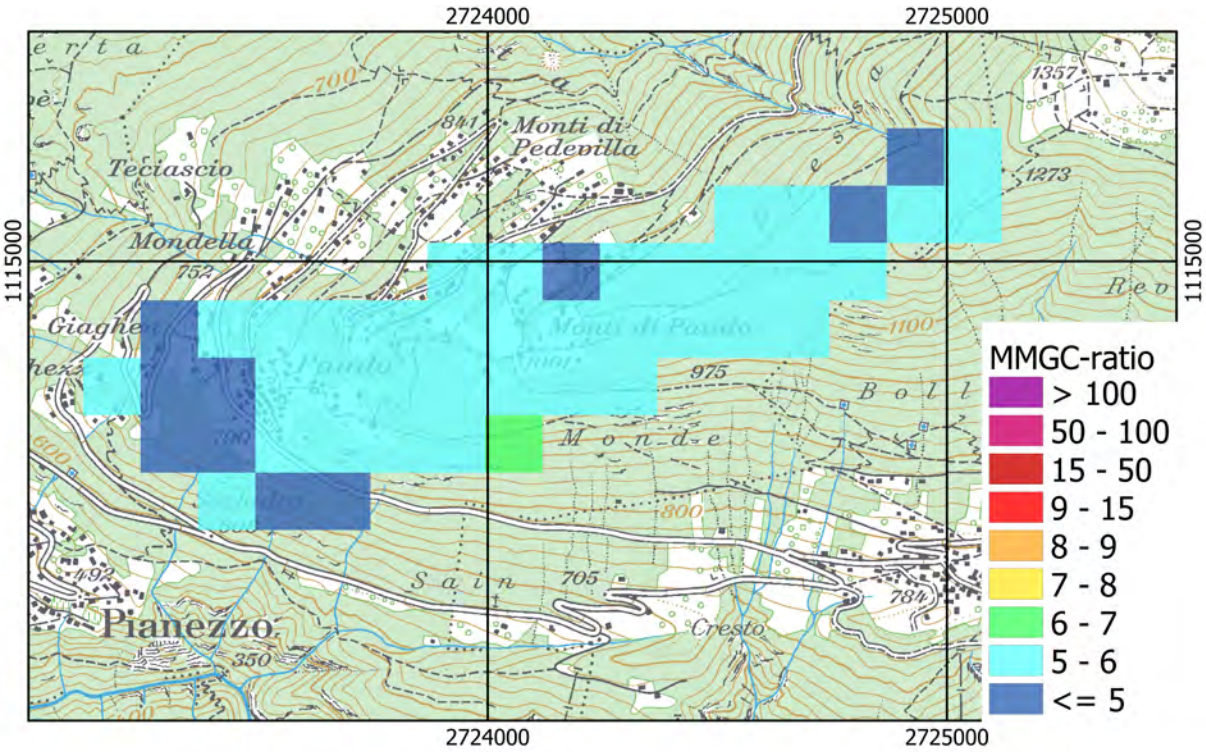

Figure 71: Man-made gross count (MMGC) ratio at the Monti di Paudo. Geodaten©swisstopo.

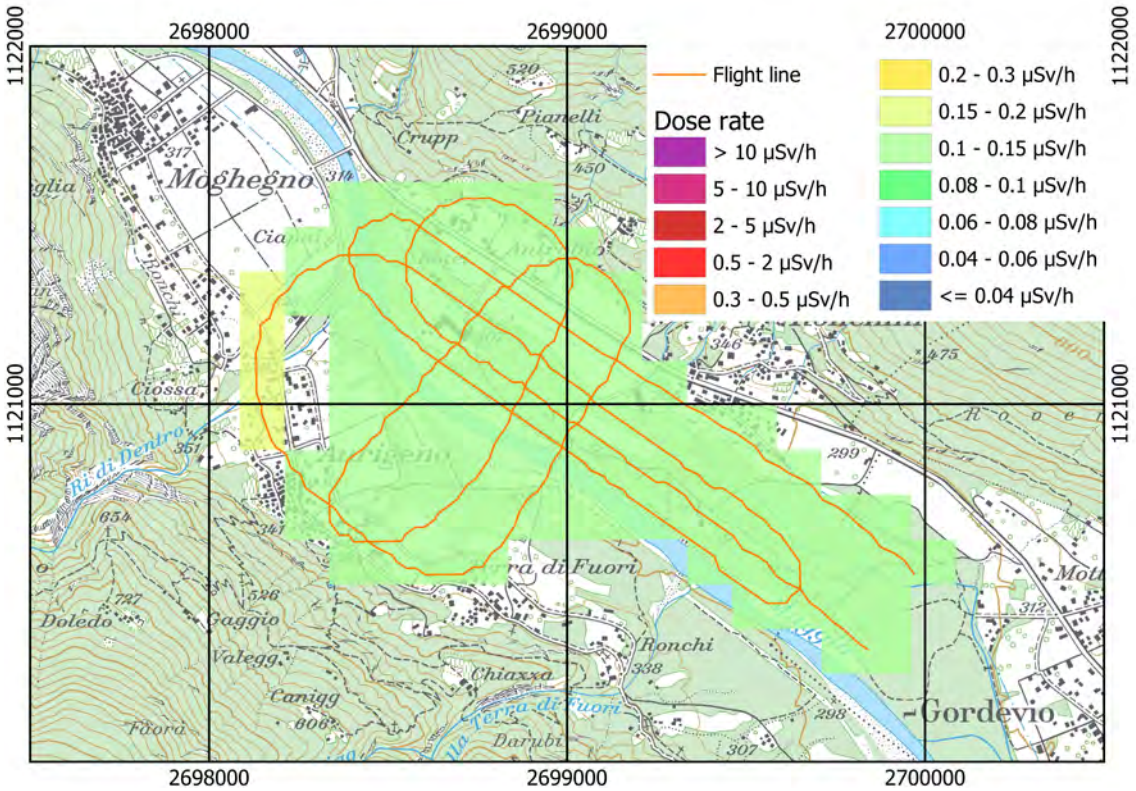

Figure 72: Dose rate over Ronchini. Geodaten©swisstopo.

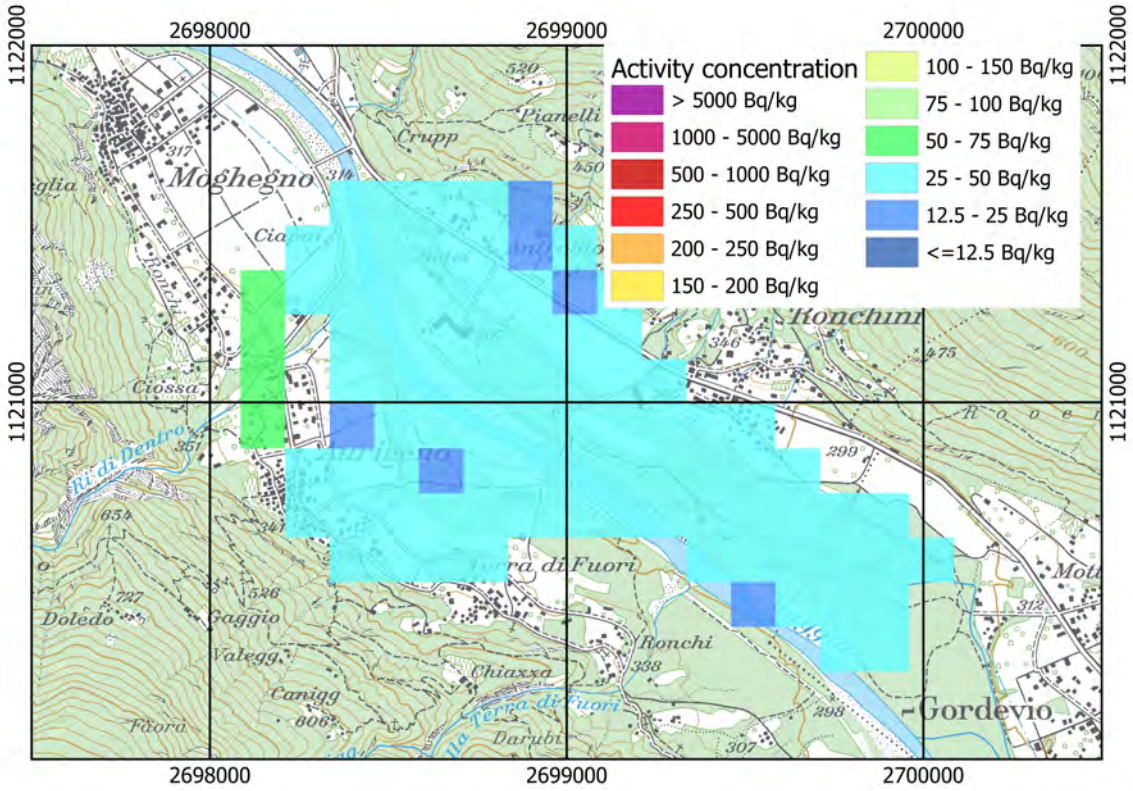

Figure 73: ^{232}Th activity concentration measured over Ronchini. Geodaten©swisstopo.

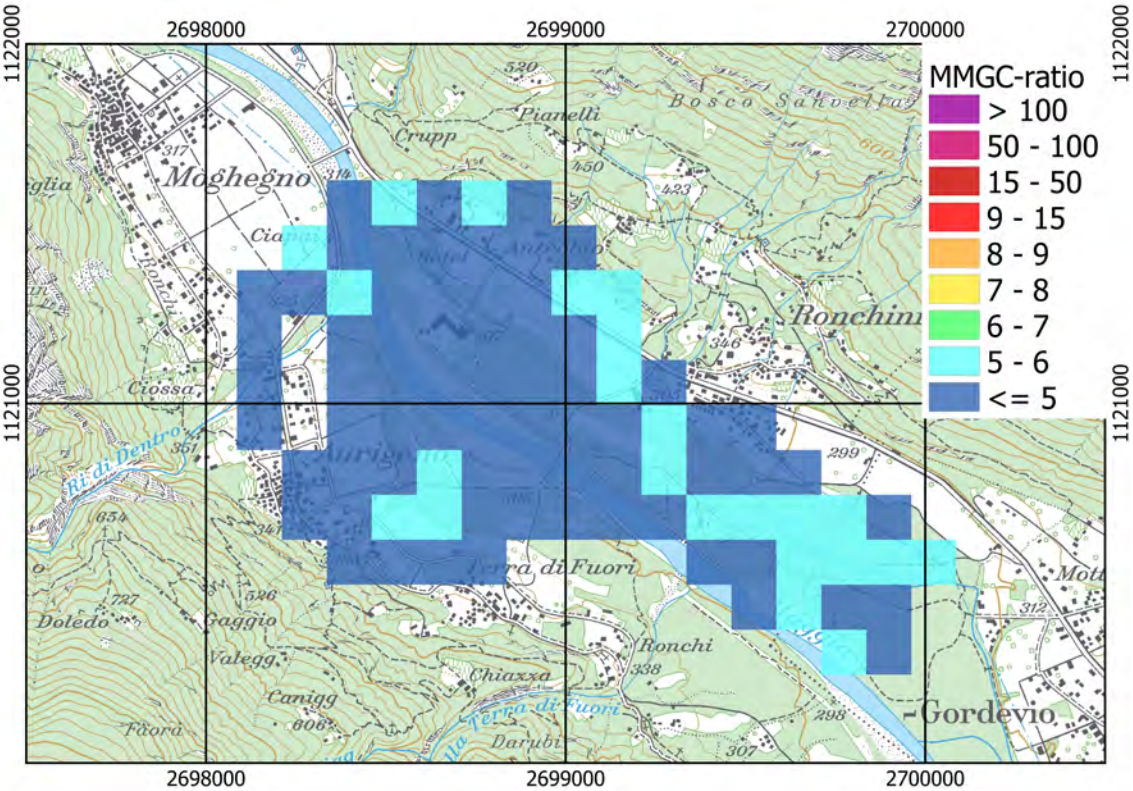

Figure 74: Man-made gross count (MMGC) ratio over Ronchini. Geodaten©swisstopo.

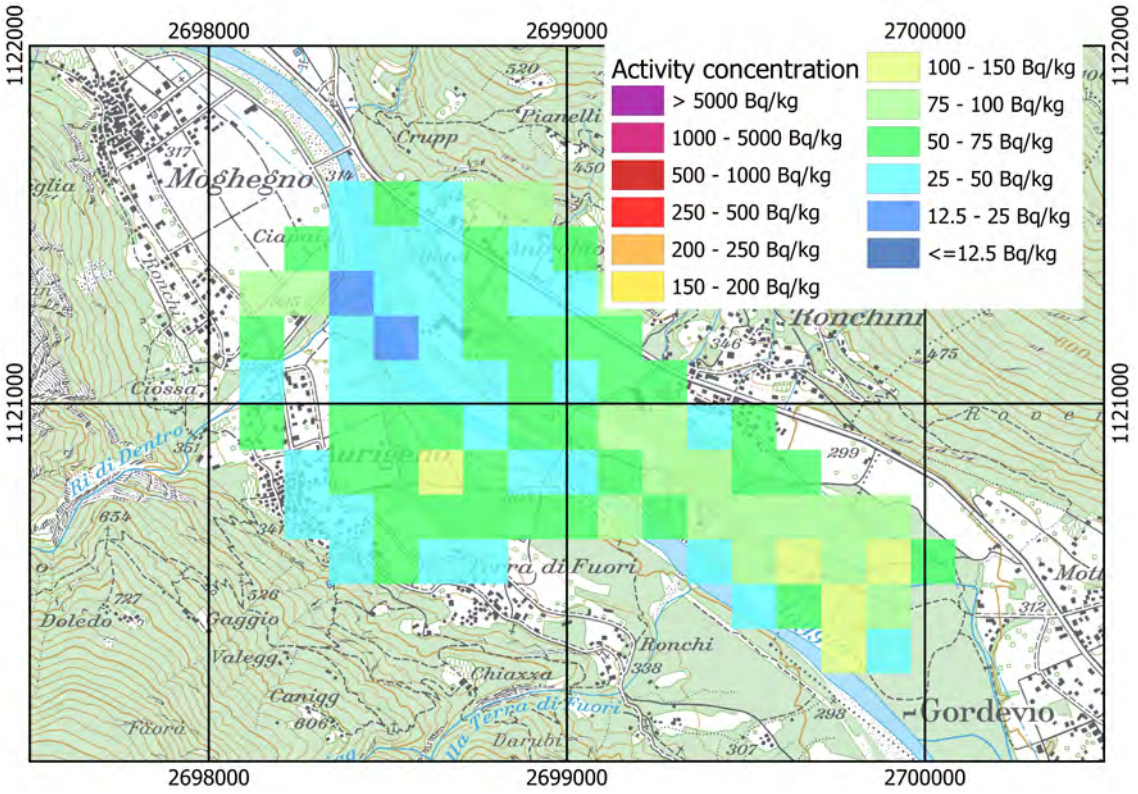

Figure 75: ^{137}Cs activity concentration measured over Ronchini. Geodaten©swisstopo.

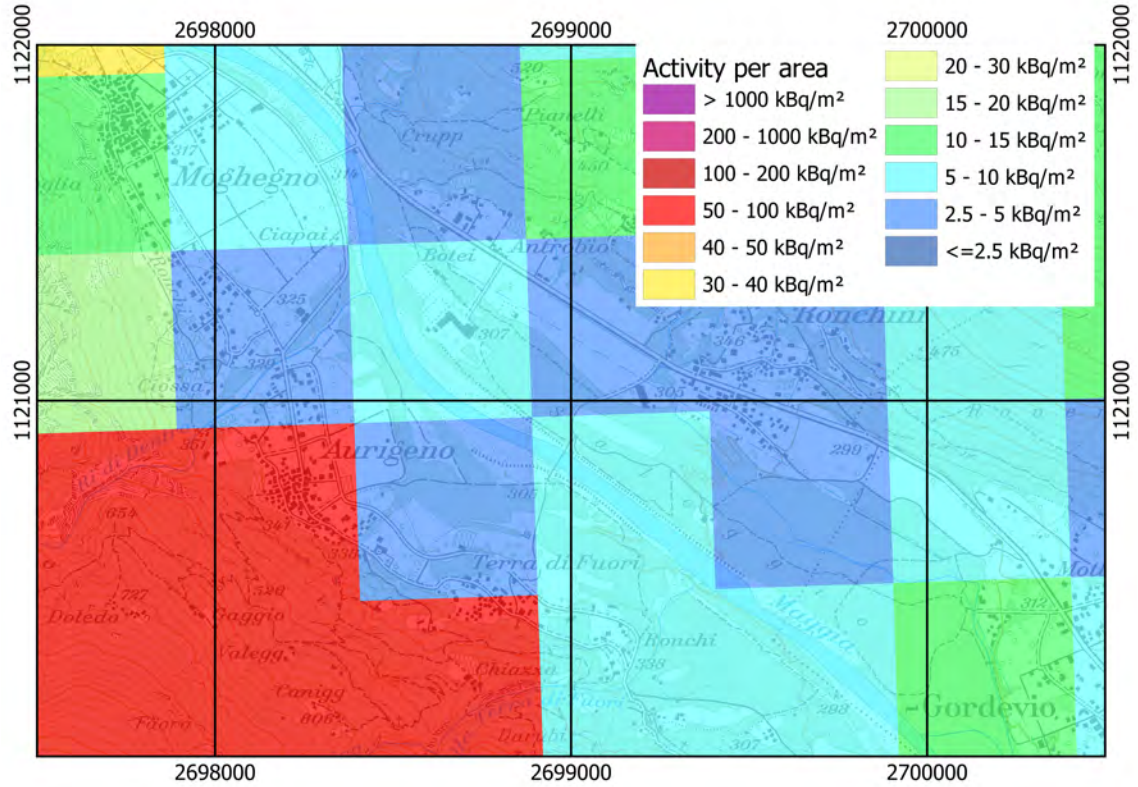

Figure 76: ^{137}Cs activity per area over Ronchini 2009 taken from baseline map. Geodaten©swisstopo, Caesium activity per area from Meusburger et al., 2020, provided electronically by ESDAC (Paganos et al. 2012).

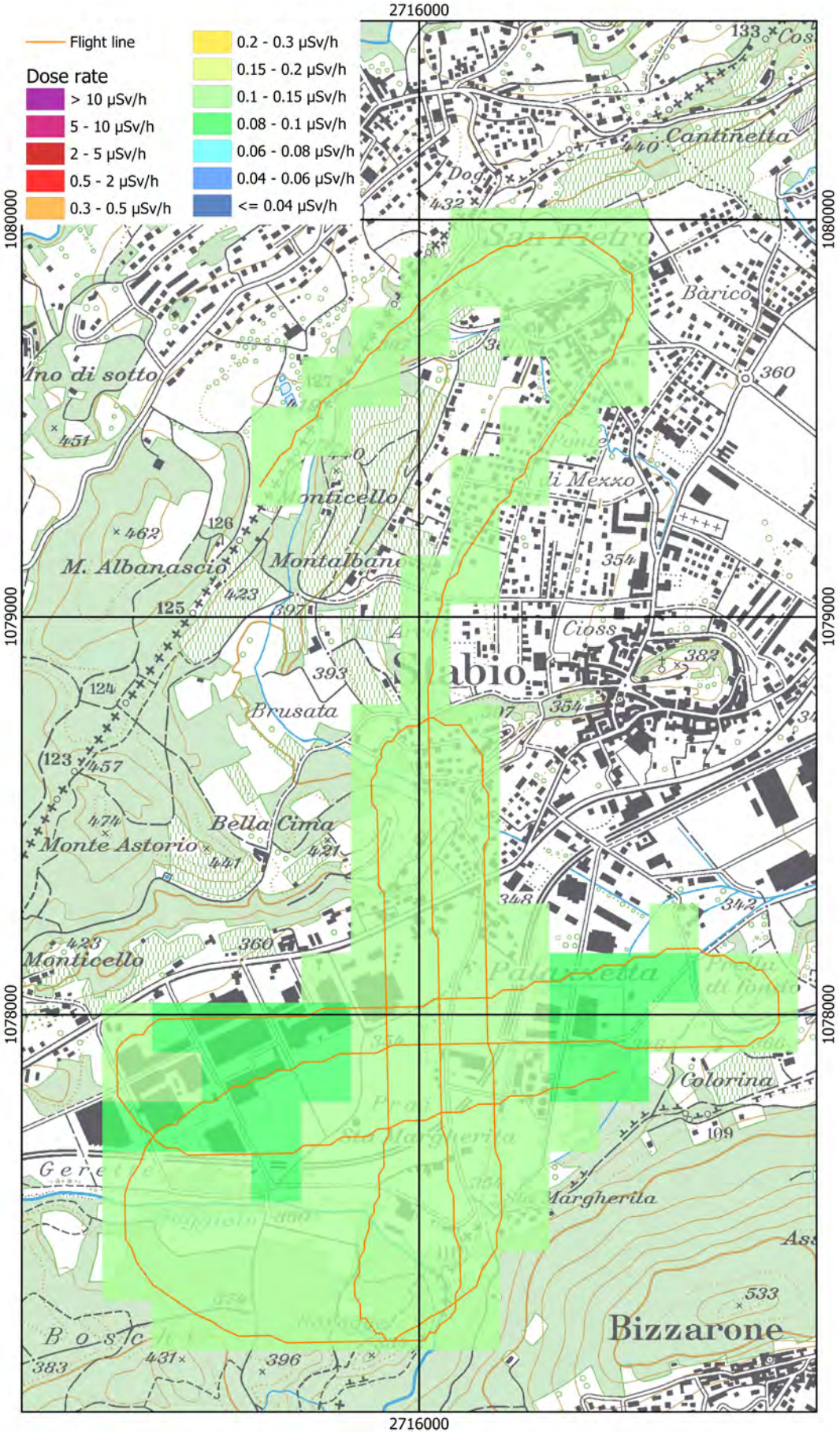

Figure 77: Dose rate over Stabio. Geodaten©swisstopo.

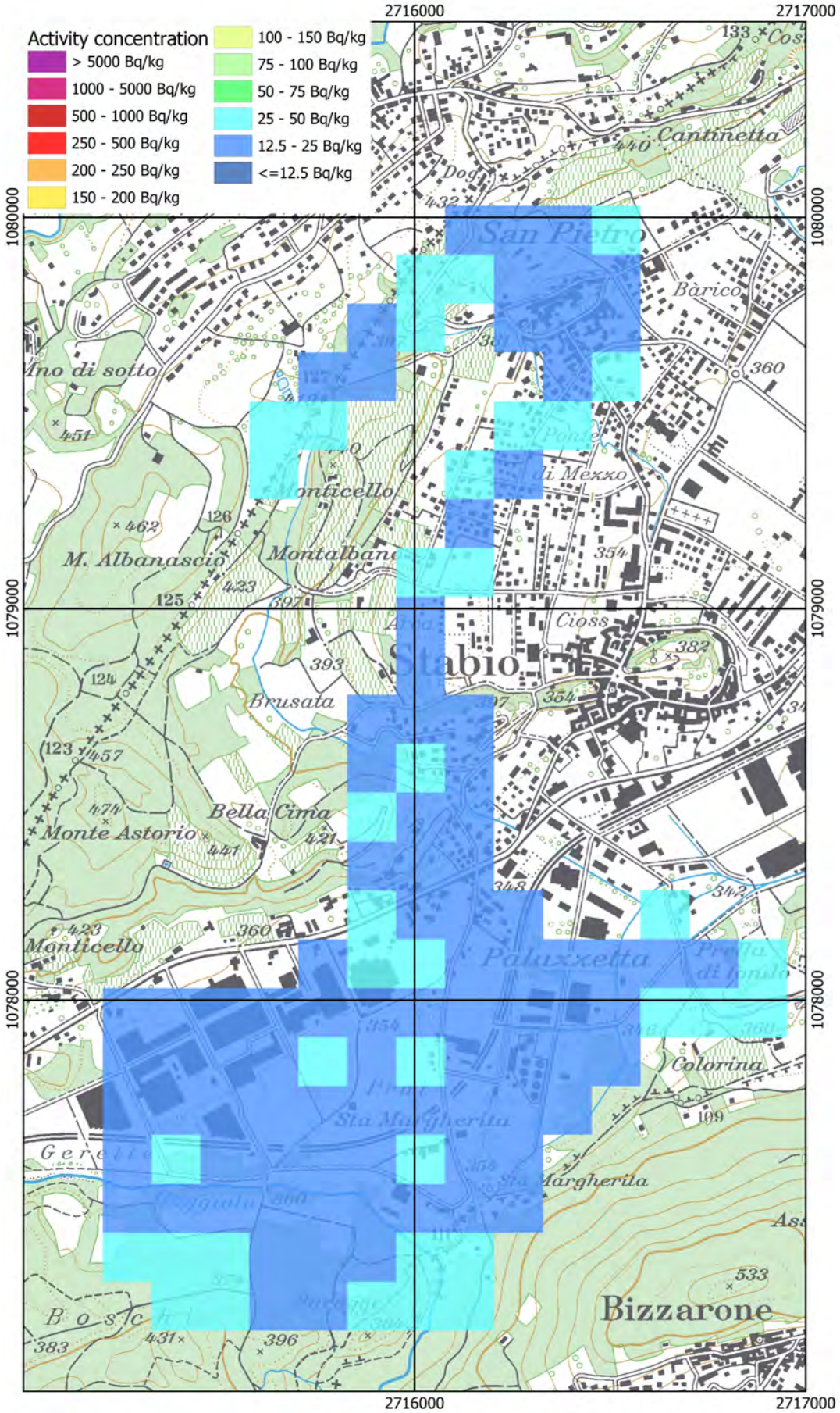

Figure 78: ^{232}Th activity concentration measured over Stabio. Geodaten©swisstopo.

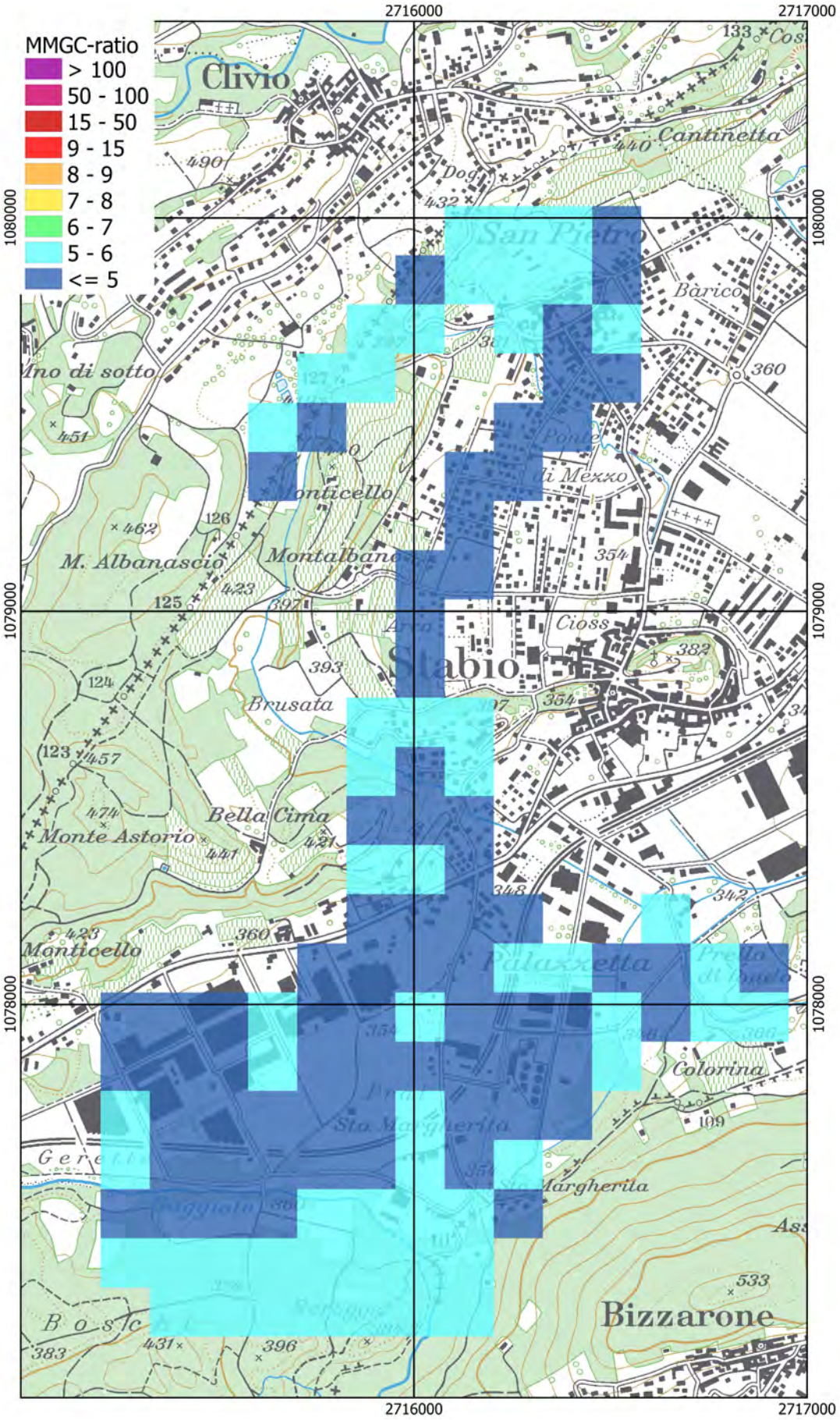

Figure 79: Man-made gross count (MMGC) ratio over Stabio. Geodaten©swisstopo.

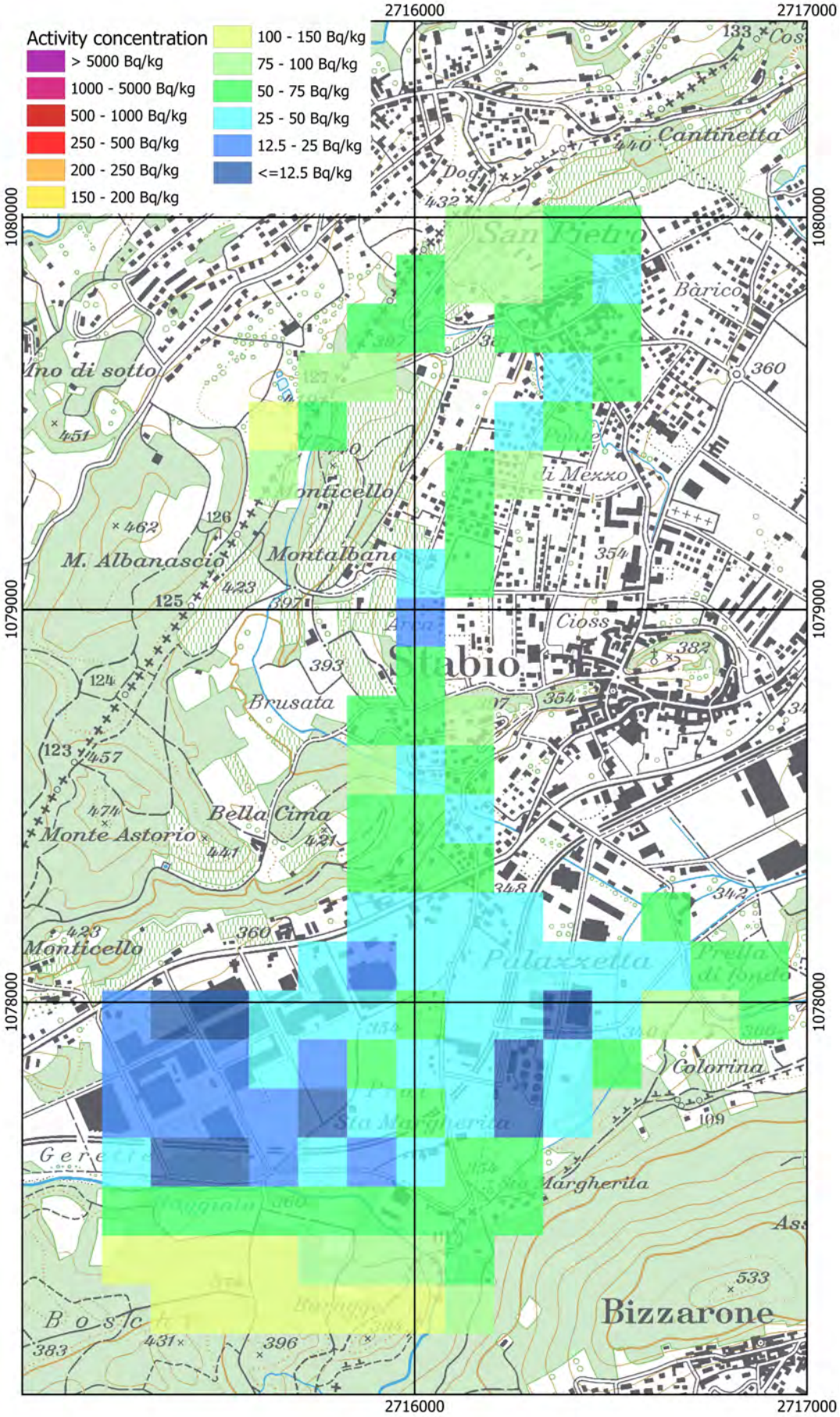

Figure 80: ^{137}Cs activity concentration measured over Stabio. Geodaten©swisstopo.

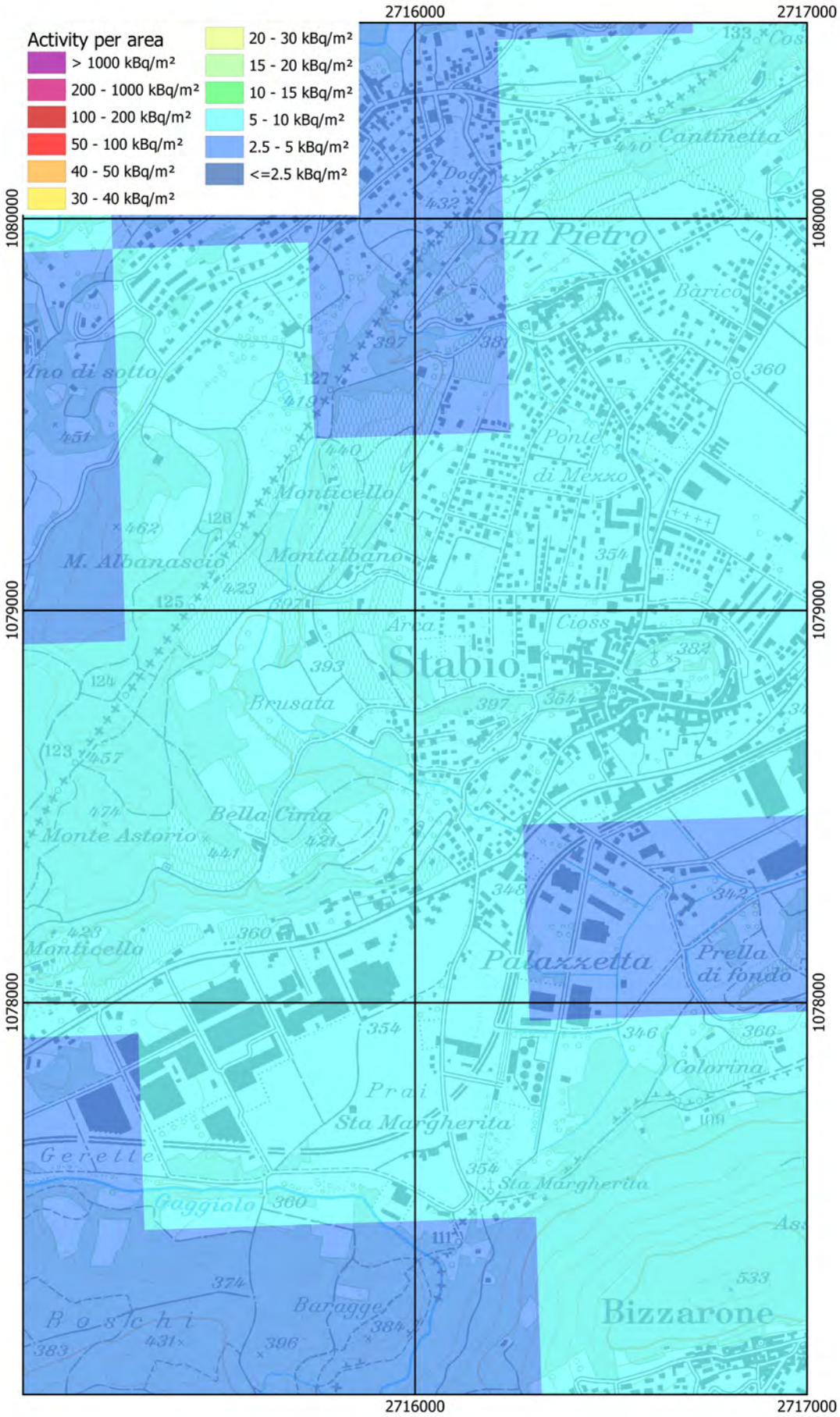

Figure 81: ^{137}Cs activity per area over Stabio 2009 taken from baseline map. Geodaten©swisstopo, Caesium activity per area from Meusburger et al., 2020, provided electronically by ESDAC (Paganos et al. 2012).

2.4.4 Comparison

Table 11 shows a comparison of ^{137}Cs activity concentrations determined in the different measurement areas.
Column "'Baseline"' was derived from the baseline map (Meusburger et al., 2020, see Figure 39). The maximum value of the provided digital data is limited to 65 kBq/m^2, which is unfortunately reached in some of the measurement areas. Values at this upper limit can be found frequently over lakes and rivers. The reason for this effect is unclear. The remaining activity per unit area was calculated using the factor of 0.76 from Table 9.
Column "'ARM21"' is based on values measured during ARM21 in the respective measuring area. The activity per wet weight in Bq/kg and per area in Bq/m^2 were calculated using the conversion factors listed in Table 5. The ratio between both conversion factors is 197 kg/m², rounded to a ratio of 200 kg/m² used for aligning activity colour scales (Section 2.4.1).
The ^{137}Cs deposited on a lake and river ground cannot be measured with airborne gamma-spectrometry due to the attenuation of photons by the water layer, leading to estimated activity concentration around zero. These low measured activity concentrations measured lead together with the observed high values of the baseline map over lakes to a bias in comparing area averages. Therefore, both maps were masked with a polygon covering the overlapping area, but excluding lakes in the respective regions. The values reported in the respective columns of Table 11 consist of the average of grid cells in the remaining polygon together with the respective minimal and maximal grid cell values.
Column "'Ground"' contains the results of the measurement of soil samples published by the Canton Ticino (Togni et al., 2016). These measurements were performed between 2013 and 2015, thus activity concentrations between 82% and 88% of the reported values would be expected at the date of ARM21. The measured activity per unit mass of soil layers at the different sites differs from the exponential distribution with a relaxation mass per unit area of β =9.5 g/cm². To render comparable values, only the results of the uppermost soil layers was used. The activity concentration in the first 5 cm of the soil profile was decay corrected for remaining activity listed in Table 9 and the associated activity concentration of a vertically homogeneous activity distribution was calculated using a transfer factor of 1.402 (Section 1.3.3). The range of activity concentrations lists minimum and maximum of decay corrected activity concentrations measured in 5 cm thick soil layers up to 25 cm depth. For the measuring area "'Joux"', the average value of the in-situ gamma-spectrometric measurements (Table 10) and the according minimum and maximum were used.
The ^{137}Cs activity concentrations determined with airborne gamma spectrometry are always lower compared to the results of ground measurements, indicating the necessity to review the according calibration factor in Table 5. The differences to the baseline map do not yield such a consistent picture. The results in the measuring areas Balerna, Joux, Lodrino, Lugano and Monti di Paudo agree reasonably well, whereas the ^{137}Cs activity concentrations measured with airborne gamma-spectrometry in the regions of Demanio, Ronchini and Stabio are two to three times larger than the gridded values predicted by the baseline map.

Area	^{137}Cs activity			
	ARM21		Ground	Baseline
	[Bq/kg]	[kBq/m^2]	[Bq/kg]	[kBq/m^2]
Balerna	42 (-42 – 124)	8.2 (-8 – 24)	84 (25 – 118)	7.3 (5 – 9)
Demanio	37 (-41 – 78)	7.3 (-8 – 15)	-	2.9 (2 – 5)
Joux	22 (-17 – 69)	4.3 (-3 – 14)	56 (30 – 157)	6.7 (0 – 49)
Lodrino	45 (-28 – 82)	8.8 (-6 – 16)	92 (17 – 129)	6.2 (4 – 10)
Lugano	43 (-39 – 152)	8.5 (-8 – 30)	156 (18 – 218)	9.8 (2 – 49)
Monti di Paudo	92 (70 – 111)	18.2 (14 – 22)	355 (81 – 497)	15.1 (2 – 49)
Ronchini	62 (22 – 146)	12.2 (4 – 29)	144 (-)	4.4 (3 – 8)
Stabio	55 (-5 – 137)	10.9 (-1 – 27)	-	4.4 (3 – 5)

Table 11: ^{137}Cs activity in the different regions. Average and range of values in map cells of the overlapping areas. Negative values of the measured data are due to statistical measurement uncertainties.

The results of previous airborne gamma-spectrometric measurements in Canton Ticino are listed in Table 12. The measured activity concentrations were decay corrected to July 1st, 2021. The mass reference was changed from dry soil to wet soil assuming a 20% water content of the soil. The average activity concentrations in Table 12 range from 14 Bq/kg to 108 Bq/kg, comparable to the range found during this exercise for the areas located in Canton Ticino between 37 Bq/kg and 92 Bq/kg.

Area	Flight number	^{137}Cs activity concentration [Bq/kg]
Magadino	1996018	77 ± 32
Magadino	1996019	84 ± 30
Magadino	1996020	78 ± 31
Cavigliano	1999016	74 ± 35
Lugano	1999017	70 ± 30
Pizzo Ometto	2011012	108 ± 33
Rasa	2011013	90 ± 45
Chiasso	2011015	36 ± 40
Novaggio	2011018	54 ± 37
Rodi	2011020	14 ± 35

Table 12: Average and standard deviation of ^{137}Cs activity concentrations measured over areas in Canton Ticino in 1996, 1999 and 2011. Measured activity concentrations were decay corrected to July 1st, 2021.

2.5 Transverses

Two parallel transverses were flown starting with the northern leg from Rüthi to Châtel-Saint-Denis and back in the southern leg from Saint-Légier-La-Chiésaz to Eschenbach (Figure 82). Only data points were considered, where a ground clearance between 30 m and 200 m was achievable. The altitude ranged from 500 m above sea level to 2200 m above sea level (Figure 83). A topographical correction based on the Swiss digital elevation DHM25 was applied in the evaluation. The total dose rate estimated for one meter above ground shows clearly the influence of the altitude dependent component due to cosmic radiation (Figure 84). The terrestrial component of the dose rate does not show this altitude dependence and also no indication of anomalous activity concentrations of natural radionuclides. The attenuation of photons emitted by terrestrial radionuclides due to the water layer of lakes crossed during the traversals marked in Figures 82 and 84 with letters A to G is clearly visible.

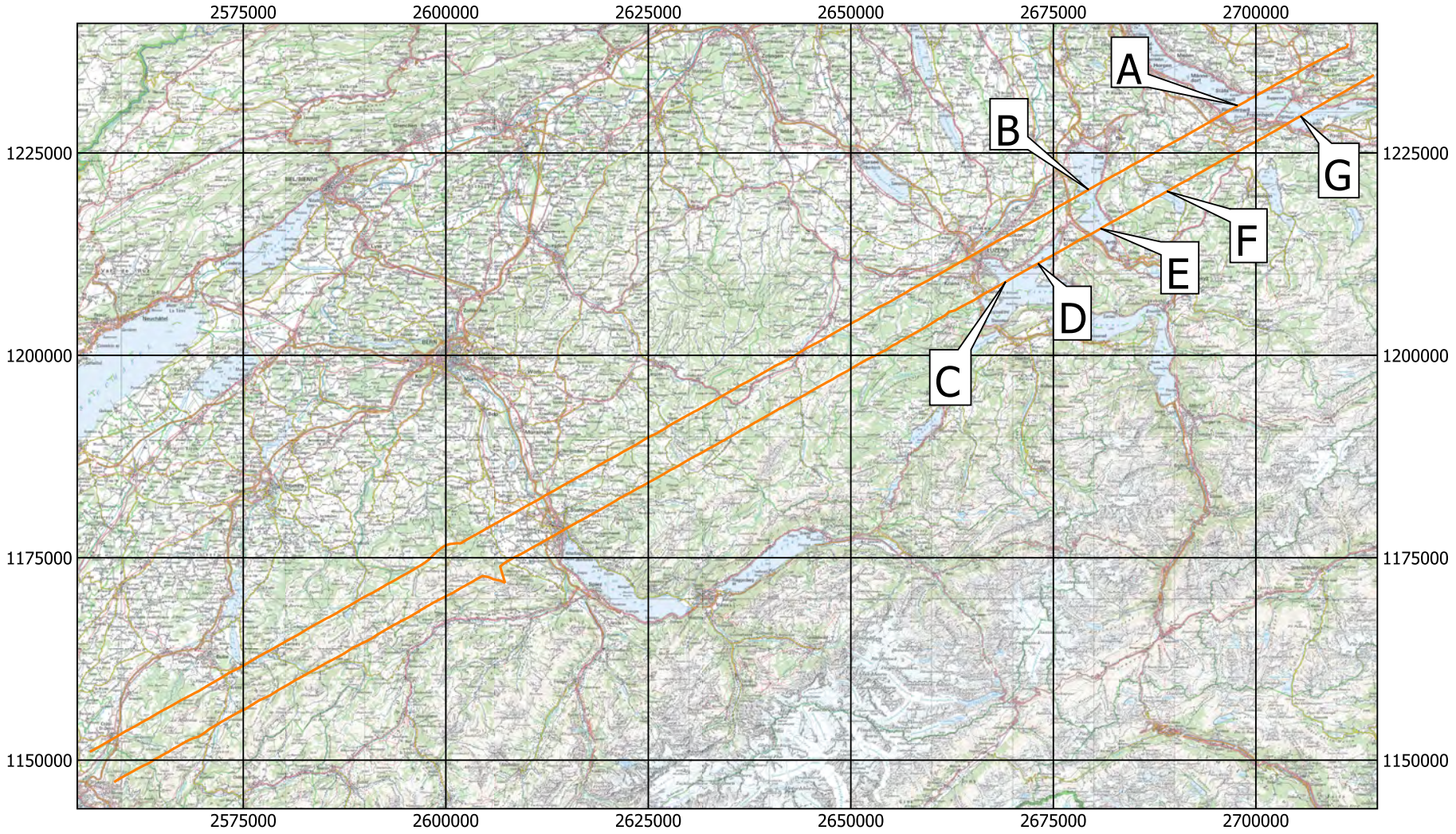

Figure 82: Flight lines of the transverses. Geodaten©swisstopo.

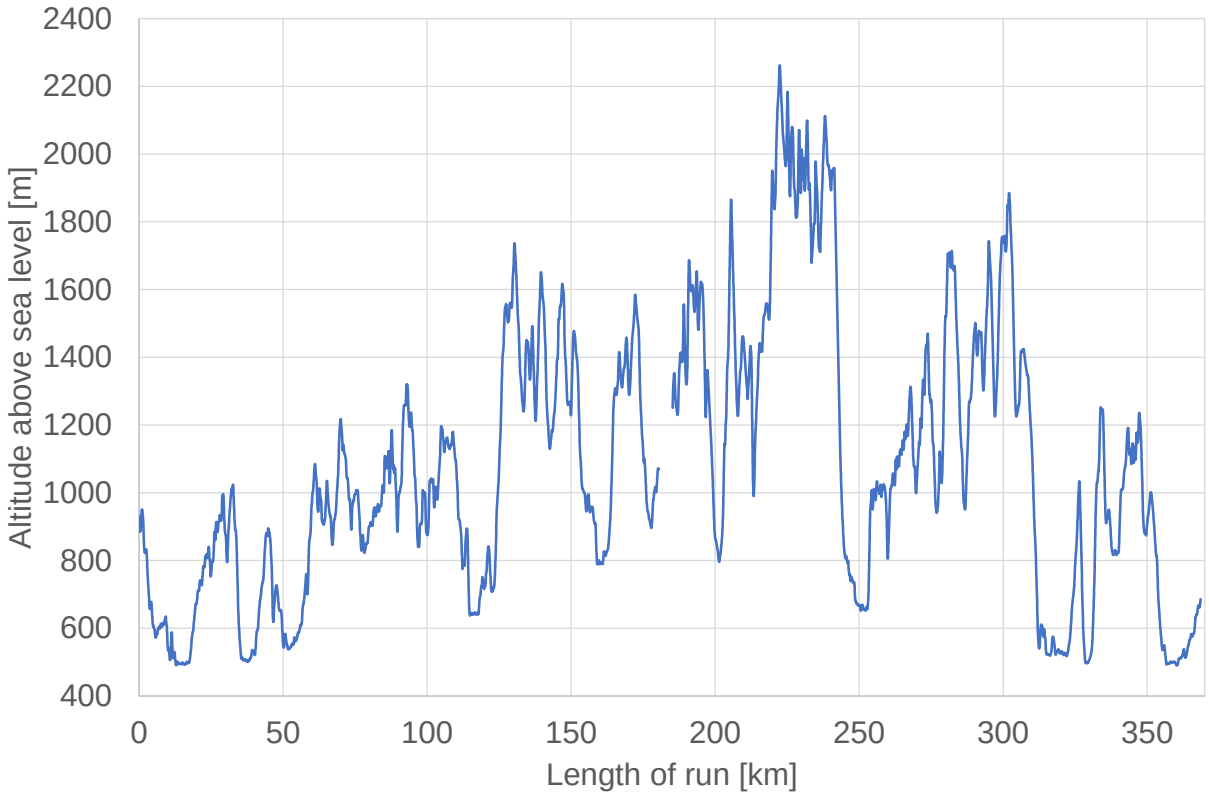

Figure 83: Altitude of the transverses.

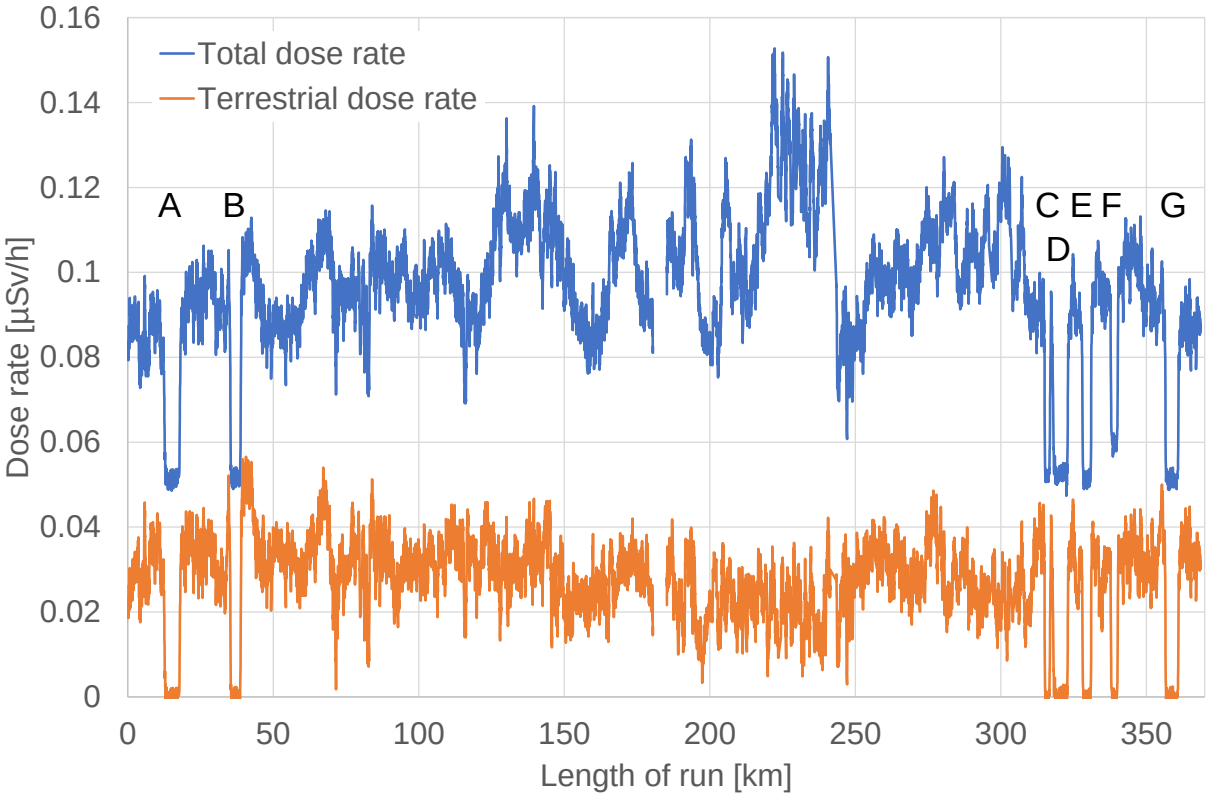

Figure 84: Total and terrestrial dose rate measured along the transverses.

3 Conclusions

The survey of the Swiss nuclear power plants Gösgen (KKM) and Mühleberg (KKM) showed no artificial radionuclides in the vicinity of the plant premises. Due to the decommissioning of KKM, radioactive material is moved from the well shielded reactor building to other sites on the premises for processing and measurement. These relocated components were clearly detected during the measuring flights.
Altitude profiles over Lake Neuchâtel were added to the database of altitude profiles measured in the past to improve the data evaluation procedure for the determination of system background and the influence of cosmic radiation.
With the exception of Lugano, measurements over several Swiss cities, over an area to the south-west of KKG and along two transverses showed the distribution of natural occurring radionuclides according to the underlying geology and the attenuation of terrestrial photons by water layers.
Lugano is located in one of the regions of Switzerland affected from radionuclide deposition of the Chernobyl accident. Residual ^{137}Cs activity can still be detected in the vicinity of Lugano and several other sites tested during ARM21 as a follow-up of the Chernobyl deposition. Comparison to results of ground measurements, maps published in the scientific literature and previous airborne measurements yielded reasonable agreement to the measurement results.
Detector RLL001 used in exercise part ARM21c continues to operate as specified. Problems with one NaI(Tl) crystal of detector RLL004 used during exercise part ARM21m indicates that not all of the crystals with poor quality have yet been identified during previous exercises.

4 Literature

Bucher, B.: Methodische Weiterentwicklungen in der Aeroradiometrie. Dissertation Nr. 13973, ETH Zürich, 2001

European Commission: Atlas of Caesium deposition on Europe after the Chernoby accident. Office for Official Publications of the European Communities, Luxembourg, ISBN92-828-3140-X, 1998

Evangeliou, N., Hamburger, T., Talerko, N., Zibtsev, S., Bondar, Y., Stohl, A., Balanski, Y., Mousseau, T.A. Møller,A.P.: Reconstructing the Chernobyl Nuclear Power Plant (CNPP) accident 30 years after. A unique database of air concentration and deposition measurements over Europe. Environmental Pollution 216, pp. 408-418, 2016

Hauptabteilung für die Sicherheit der Kernanlagen: Der Unfall Chernobyl - Ein Überblick über Ursachen und Auswirkungen, HSK-report HSK-AN-1816 Rev. 1, Würenlingen, Switzerland, 1986

International Commission on Radiation Units and Measurements (ICRU): Gamma-Ray Spectrometry in the Environment, ICRU Report 52, Bethesda, Maryland, USA, 1994.

Lemercier, M., Gurriaran, R., Bouisset, P., Cagnat, X.: Specific activity to H*(10) conversion coefficients for in situ gamma spectrometry. Radiat. Prot. Dosim. 128(1), pp. 83-89, 2007

Meusburger, K., Evrard, O., Alewell, C., Borrelli, P., Cinelli, G., Ketterer, M., Mabit, L., Panagos, P., van Oost, K., Ballabio, C: Plutonium aided reconstruction of caesium atmospheric fallout in European topsoils. Scientific Reports 10: 11858, 2020. https://doi.org/10.1038/s41598-020-68736-2

Panagos P., Van Liedekerke M., Jones A., Montanarella L.: “European Soil Data Centre: Response to European policy support and public data requirements”; Land Use Policy, 29 (2), pp. 329-338. doi:10.1016/j.landusepol.2011.07.003 European Soil Data Centre (ESDAC), esdac.jrc.ec.europa.eu, European Commission, Joint Research Centre, 2012

Riesen, T.K., Zimmermann, S., Blaser, P.: Spatial distribution of ^{137}Cs in forest soils of Switzerland. Water, Air and Soil Pollution 114, pp. 277-285, 1999

Schwarz, G. F.: Methodische Entwicklungen zur Aerogammaspektrometrie. Beiträge zur Geologie der Schweiz, Geophysik Nr. 23, Schweizerische Geophysikalische Kommission, 1991

Togni, V., Pancera, S., Solcà, N.: Cs-137 nei suoli boschivi in Ticino a 30 anni dall’incidente di Chernobyl , Canton Ticino, Ufficio della gestione dei rischi ambientali e del suolo, https://www4.ti.ch/fileadmin/DT/temi/protezione_suolo/documenti/Cesio137_suoli_boschi.pdf, 2016

5 Previous reports

Schwarz, G. F., Klingelé, E. E., Rybach, L.: Aeroradiometrische Messungen in der Umgebung der schweizerischen Kernanlagen. Bericht für das Jahr 1989 zuhanden der Hauptabteilung für die Sicherheit der Kernanlagen (HSK). Interner Bericht, Institut für Geophysik, ETH Zürich, 1990.

Schwarz, G. F., Klingelé, E. E., Rybach, L.: Aeroradiometrische Messungen in der Umgebung der schweizerischen Kernanlagen. Bericht für das Jahr 1990 zuhanden der Hauptabteilung für die Sicherheit der Kernanlagen (HSK). Interner Bericht, Institut für Geophysik, ETH Zürich, 1991.

Schwarz, G. F., Klingelé, E. E., Rybach, L.: Aeroradiometrische Messungen in der Umgebung der schweizerischen Kernanlagen. Bericht für das Jahr 1991 zuhanden der Hauptabteilung für die Sicherheit der Kernanlagen (HSK). Interner Bericht, Institut für Geophysik, ETH Zürich, 1992.

Schwarz, G. F., Klingelé, E. E., Rybach, L.: Aeroradiometrische Messungen in der Umgebung der schweizerischen Kernanlagen. Bericht für das Jahr 1992 zuhanden der Hauptabteilung für die Sicherheit der Kernanlagen (HSK). Interner Bericht, Institut für Geophysik, ETH Zürich, 1993.

Schwarz, G. F., Klingelé, E. E., Rybach, L.: Aeroradiometrische Messungen in der Umgebung der schweizerischen Kernanlagen. Bericht für das Jahr 1993 zuhanden der Hauptabteilung für die Sicherheit der Kernanlagen (HSK). Interner Bericht, Institut für Geophysik, ETH Zürich, 1994.

Schwarz, G. F., Rybach, L.: Aeroradiometrische Messungen im Rahmen der Übung ARM94. Bericht für das Jahr 1994 zuhanden der Fachgruppe Aeroradiometrie (FAR). Interner Bericht, Institut für Geophysik, ETH Zürich, 1995.

Schwarz, G. F., Rybach, L.: Aeroradiometrische Messungen im Rahmen der Übung ARM95. Bericht für das Jahr 1995 zuhanden der Fachgruppe Aeroradiometrie (FAR). Interner Bericht, Institut für Geophysik, ETH Zürich, 1996.

Schwarz, G. F., Rybach, L., Bärlocher, C.: Aeroradiometrische Messungen im Rahmen der Übung ARM96. Bericht für das Jahr 1996 zuhanden der Fachgruppe Aeroradiometrie (FAR). Interner Bericht, Institut für Geophysik, ETH Zürich, 1997.

Bucher, B., Rybach, L., Schwarz, G., Bärlocher, C.: Aeroradiometrische Messungen im Rahmen der Übung ARM97. Bericht für das Jahr 1997 zuhanden der Fachgruppe Aeroradiometrie (FAR). Interner Bericht, Institut für Geophysik, ETH Zürich, 1998.

Bucher, B., Rybach, L., Schwarz, G., Bärlocher, C.: Aeroradiometrische Messungen im Rahmen der Übung ARM98. Bericht für das Jahr 1998 zuhanden der Fachgruppe Aeroradiometrie (FAR). Interner Bericht, Institut für Geophysik, ETH Zürich, 1999.

Bucher, B., Rybach, L., Schwarz, G., Bärlocher, C.: Aeroradiometrische Messungen im Rahmen der Übung ARM99. Bericht für das Jahr 1999 zuhanden der Fachgruppe Aeroradiometrie (FAR). Interner Bericht, Institut für Geophysik, ETH Zürich, 2000.

Bucher, B., Rybach, L., Schwarz, G., Bärlocher, C.: Aeroradiometrische Messungen im Rahmen der Übung ARM00. Bericht für das Jahr 2000 zuhanden der Fachgruppe Aeroradiometrie (FAR). Interner Bericht, Institut für Geophysik, ETH Zürich, 2001.

Bucher, B., Rybach, L., Schwarz, G., Bärlocher, C.: Aeroradiometrische Messungen im Rahmen der Übung ARM01. Bericht für das Jahr 2001 zuhanden der Fachgruppe Aeroradiometrie (FAR). Interner Bericht, Paul Scherrer Institut, Villigen, Schweiz, 2002.

Bucher, B., Rybach, L., Schwarz, G., Bärlocher, C.: Aeroradiometrische Messungen im Rahmen der Übung ARM02. Bericht für das Jahr 2002 zuhanden der Fachgruppe Aeroradiometrie (FAR). Interner Bericht, Paul Scherrer Institut, Villigen, Schweiz, 2003.

Bucher, B., Rybach, L., Schwarz, G.: Aeroradiometrische Messungen im Rahmen der Übung ARM03. PSI-Bericht 04-14, ISSN 1019-0643, Paul Scherrer Institut, Villigen, Schweiz, 2004.

Bucher, B., Butterweck, G., Rybach, L., Schwarz, G.: Aeroradiometrische Messungen im Rahmen der Übung ARM04. PSI-Bericht 05-10, ISSN 1019-0643, Paul Scherrer Institut, Villigen, Schweiz, 2005.

Bucher, B., Butterweck, G., Rybach, L., Schwarz, G.: Aeroradiometrische Messungen im Rahmen der Übung ARM05. PSI-Bericht 06-06, ISSN 1019-0643, Paul Scherrer Institut, Villigen, Schweiz, 2006.

Bucher, B., Butterweck, G., Rybach, L., Schwarz, G.: Aeroradiometrische Messungen im Rahmen der Übung ARM06. PSI-Bericht 07-02, ISSN 1019-0643, Paul Scherrer Institut, Villigen, Schweiz, 2007.

Bucher, B., Guillot, L., Strobl, C., Butterweck, G., Gutierrez, S., Thomas, M., Hohmann, C., Krol, I., Rybach, L., Schwarz, G.: International Intercomparison Exercise of Airborne Gammaspectrometric Systems of Germany, France and Switzerland in the Framework of the Swiss Exercise ARM07. PSI-Bericht Nr. 09-07, ISSN 1019-0643, Paul Scherrer Institut, Villigen, Schweiz, 2009.

Bucher, B., Butterweck, G., Rybach, L., Schwarz, G.: Aeroradiometrische Messungen im Rahmen der Übung ARM08. PSI-Bericht Nr. 09-02, ISSN 1019-0643, Paul Scherrer Institut, Villigen, Schweiz, 2009.

Bucher, B., Butterweck, G., Rybach, L., Schwarz, G., Strobl, C.: Aeroradiometrische Messungen im Rahmen der Übung ARM09. PSI-Bericht Nr. 10-01, ISSN 1019-0643, Paul Scherrer Institut, Villigen, Schweiz, 2010.

Bucher, B., Butterweck, G., Rybach, L., Schwarz, G., Mayer, S.: Aeroradiometrische Messungen im Rahmen der Übung ARM10. PSI-Bericht Nr. 11-02, ISSN 1019-0643, Paul Scherrer Institut, Villigen, Schweiz, 2011.

Bucher, B., Butterweck, G., Rybach, L., Schwarz, G., Mayer, S.: Aeroradiometric Measurements in the Framework of the Swiss Exercise ARM11. PSI-Report No. 12-04, ISSN 1019-0643, Paul Scherrer Institut, Villigen, Switzerland, 2012.

Butterweck, G., Bucher, B., Rybach, L., Schwarz, G., Hödlmoser, H., Mayer, S., Danzi, C. Scharding, G.: Aeroradiometric Measurements in the Framework of the Swiss Exercise ARM12. PSI-Report No. 13-01, ISSN 1019-0643, Paul Scherrer Institut, Villigen, Switzerland, 2013.

Butterweck, G., Bucher, B., Rybach, L., Schwarz, G., Hohmann, E., Mayer, S., Danzi, C. Scharding, G.: Aeroradiometric Measurements in the Framework of the Swiss Exercise ARM13. PSI-Report No. 15-01, ISSN 1019-0643, Paul Scherrer Institut, Villigen, Switzerland, 2015.

Butterweck, G., Bucher, B., Rybach, L., Schwarz, G., Hohmann, E., Mayer, S., Danzi, C. Scharding, G.: Aeroradiometric Measurements in the Framework of the Swiss Exercises ARM14 and FTX14. PSI-Report No. 15-02, ISSN 1019-0643, Paul Scherrer Institut, Villigen, Switzerland, 2015.

Butterweck, G., Bucher, B., Rybach, L., Schwarz, G., Hofstetter-Boillat, B., Hohmann, E., Mayer, S., Danzi, C. Scharding, G.: Aeroradiometric Measurements in the Framework of the Swiss Exercises ARM15, GNU15 and the International Exercise AGC15. PSI-Report No. 15-04, ISSN 1019-0643, Paul Scherrer Institut, Villigen, Switzerland, 2015.

Butterweck, G., Bucher, B., Rybach, L., Poretti, C., Maillard, S., Schwarz, G., Hofstetter-Boillat, B., Hohmann, E., Mayer, S., Scharding, G.: Aeroradiometric Measurements in the Framework of the Swiss Exercises ARM16 and LAURA. PSI-Report No. 17-01, ISSN 1019-0643, Paul Scherrer Institut, Villigen, Switzerland, 2017.

Butterweck, G., Bucher, B., Gryc, L., Debayle, C., Strobl, C., Maillard, S., Thomas, M., Helbig, A., Krol, I., Chuzel, S., Couvez, C., Ohera, M., Rybach, L., Poretti, C., Hofstetter-Boillat, B., Mayer, S., Scharding, G.: International Intercomparison Exercise of Airborne Gamma-Spectrometric Systems of the Czech Republic, France, Germany and Switzerland in the Framework of the Swiss Exercise ARM17. PSI-Report No. 18-04, ISSN 1019-0643, Paul Scherrer Institut, Villigen, Switzerland, 2018.

Butterweck, G., Bucher, B., Rybach, L., Poretti, C., Maillard, S., Schindler, M., Hofstetter-Boillat, B., Mayer, S., Scharding, G.: Aeroradiometric Measurements in the Framework of the Swiss Exercises ARM18 and the International Exercise CONTEX 2018. PSI-Report No. 19-01, ISSN 1019-0643, Paul Scherrer Institut, Villigen, Switzerland, 2019.

Butterweck, G., Bucher, B., Rybach, L., Poretti, C., Maillard, S., Schindler, M., Hofstetter-Boillat, B., Mayer, S., Scharding, G.: Aeroradiometric Measurements in the Framework of the Swiss Exercise ARM19. PSI-Report No. 20-01, ISSN 1019-0643, Paul Scherrer Institut, Villigen, Switzerland, 2020.

Butterweck, G., Bucher, B., Breitenmoser, D., Rybach, L., Poretti, C., Maillard, S., Kasprzak, M., Ferreri, G., Gurtner, A., Astner, M., Hauenstein, F., Straub, M., Bucher, M., Harm, C., Scharding, G., Mayer, S.: Aeroradiometric Measurements in the Framework of the Swiss Exercise ARM20. PSI-Report No. 21-01, ISSN 1019-0643, Paul Scherrer Institut, Villigen, Switzerland, 2021.

The reports since 1994 can be found and downloaded from the FAR website `https://far.ensi.ch`.

6 Evaluation parameters

The parameters used for data evaluation are stored in the header section of each generated ERS 2.0 file. The header sections used in the current exercise are listed below.

6.1 Detector RLL001

These evaluation parameters were used for the evaluation of exercise part ARM21c with detector RLL001.

```
V 2.0
HSW AGS_CH_V0.0
/* Parameters used for data evaluation-------------------------------------------------------------
/* No data value;MND -999
/* Energy calibration;ISE0 0;ISE1 3;ISE2 0
/* Energy windows---------------------------------------------------------------------------------
ISW Total;ISWE1_Total 401;ISWE2_Total 2997;ISWB_Total 125.3;ISWC_Total 5.65;ISWT_Total 0.006;ISWRA_Total 0;ISWRB_Total 0
ISW K-40;ISWE1_K-40 1369;ISWE2_K-40 1558;ISWB_K-40 9.1;ISWC_K-40 0.3;ISWT_K-40 0.008;ISWRA_K-40 0;ISWRB_K-40 0
ISW U-238;ISWE1_U-238 1664;ISWE2_U-238 1853;ISWB_U-238 5.8;ISWC_U-238 0.23;ISWT_U-238 0.0055;ISWRA_U-238 0;ISWRB_U-238 0
ISW Th-232;ISWE1_Th-232 2407;ISWE2_Th-232 2797;ISWB_Th-232 0.5;ISWC_Th-232 0.28;ISWT_Th-232 0.006;ISWRA_Th-232 0;ISWRB_Th-232 0
ISW Cs-137;ISWE1_Cs-137 600;ISWE2_Cs-137 720;ISWB_Cs-137 19.6;ISWC_Cs-137 0.58;ISWT_Cs-137 0.01;ISWRA_Cs-137 0;ISWRB_Cs-137 0
ISW Co-60;ISWE1_Co-60 1100;ISWE2_Co-60 1400;ISWB_Co-60 12.2;ISWC_Co-60 0.65;ISWT_Co-60 0.008;ISWRA_Co-60 0;ISWRB_Co-60 0
ISW MMGC1;ISWE1_MMGC1 400;ISWE2_MMGC1 1400;ISWB_MMGC1 0;ISWC_MMGC1 0;ISWT_MMGC1 0.006;ISWRA_MMGC1 0;ISWRB_MMGC1 0
ISW MMGC2;ISWE1_MMGC2 1400;ISWE2_MMGC2 2997;ISWB_MMGC2 0;ISWC_MMGC2 0;ISWT_MMGC2 0.0065;ISWRA_MMGC2 0;ISWRB_MMGC2 0
ISW LOW;ISWE1_LOW 100;ISWE2_LOW 400;ISWB_LOW 0;ISWC_LOW 0;ISWT_LOW 0.02;ISWRA_LOW 0;ISWRB_LOW 0
ISW MID;ISWE1_MID 720;ISWE2_MID 2997;ISWB_MID 0;ISWC_MID 0;ISWT_MID 0.015;ISWRA_MID 0;ISWRB_MID 0
ISW SDI;ISWE1_SDI 240;ISWE2_SDI 2997;ISWB_SDI 85.5;ISWC_SDI 4.26;ISWT_SDI 0.0053;ISWRA_SDI 0;ISWRB_SDI 0
/* Stripping factors------------------------------------------------------------------------------
ISWS_U-238_K-40 0.931
ISWS_Th-232_K-40 0.478
ISWS_Co-60_K-40 0.067
ISWS_Th-232_U-238 0.362
ISWS_U-238_Th-232 0.049
ISWS_K-40_Cs-137 0.450
```

```
ISWS_U-238_Cs-137 3.161
ISWS_Th-232_Cs-137 1.654
ISWS_Co-60_Cs-137 0.154
ISWS_K-40_Co-60 0.758
ISWS_U-238_Co-60 2.370
ISWS_Th-232_Co-60 0.684
/* Conversion factors----------------------------------------------------------------------------
ISWA_AW_K-40 5.58
ISWA_AW_U-238 3.57
ISWA_AW_Th-232 1.22
ISWA_AW_Cs-137 1.02
ISWA_AA_Cs-137 201
ISWA_AP_Cs-137 2511000
ISWA_AP_Co-60 1505000
ISD_SDI 5.65E-08
ISWD_K-40 0.000289
ISWD_U-238 0.00197
ISWD_Th-232 0.000971
ISWD_Cs-137 0.000191
/* Corrections-----------------------------------------------------------------------------------
/* Definition of additional Identifiers for corrected altitude and ground clearance, an indicator for a new flight and the factor for calcul
DEFINE&PZ_korr Corrected altitude im m; DEFINE&PH_korr Corrected ground clearance in m;DEFINE&New_Flight Switch for data composed of several
/* Factor for the calculation of synthetic cosmic counts;&Factor_COS 14.35
/* Topographic correction;MTC Y
/* Radon correction;MRC N
```

6.2 Detector RLL004

These evaluation parameters were used for the evaluation of exercise part ARM21m with detector RLL004. The evaluation parameters for the complete detector take into account that spectra of NaI crystal 2 were replaced with spectra of crystal 3.

```
V 2.0
HSW AGS_CH_V0.0
/* Parameters used for data evaluation-----------------------------------------------------------
/* No data value;MND -999
/* Altitude reference WGS84 ellipsoid
/* Energy calibration;ISE0 0;ISE1 3;ISE2 0
/* Energy windows-------------------------------------------------------------------------------
ISW Total;ISWE1_Total 401;ISWE2_Total 2997;ISWB_Total 149.9;ISWC_Total 5.65;ISWT_Total 0.006;ISWRA_Total 0;ISWRB_Total 0
ISW K-40;ISWE1_K-40 1369;ISWE2_K-40 1558;ISWB_K-40 10.2;ISWC_K-40 0.30;ISWT_K-40 0.008;ISWRA_K-40 0;ISWRB_K-40 0
ISW U-238;ISWE1_U-238 1664;ISWE2_U-238 1853;ISWB_U-238 7.7;ISWC_U-238 0.23;ISWT_U-238 0.0055;ISWRA_U-238 0;ISWRB_U-238 0
ISW Th-232;ISWE1_Th-232 2407;ISWE2_Th-232 2797;ISWB_Th-232 0.9;ISWC_Th-232 0.28;ISWT_Th-232 0.006;ISWRA_Th-232 0;ISWRB_Th-232 0
ISW Cs-137;ISWE1_Cs-137 600;ISWE2_Cs-137 720;ISWB_Cs-137 24.9;ISWC_Cs-137 0.58;ISWT_Cs-137 0.01;ISWRA_Cs-137 0;ISWRB_Cs-137 0
ISW Co-60;ISWE1_Co-60 1100;ISWE2_Co-60 1400;ISWB_Co-60 15.6;ISWC_Co-60 0.65;ISWT_Co-60 0.008;ISWRA_Co-60 0;ISWRB_Co-60 0
ISW MMGC1;ISWE1_MMGC1 400;ISWE2_MMGC1 1400;ISWB_MMGC1 0;ISWC_MMGC1 0;ISWT_MMGC1 0.006;ISWRA_MMGC1 0;ISWRB_MMGC1 0
ISW MMGC2;ISWE1_MMGC2 1400;ISWE2_MMGC2 2997;ISWB_MMGC2 0;ISWC_MMGC2 0;ISWT_MMGC2 0.0065;ISWRA_MMGC2 0;ISWRB_MMGC2 0
ISW LOW;ISWE1_LOW 100;ISWE2_LOW 400;ISWB_LOW 0;ISWC_LOW 0;ISWT_LOW 0.02;ISWRA_LOW 0;ISWRB_LOW 0
ISW MID;ISWE1_MID 720;ISWE2_MID 2997;ISWB_MID 0;ISWC_MID 0;ISWT_MID 0.015;ISWRA_MID 0;ISWRB_MID 0
ISW SDI;ISWE1_SDI 240;ISWE2_SDI 2997;ISWB_SDI 101.0;ISWC_SDI 4.26;ISWT_SDI 0.0053;ISWRA_SDI 0;ISWRB_SDI 0
/* Stripping factors----------------------------------------------------------------------------
ISWS_U-238_K-40 0.921
ISWS_Th-232_K-40 0.474
ISWS_Co-60_K-40 0.035
ISWS_Th-232_U-238 0.338
ISWS_U-238_Th-232 0.052
ISWS_K-40_Cs-137 0.372
ISWS_U-238_Cs-137 2.784
ISWS_Th-232_Cs-137 1.442
ISWS_Co-60_Cs-137 0.120
ISWS_K-40_Co-60 0.656
```

```
ISWS_U-238_Co-60 2.257
ISWS_Th-232_Co-60 0.646
/* Conversion factors----------------------------------------------------------------------------
ISWA_AW_K-40 5.58
ISWA_AW_U-238 3.57
ISWA_AW_Th-232 1.22
ISWA_AW_Cs-137 1.02
ISWA_AA_Cs-137 201
ISWA_AP_Cs-137 2511000
ISWA_AP_Co-60 1505000
ISD_SDI 5.65E-08
ISWD_K-40 0.000289
ISWD_U-238 0.00197
ISWD_Th-232 0.000971
ISWD_Cs-137 0.000191
/* Corrections----------------------------------------------------------------------------------
/* Definition of additional Identifiers for corrected altitude and ground clearance, an indicator for a new flight and the factor for calcul
DEFINE&PZ_korr Corrected altitude im m; DEFINE&PH_korr Corrected ground clearance in m;DEFINE&New_Flight Switch for data composed of several
/* Factor for the calculation of synthetic cosmic counts;&Factor_COS 14.35
/* Topographic correction;MTC Y
/* Radon correction;MRC N
```

Paul Scherrer Institut :: Forschungsstrasse 111 :: 5232 Villigen PSI :: Switzerland :: Tel. +41 56 310 21 11 :: www.psi.ch